The influence of interstitial gas on powder handling

THE INFLUENCE OF INTERSTITIAL GAS ON POWDER HANDLING

WARD COTTAAR

THE INFLUENCE OF INTERSTITIAL GAS ON POWDER HANDLING

THE INFLUENCE OF INTERSTITIAL GAS ON POWDER HANDLING

PROEFSCHRIFT

TER VERKRIJGING VAN DE GRAAD VAN DOCTOR IN DE TECHNISCHE WETENSCHAPPEN AAN DE TECHNISCHE HOGESCHOOL EINDHOVEN, OP GEZAG VAN DE RECTOR MAGNIFICUS, PROF. DR. S. T. M. ACKERMANS, VOOR EEN COMMISSIE AANGEWEZEN DOOR HET COLLEGE VAN DEKANEN IN HET OPENBAAR TE VERDEDIGEN OP DINSDAG 16 APRIL 1985 TE 16.00 UUR

DOOR

EDUARDUS JOHANNES EMIEL COTTAAR

GEBOREN TE HEERLEN

Druk: Dissertatiedrukkerij Wibro, Helmond.

Dit proefschrift is goedgekeurd door
de promotor:
prof.dr. K. Rietema

co-promotor:
ir. S. Stemerding

CONTENTS

1 INTRODUCTION

1.1 SCOPE OF THIS THESIS

This thesis will treat the effect of the interstitial gas, i.e. the gas in the pores between the powder particles, on the handling of fine powders. The reason for such a research project is that up till now almost all research on powders only considered properties of the particles, like particle size, particle weight and so on. A powder is in essence, however, a two-phase system: it consists of a dispersed solid phase, the particles, and a continuous gaseous phase, the interstitial gas. For a complete understanding of the phenomena occuring during the handling of fine powders one should deal therefore with both phases. In this thesis the effects of the properties of the gaseous phase will be investigated.

That the gaseous phase may indeed highly influence the properties of the whole powder system may be clear from the field of fluidization: due to induced gas velocities a powder changes into a more or less turbulent mass with very large variations in voidage, e.g. "bubbles". Of course, in fluidization these gas flows are deliberately created. However, also in many other powder handling apparatus velocity differences between the particles and the gas are created through a continuous reshuffling of the powder. This may cause a significant aeration of the powder, although the velocities are generally not as high as in fluidized beds. Since this hydrodynamic interaction is due to the viscosity of the gas, this viscosity is the first property of the gas to influence the powder behavior.

A second property of the gas which may influence the behavior of the powder is the adsorption of the gas on the powder surface. This adsorption may increase the interparticle forces. The effect of this adsorption for the field of fluidization was reported on by Piepers e.a. [1]. From these results it can be concluded that also in other powder processes this influence may be of importance.

1.2 OTHER RESEARCH

Most attention so far has been paid to the effect of interstitial gas in the field of solids flow from bunkers. Both the effects of gas flows induced by the flowing particles (3,4,5) and the effects of a deliberate aeration of the powder mass in the bunker (4,5,6,7,8,9) have been investigated. Also the effects during the filling of bunkers are sometimes mentioned (4).

Further attention has been paid to the effect of aeration on more fundamental flow properties. Ishida e.a. (10) investigated the flow of powders in an aerated inclined channel. Judd and Dixon (11) studied the dynamic angle of repose of a powder flowing in a rotating drum, which is aerated through a porous wall. Bridgewater (12) reports on the effects of fluid flow through a powder bed on the stability of the slope of the powder. Van den Langenberg-Schenk and Rietema (13) established parameters of a homogeneously fluidized powder flowing in a vertical standpipe. In all this research gas flow has been deliberately induced like in fluidization. Although such research is of course very important to the development of an understanding of the two phase powder-gas system, it does not give any direct information on the powder flow in apparatus in which no gas flow is created on purpose.

Papers which are intended to develop models for the flow of powders (15,16) do not take the gas influence into account.

1.3 CONTENTS OF THIS THESIS

The part of the research project, which is presented in this thesis, mainly deals with two practical situations in powder handling: the dry milling and mixing of fine powders.

Chapters 2 through 4 all deal with dry milling. Chapter 2 contains the experimental set-up, the way of analysis of the milling experiments and some preliminary results. Chapter 3 gives results on some different types of powders and explores any practical possibilities of using the gas influence in milling processes. Chapter 4 contains a model and ex-

periments to obtain more insight in the important parameters of the milling process.

Chapter 5 presents the most important results of gas influence on dry mixing. From these results some rules of thumb can be derived for real mixing problems.

Chapter 6, finally, contains a theoretical study on the influence of gas adsorption on interparticle forces. It is shown that such is indeed quite possible.

All chapters are either published in Powder Technology or submitted for publication. References in a chapter to other chapters are therefore expressed by referring to the publications in Powder Technology. Generally, it will however be directly clear which chapters are meant.

1.4 LITERATURE

1 H. Piepers, W. Cottaar, A. Verkooijen and K. Rietema
Powder Technology 37(1984)55

2 K. Rietema, J. Boonstra, G. Schenk and A. Verkooijen
Proc.Eur.Symp. Particle Technology
Amsterdam (1980)981

3 J. Johanson and A. Jenike Proc. Powtech (1971)207

4 W. Bruff and A. Jenike Powder Technology 1(1967)252

5 I. McDougall Brit.Chem.Eng. 14(1969)1079

6 H. Kurz adn H. Rumpf Powder Technology 11(1976)147

7 R. Neddermann, U. Tüzün and S. Savage
Chem.Eng.Sci. 37(1982)1597

8 R. Neddermann, U. Tüzün and R. Thorpe
Powder Technology 35(1983)69

9 L. Bates Fachb. Rohstoff-Eng. 105(1981)484

10 M. Ishida, H. Hatano and T. Shirai
Powder Technology 27(1980)7

11 M. Judd and P. Dixon Trans.I.Chem.Eng. 57(1979)67

12 J. Bridgewater Powder Technology 11(1975)199

13 G. v.d. Langenberg-Schenk and K. Rietema
Powder Technology 38(1984)23

14 U. Tüzün and R. Neddermann Powder Technology 24(1979)257
15 J. Johanson Powder Technology 5(1971)93

2 THE EFFECT OF INTERSTITIAL GAS ON MILLING

Published in Powder Technology 38(1984)183-194
Coauthor: K. Rietema.

2.0 ABSTRACT

In a research program on the influence of interstitial gas on the handling of fine powders, particle diameter less than 100 μm, the effect on milling is also investigated.

The influence of the interstitial gas is exhibited through the drag force, due to velocity differences, which the gas exerts on the solid particles of the powder. These forces strongly influence the behavior of the powder.

Our investigations of milling showed that the milling parameters, i.e. the specific rates of breakage and the breakage parameter, were dependent on the powder flow behavior. Two extremes were the regime of free flowing powder, where the rate of breakage was high and the grinding of the individual particles was rather ineffective, and the regime in which the powder did not flow at all, where the rate of breakage was low, but where the grinding of the single particles was rather fine.

2.1 INTRODUCTION

This paper reports on the influence of interstitial gas on the milling parameters, when milling fine powders (d_p = 10 to 100 μm) in a ball mill. The research is a part of our present research on the influence of gas on powder handling.

The influence of interstitial gas is exhibited by the forces which arise from a velocity difference between the dispersed solid and the continuous gas phase of the powder. When there is a velocity difference U_s, the so called slip velocity, between solid particles with a typical particle size d_p and a gas with viscosity μ, the interaction force F_i is given by Carman (1). To a first approximation it follows

$$F_i = \frac{150\ \mu}{d_p^2}\ h(\varepsilon)\ U_s \qquad (2.1)$$

Where $h(\varepsilon)$ is a function of the porosity ε, which is of the order of unity, when ε is of the order of 0.5. This relation is well known in the field of fluidization.

In many powder-handling operations like milling and mixing, the powder is continuously reshuffled, while at the same time gas is entrapped in the pores between the solid particles. In this way, pressure differences are created, which create a gas flow, which in turn will exhibit a force on the solid particles as given by equation (2.1). In the stationary case, the velocity of the gas flow will be of the order of a typical speed of the apparatus, U_a. The force of the outflowing gas, generally in the upward direction, can, however, never exceed the weight of the solid particles. Hence, we can write

$$(1-\varepsilon)\ \rho_d\ g \geq \frac{150\ \mu}{d_p^2}\ h(\varepsilon)\ U_a \qquad (2.2)$$

As long as the bulk weight of the particles is higher than the drag force of the gas the value of the porosity ε will equal the lowest possible value ε_0. As U_a increases, a point will be reached, where both sides in equation (2.2) are equal, while ε is still ε_0.

When U_a increases still further, ε must change for the formula still to hold. Hence, a stage is reached where the porosity of the powder is changed (increased). This change will have a marked influence on the powder flow behavior.

From equation (2.2) we can derive a criterion for gas influence. Using $h(\varepsilon) = ((1-\varepsilon)/\varepsilon)^2$ and $\varepsilon_0 = 0.4$, it follows there will be a gas influence if

$$\frac{\rho_d\ g\ d_p^2}{\mu\ U_a} < 500 \qquad (2.3)$$

From equation (2.3) we can see that for smaller or less heavy particles there will be more influence, as the left side of equation (2.3) is smaller. The same goes for more viscous gases or a higher apparatus speed.

Using some typical values of our experiments: $\rho_d = 1000$, $g = 10$, $d_p = 10^{-4}$, $\mu = 10^{-5}$, $U_a = 0.1$, all in SI-units, we get a value of 100 for the left side.

So far, we have assumed the value of gas viscosity to be a property of the gas itself, independent of other parameters. This concept is, however, only true, when the free path of the gas molecules is much smaller than any other specific length of the system considered. In general, this path is in the order of 0.1 μm at 1 bar and inversely proportional to the pressure. So at 0.01 bar, the free path is 10 μm and is therefore in the order of the particle diameter. The force exhibited by the flowing gas will then decrease as the interaction between gas molecules and so their momentum exchange becomes less important. The apparent viscosity will therefore also decrease. In the rest of this paper, the conceptions of smaller and larger viscosity or pressure will therefore be highly equivalent (see also the appendix 2.A).

To examine the influence on the milling process, we performed milling experiments with one specific powder using several gases and pressures. From these we derived specific milling parameters, i.e. the specific rate of breakage and the breakage parameter. The range of gases and pressures was wide enough to change the powder from a very airy free flowing powder to a completely stiff mass, which showed no flow at all. All other parameters have been kept constant as their effect has been reported extensively elsewhere, e.g. ball size [2,3], fines content [4], moisture [5,6], additives [7], ball and powder loading [8,9].

2.2 DESCRIPTION OF THE MILLING PROCESS

To describe the milling process, we used a method which is quite common in the literature [3,4,5,10,11,12]. The model is based on mass-balance equations and, although it is not a priori evident that all the assumptions made are valid, the model has proved to be quite useful and, as will be shown, does also agree satisfactorily with our experiments. Some other, but closely related methods have also been used [13].

To describe the process, we split the weight size distribution of the solid into n intervals with a constant lower to upper size ratio. The first interval contains the largest particles. The nth interval contains all the particles below the upper size of the nth interval. We assume the decrease of the weight fraction of an interval due to milling of that fraction to be first order, i.e. proportional to the weight fraction. So we can write

$$\frac{dw_i}{dt} \sim -S_i w_i \tag{2.4}$$

Where w_i is the weight fraction and S_i the specific rate of breakage, both for the ith interval.

Furthermore we assume particles do only get smaller and so do not agglomerate. The portion of the milled fraction of the jth interval which falls into the ith interval is denoted by b_{ij}. So we can write

$$\frac{dw_i}{dt} = -S_i w_i + \sum_{j=1}^{i-1} b_{ij} S_j w_j \tag{2.5}$$

where

$$S_n = 0 \tag{2.6}$$

because particles which fall into the nth interval remain inside this interval even when milled. And

$$\sum_{i=j+1}^{n} b_{ij} = 1 \tag{2.7}$$

because all milling products of size j have to fall into some higher interval i. More extensive discussions of this method and its assumptions can be found in the literature (12,14).

The solution of these equations, which can be solved analytically, is very easy if a digital computer is used. In fact, these equations form an eigenvalue problem, with eigenvalues S_i. The general solution can be written as

$$w_i(t) = \sum_{j=1}^{i} c_j a_{ij} \exp(-S_j t) \tag{2.8}$$

where a_{ij} (i=1,n) is the eigenvector belonging to eigenvalue S_j. a_{ij} is completely determined by all the parameters S_i and b_{ij}. The constants c_j are determined by the initial values of $w_i(t)$, i.e. $w_i(0)$. For the first interval the equation is

$$w_1(t) = w_1(0) \exp(-S_1 t) \tag{2.9}$$

To reduce the number of parameters we assume the values of b_{ij} to be normalized, which means that

$$b_{ij} = b_{i-1,j-1} \tag{2.10}$$

while the value of b_{nj} will be determined by

$$b_{nj} = 1 - \sum_{i=j+1}^{n-1} b_{ij} \tag{2.11}$$

This means that the relative size of the daughter particles with respect to the parent particle size is independent of the parent particle size. Of course, this is still a further restriction in our model, which has no physical ground.

For later use, we also define the cumulative breakage parameter as

$$B_i = \sum_{j=i}^{n} b_{j1} \tag{2.12}$$

2.3 COMPUTER ANALYSIS

A second step is to derive from our measurements the parameters S_i and b_{ij}. Therefore we measure at certain moments the particle size distribution inside the mill (see also the next section). From this, we derive the weight fractions of the several intervals, which we will denote as $v_i(t)$. These values have, of course, an experimental error, $s_i(t)$, which consists of two parts.

The first error is introduced through sampling, i.e. the sample measured with the Coulter Counter is not exactly representative of the contents of the mill. This error was determined experimentally by taking many samples at one moment during the milling. It was of the order of 0.5% per interval.

The second error is the statistical error of the measurement of the particle size distribution itself. It can easily be calculated because if m is the number of particles counted by the Coulter Counter in an interval, then the statistical error in this number is equal to the square root of m (see also section 2.4.2 on particle size measurement).

Our aim is now to find those values of S_i and b_{ij} which, given $w_i(0)$, give the same sets $w_i(t)$ as the measured sets $v_i(t)$. The deviation between these two values may be of the order of $s_i(t)$. To reach this aim we use a least-squares method, which minimizes Q, where Q is given by

$$Q = \sum_{i,t} \left\{ \frac{v_i(t) - w_i(t)}{s_i(t)} \right\}^2 \qquad (2.13)$$

Such a least-squares method will give the most likely values of the parameters for the given experiment, assuming the experimental errors have a Gaussian distribution. Also, the statistical errors of the parameters are a result of the analysis, a fact which is often ignored in the literature (more on the method used can be found in the appendix 2.B).

Using this method enables us to determine directly all values of S_i and b_{ij}. Using narrow starting size fractions and studying the parameters only for that interval is therefore unnecessary [15]. Care should be taken to ensure that the number of measurements is much larger than the number of parameters (order of ten). This fact is sometimes neglected in the literature, which results in numerous, but insignificant numbers [10].

2.4 MEASUREMENTS

2.4.1 experimental set-up

A schematic drawing of the set-up is given in figure 2.1. The mill was made of steel with an internal diameter of 150 mm and an internal length of 195 mm. In all reported experiments, it was run at a speed of 80 rpm, which is 73% of the critical speed.

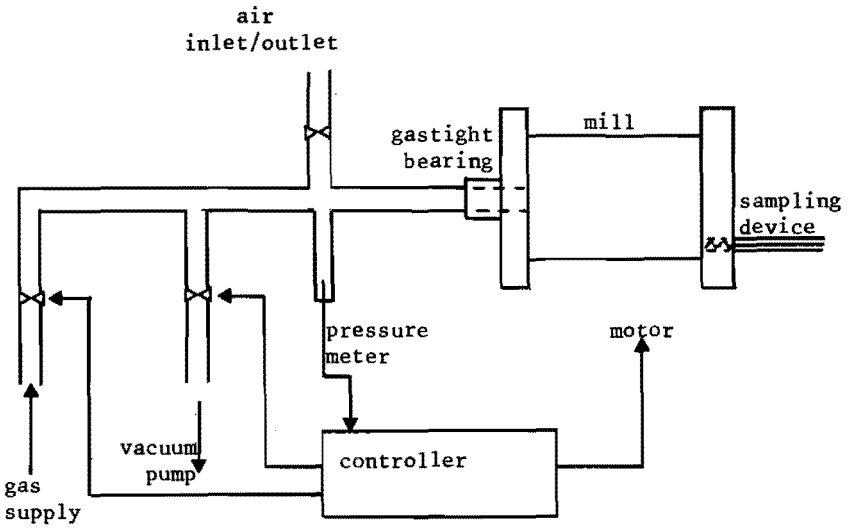

Figure 2.1. Schematics of the experimental set-up.

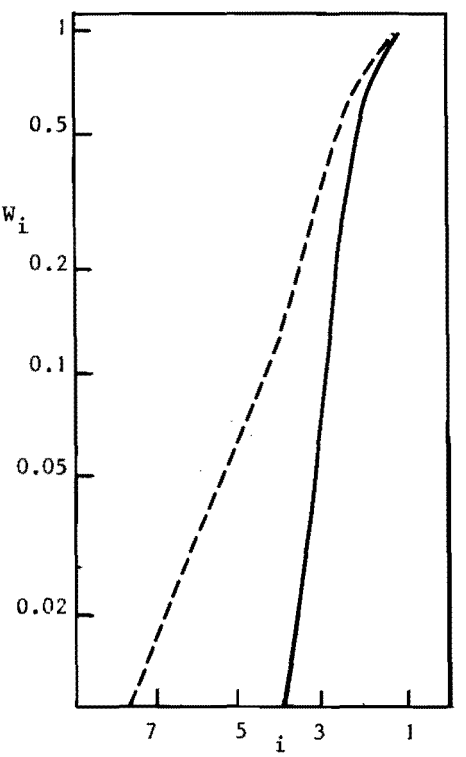

Figure 2.2. The initial distribution; ——, *coarse distribution;* – – –, *fine distribution.*

The ball filling consisted of 240 steel balls with a diameter of 16 mm. The total ball volume was therefore equal to 15% of the mill volume. The bulk volume of the balls was about 30% of the mill volume. The bulk volume of the powder was equal to 15% of the total mill volume. The powder used was a quartz sand consisting of 99% SiO_2. Two initial particle size distributions were used, a coarse one and a fine one. The fine one was obtained by milling the coarse one in air for one hour in the same mill as described above (see figure 2.2).

During each experiment, around 30 samples were taken from the mill at certain moments, depending on the milling speed. The samples with a weight of the order 0.5 g were taken with a special sampling device (figure 2.3), consisting of a cork screw closely fitting inside a hollow tube. This was inserted in the mill through a ball valve and, by turning the cork screw via an axis connected to it some powder was pulled into the tube. The whole assembly was air-tight so no leakage of gas was possible. However, each time some contamination entered the mill due to the air volume of the hollow tube. Although this volume equals only 0.05% of the mill volume at low pressures it could still heavily contaminate the contents, because the tube was filled with air at 1 bar. Therefore, the contents of the mill were renewed after each sample.

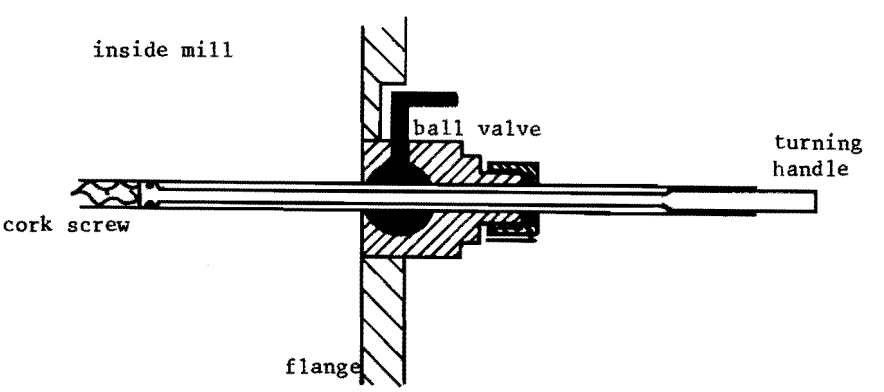

Figure 2.3. The sampling device.

gas	density (kg/m^3)	viscosity (kg/ms)	free path (μm) (1 bar)
dry air	1.290	$1.88 \cdot 10^{-5}$	0.05
hydrogen	0.089	$0.88 \cdot 10^{-5}$	0.09
neon	0.890	$3.10 \cdot 10^{-5}$	0.11

Table 2.1. Data on used gases.

By means of an air-tight bearing, the mill - which was of course also air-tight - was connected to the gas-supply system. This system could handle pressures in the range of 0.001 to 10 bar. The system was controlled by a device, which has the following functions:

(1) After a sample has been taken the mill is evacuated.
(2) Gas is supplied to the mill until a preset pressure is reached. At low pressures an excess of gas is supplied, whereafter part of it is pumped away.
(3) The mill is run for a preset time.

Steps (1) and (2) can be repeated several times, up to ten, if the gas contents of the mill are severely contaminated.

Three gases, dry air, hydrogen and neon, were used during the experiments. These were chosen because of the large range of viscosity, which is covered by these gases. Data can be found in table 2.1.

2.4.2 particle size measurement

To measure the size distribution, a Coulter Counter connected to a channel-analyzer was used. The schematics of the set-up is given in figure 2.4. The main advantage of this method over more conventional ones like sieving or sedimentation is the measuring speed. The measurement of one sample took in the order of five minutes, while a diameter ratio of twenty-five was reached. Another advantage is the small amount of powder needed for analysis, which can be neglected compared to the total powder contents of the mill.

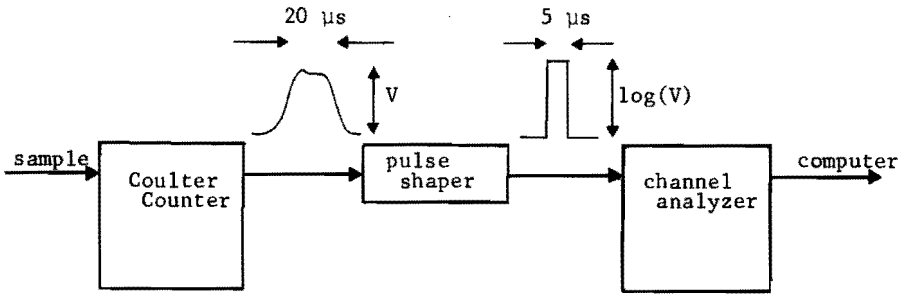

Figure 2.4. Schematics of the particle size measurement.

A disadvantage is that the Coulter Counter is in essence a particle counting technique, while for the further analysis, volume fractions, i.e. weight fractions, are needed. Therefore, a conversion has to be made. Of course, this conversion can be done very accurately through calibration. However, especially with a wide size distribution, which is often the case in milling, a few large particles can count for a volume as large as thousands of small particles. Because, as mentioned above, the statistical error is equal to the square root of the number of counted particles, the relative error in the number of counted particles as well as in the calculated volume is inversely proportional to the square root of the number of counted particles. For the intervals with the larger particles, this relative error can become very large, even of the order of one.

The small volume of the samples, given as an advantage, can also be a disadvantage when the mill is not fully mixed. In that case, the sample would not be representative for the contents of the mill. As mentioned above this error was measured experimentally.

The electrolyte used consisted of 50% water and 50% glycerol in which 10 g NaCl per liter was soluted. The powder was dispersed using a stirrer. To test the effectiveness of this procedure some samples were also dispersed using an ultrasonic bath. Even after 30 minutes, no effect could be detected on the measured particle size distribution.

The pulses of the Coulter Counter, the height of which is proportional to the volume of the measured particles, pass through a pulse-shaper, which adapts the pulses for the channel-analyzer. Its output pulses have a height proportional to the logarithm of the input pulses and are therefore proportional to the logarithm of the volume, i.e. to the diameter of the particles.

Finally the height of these pulses is analyzed by the channel-analyzer and one particle added to the specific channel, in which bounds the height of the pulse falls. Thus, a particle size distribution of the number of particles versus the logarithm of particle diameter is obtained.

The measured size distributions were punched on tape and fed into a MINC-11 mini-computer, which first calculated the correction for coincidence in the measuring volume of the Coulter Counter and the dead time of the channel-analyzer. Using calibration data, the number of particle distribution was then converted to a volume distribution. Also the statistical error could be calculated. Thus a distribution was obtained of about 50 intervals per sample with an upper to lower size ratio of 1.08.

2.4.3 analysis

As explained in the previous section, a size distribution is obtained with about 50 intervals. As this would lead to enormous numbers of variables and equations in the least-squares procedure, for our analysis each time several volume fractions (usually six) as well as their errors were taken together to form a new interval. The volume fractions were just added, while the errors were added quadratically.

These intervals, however, contain only particles above a certain minimum size. The nth interval should contain all particles below its upper size level. To correct for the volume of the not counted particles, we assume that if we would measure any particles in intervals above the nth, the volume ratio of these intervals would be constant, i.e.

$$\frac{v_i}{v_{i-1}} = C \qquad i > n \tag{2.14}$$

where C is a constant smaller than one. So now the contents of all intervals above n, including the nth interval, is given by

$$\sum_{i=0}^{\infty} v_n C^i \tag{2.15}$$

The constant C is calculated using the intervals n-3 to n, assuming equation (2.14) also holds for these intervals. The correction was generally in the order of a few percent on the total distribution. From all measured volumes v_i at different moments t, using the least-squares method, the values of S_i and b_{il} can be obtained.

Figures 2.5 and 2.6 give the results of two of these fits. Shown is the cumulative weight fraction W_i defined by

$$W_i = \sum_{j=n}^{i} w_j \tag{2.16}$$

as a function of time. The drawn curves are the results of a computer simulation using the values of S_i and b_{il} given by the least-squares fit. As can be seen in figure 2.6, not all the measurements are neatly described by the used model. This was more evident in the experiments with more viscous gases. A computer fit using non-normalized values of b_{ij} yielded better results (broken line in figure 2.6). However, the significance of the results for S_i and b_{ij} decreased due to the larger number of parameters to be fitted. Hence, normalized values were always used. This is also quite common in the literature, although some work has been done on non-normalized values (16).

To investigate the influence of the number and size of the intervals, several measurements were analyzed using other numbers and sizes. Some results are shown in figures 2.7 and 2.8. Here S and B are not shown as functions of interval number, but as functions of particle size x, as the intervals of the different analyses do not coincide. With S, the value of x corresponds to the mean particle size of a given interval; with B, it corresponds to the uppermost size of an interval, which is in accordance with the definition of B.

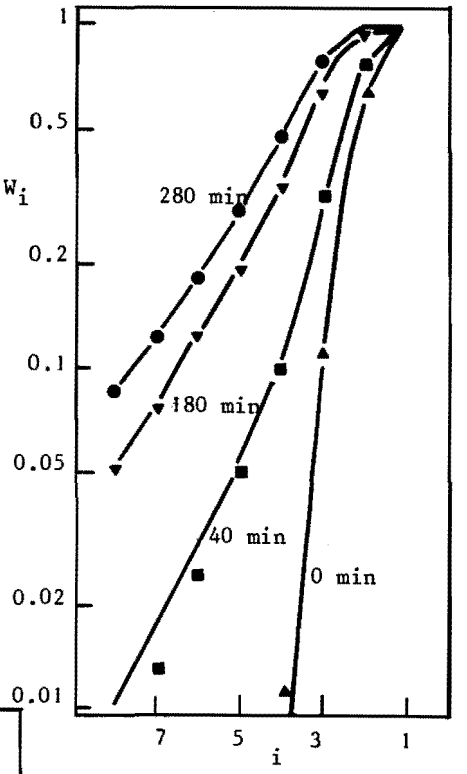

Figure 2.5. The cumulative weight fraction as a function of the interval number at several moments, when milling in air at 0.01 bar, using the coarse starting distribution. The drawn lines are the result of a computer fit using normalized b_{ij}.

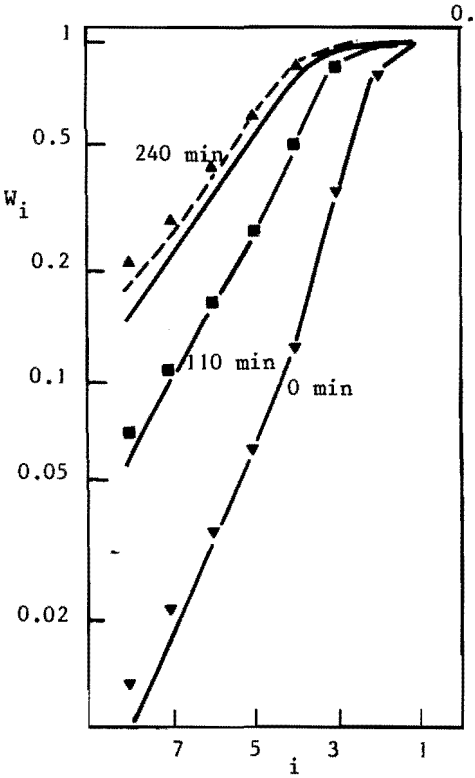

Figure 2.6. The cumulative weight fraction as a function of the interval number at several moments, when milling in air at 7 bar, using the fine starting distribution. The drawn lines are the result of a computer fit using normalized b_{ij}; the broken line is the result of a fit using non-normalized b_{ij}.

From figures 2.7 and 2.8 we can see there is good agreement between the different analyses. Deviations are in the order of the experimental error for all sizes. In order to keep the number of parameters low, we will use the analysis with eight intervals and an upper to lower size ratio of 1.56 for our further results.

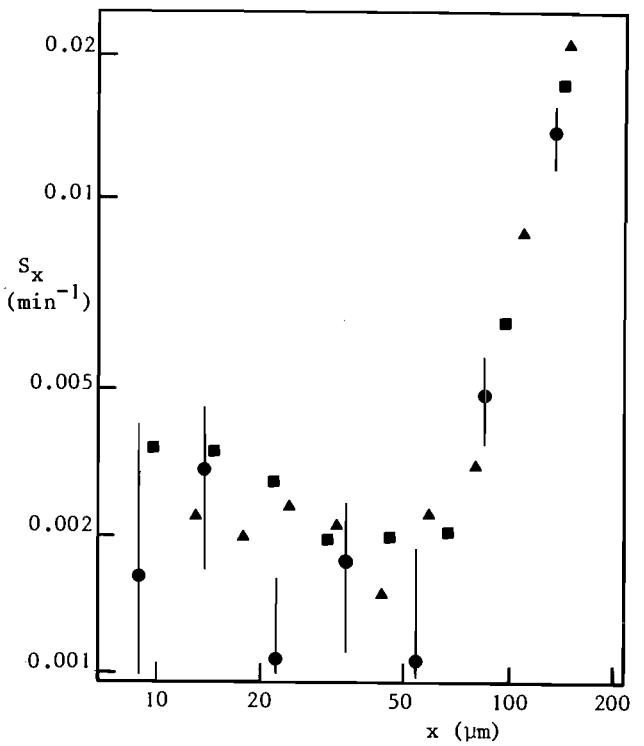

Figure 2.7. The specific rates of breakage as a function of the particle diameter using different numbers of intervals and interval sizes:

●, *8 intervals, size ratio 1.56;*

■, *10 intervals, size ratio 1.46;*

▲, *10 intervals, size ratio 1.36.*

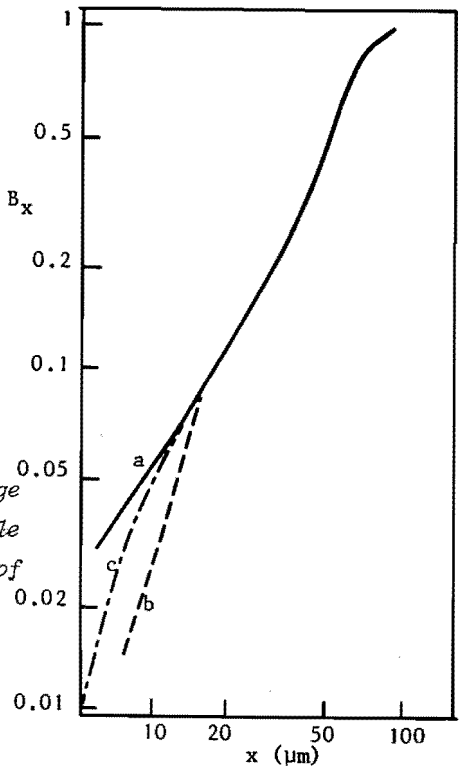

Figure 2.8. The cumulative breakage parameter as a function of particle diameter using different numbers of intervals and interval sizes: a, 8 intervals, size ratio 1.56; b, 10 intervals, size ratio 1.46; c, 10 intervals, size ratio 1.36.

As can also be seen from figure 2.7 for the higher intervals, smaller particles, the experimental error is of the same order of magnitude as the value of the parameter. These errors can be understood, as the total milling time of one single experiment was of the order of $10/S_1$. Hence, the lowest possible value of S_i to be determined will be of the order of $S_1/10$. No conclusions can therefore be drawn for the higher intervals and we will present only results for the four lowest intervals, largest particles.

No attempt has been made to fit the values of S_i and b_{il} to any functional forms, as there is no common understanding of these functions and their physical meaning [12,16,17].

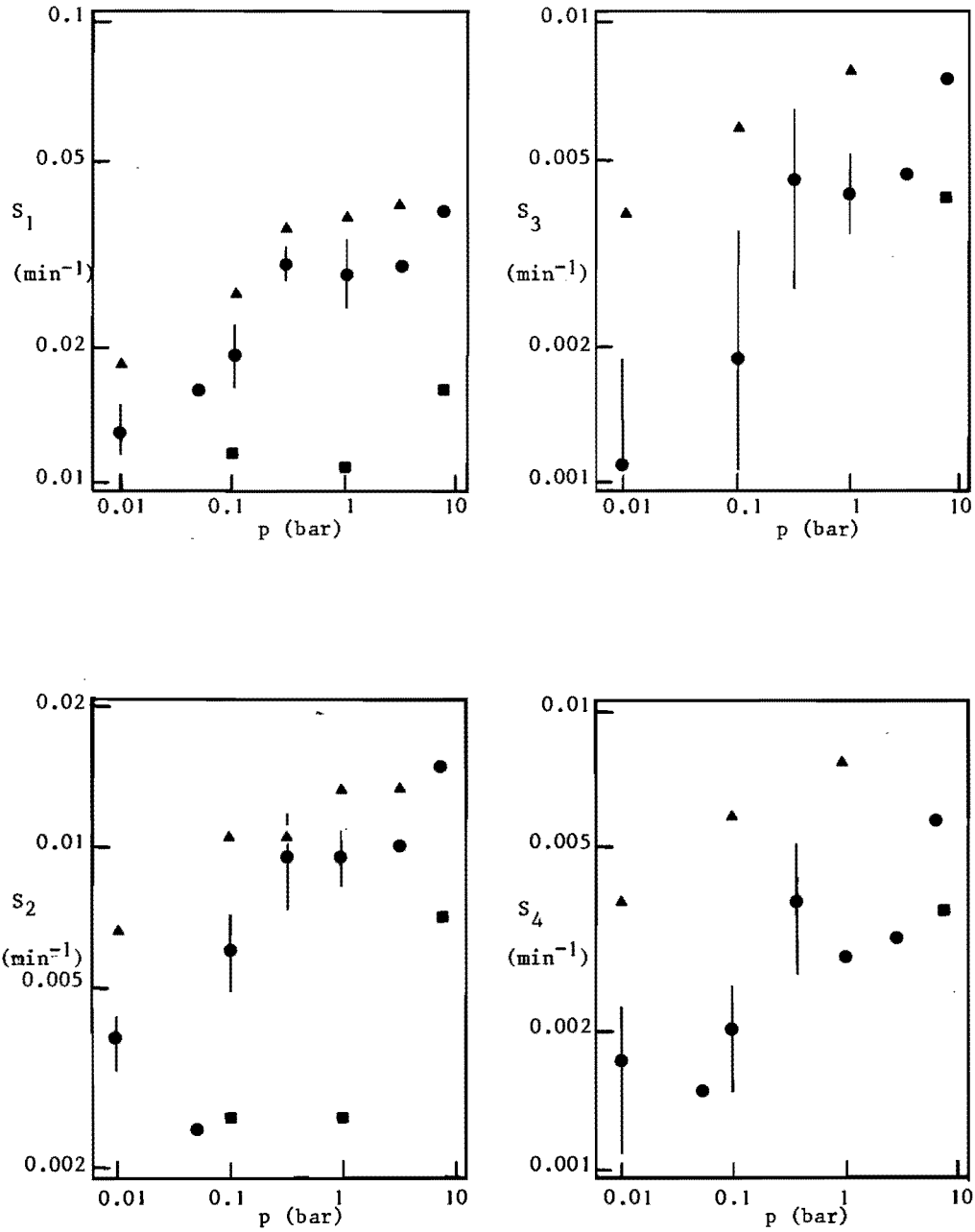

Figure 2.9. The values of the specific rates of breakage as a function of pressure for three gases: ●, air; ■, hydrogen; ▲, neon.

2.5 RESULTS

Figures 2.9 and 2.10 give the results of the experiments for the specific rates of breakage and the breakage parameters. All were obtained using the fine starting distribution.

For the specific rate of breakage, we see a general increase in the rate when the pressure or the viscosity of the gas is increased. For air, we see a rather flat region in the range between 0.3 and 3 bar. For hydrogen the rate is constant below 0.1 bar, while for neon, a flat region seems to exist above 1 bar, although no measurements were performed above 3 bar. For neon, at 3 bar only the values of S_1 and S_2 were determined due to the short milling time in this particular experiment.

Of the breakage parameter, only the values of b_{21} and b_{31} are given. The other values were always small, less than 0.1, and showed very high scatter between the individual experiments. As can be seen at high pressures or viscosities, the value of b_{21} is high, about 0.8, i.e. when a particle is milled, most of the product falls into the interval directly below the original one. When pressure or viscosity is decreased, the process gets finer: the value of b_{21} decreases and the value of b_{31}, and also of b_{41}, increases.

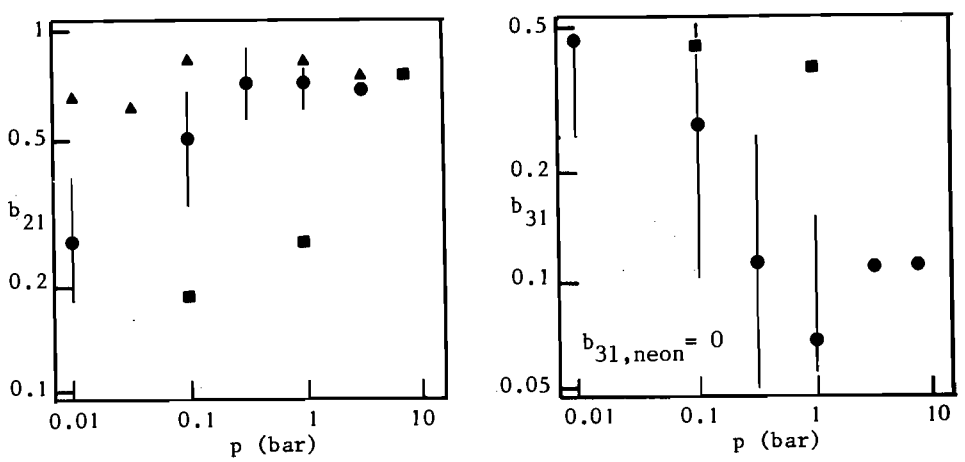

Figure 2.10. The value of the breakage parameter as a function of pressure for three gases: ●, air; ■, hydrogen; ▲, neon.

The error bars in figures 2.9 and 2.10 are an illustration of the accuracy. The errors of the points, where no bars are shown, are of the same order of magnitude.

Some experiments were also performed using the coarser powder at the start. A result is shown in figure 2.11, where the weight fraction of the first interval is shown as a function of time. At a certain moment there is a change in the specific rate of breakage. After this time, the milling could be described by the parameters as given in the figures 2.9 and 2.10. Before this time, the rate of breakage was in the order 0.01 min^{-1} and was independent of viscosity or pressure. The change only occured for air and neon at pressures above 0.1 bar. For the other cases, the results using the coarse and the fine starting distribution were the same.

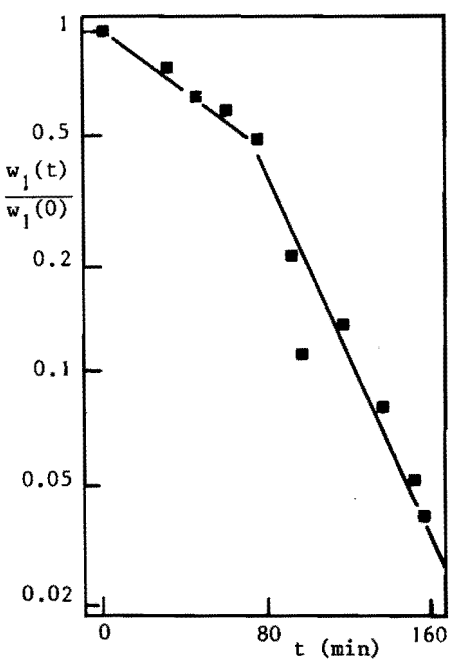

Figure 2.11. The weight fraction of the first interval when milling in air at 7 bar, milling the coarse powder.

2.6 DISCUSSION

It is believed that the results should be correlated to the flow behavior of the powder in the mill. Using a highly viscous gas or a high pressure, the powder flows very easily, like a liquid, while the bulk volume is high. When decreasing the viscosity, the flow properties of the powder decrease. At very low pressure, the powder does not flow at all. It sticks to the wall of the mill, is carried up and falls down together with the balls from the point, where equilibrium is reached between the gravitational and centrifugal forces. These effects are shown in figure 2.12, where the dynamic angle of repose is given for several gases and pressures. This angle is defined as shown in figure 2.13. The measurements were performed in the same apparatus and at the same speed as the milling experiments.

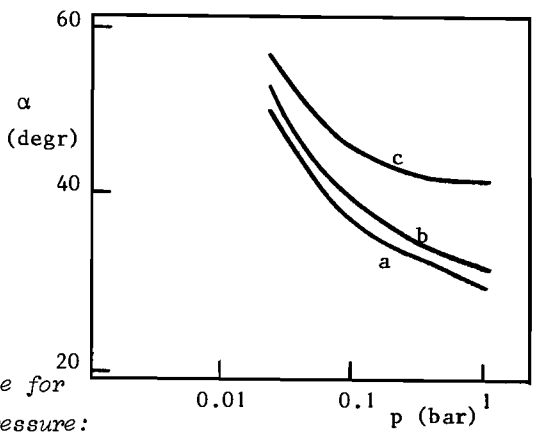

Figure 2.12. The angle of repose for three gases as a function of pressure: a, neon; b, air; c, hydrogen. d_p *= 50 μm.*

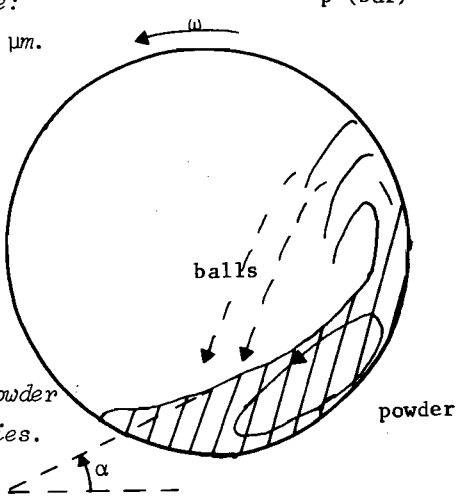

Figure 2.13. The flow of balls and powder inside the mill at high gas viscosities.

A second indication is the sound of the mill: at high viscosity, a soft scraping noise can be heard together with the sound of light collisions. At low viscosity, the balls are really banging. So far it has not been distinguished if this sound comes from collisions with the wall, between balls, or both.

From these observations, it seems plausible that frequency and violence of ball collisions with each other and with the wall of the mill are strongly influenced by the flow behavior of the powder and further, that the effectiveness of the milling process should be correlated with this ball behavior.

The results at pressures above 1 bar cannot be explained using the concept of the dependence of viscosity on pressure. Since at 1 bar the free path of the molecules is already much smaller than the particle size, the gas viscosity is constant at pressures above 1 bar. The further change in the milling behavior is ascribed by us to the adsorption of gas on the particles, which influences the interparticle forces, which in their turn influence the flow behavior. In fluidization, this adsorption does have a marked influence on the range of homogeneous fluidization of fine powders.

We are continuing our investigations on both aspects, the ball behavior in relation to the powder flow as well as the effects of gas adsorption on powder flow.

2.7 CONCLUSIONS

The interstitial gas does have a marked influence on the milling parameters. This influence can be easily understood qualitatively when considering the powder flow. The changes in powder flow are a result of the interaction between the two constituents of a powder, the gas and the solid particles, and will be the subject of our future research. From the results, it also follows that during the milling the rate of breakage can change due to the creation of finer particles and a resulting change in powder flow. We measured an increase. Therefore when milling fine powders (d_p < 100 μm), the powder flow should be taken into account.

2.8 LIST OF SYMBOLS

a_{ij}		eigenvector belonging to the eigenvalue S_j in the solution of the mass-balance equations
B		cumulative breakage parameter
b_{ij}		breakage parameter, part of interval j falling into interval i
C		ratio of weight fractions for the highest intervals
c_j		constant in solution of mass-balance equations
d_p	L	particle size
F_i	$ML^{-2}T^{-2}$	interaction force between gas and particles per unit volume
g	LT^{-2}	gravitational acceleration
i		interval number
j		interval number
m		number of particles counted in an interval
n		number of intervals
p	$ML^{-1}T^{-2}$	gas pressure
Q		residue of the least-squares method
S	T^{-1}	specific rate of breakage
s_i		error in measured weight fraction of the ith interval
t	T	time
U_a	LT^{-1}	typical speed of apparatus
U_s	LT^{-1}	slip velocity between gas and particles
v_i		measured weight fraction in the ith interval
W_i		cumulative weight fraction
w_i		weight fraction in the ith interval
x	L	particle size
ε		porosity
ε_0		lowest possible porosity
μ	$ML^{-1}T^{-1}$	gas viscosity
ρ_d	ML^{-3}	particle density

2.9 LITERATURE

1	P.C. Carman	Trans.Inst.Chem.Eng. 15(1937)15
2	L.G. Austin, K. Shoji and P.T. Luckie	Powder Technology 14(1976)71
3	V.K. Gupta and P.C. Kapar	Powder Technology 10(1974)217
4	L.G. Austin and P. Bagga	Powder Technology 28(1981)83
5	M.A. Berube, Y. Berube and R. Le Houillier	Powder Technology 23(1979)169
6	C. Bernhardt, H.J. Schulze and M. Ortelt	Powder Technology 25(1980)15
7	H. v. Seebach	Zement, Kalk und Gips 5(1969)2
8	K. Shoji, S. Lohrast and L.G. Austin	Powder Technology 25(1980)109
9	K. Shoji, L.G. Austin and F. Smaila	Powder Technology 31(1982)121
10	A. Auer	Powder Technology 28(1981)65
11	L.G. Austin and P.T. Luckie	Powder Technology 5(1971)215
12	L.G. Austin	Powder Technology 5(1971)1
13	G.W. Cutting	Powder Technology 15(1976)21
14	K.J. Reid	Chem.Eng.Sci. 20(1965)953
15	L.G. Austin and V.K. Bhatia	Powder Technology 5(1971)261
16	L.G. Austin and P.T. Luckie	Powder Technology 5(1971)267
17	V.K. Gupta, D. Hodouin, M.A. Berube and M.D. Everell	Powder Technology 28(1981)97

APPENDICES

2.A VISCOSITY AT LOW PRESSURES

We will compare the force F exhibited by a flowing gas, speed U, on a tube with radius R and length L, where $L \gg R$. We will consider two extreme cases : first, the case of viscous flow, where the free path λ of the molecules is much smaller than R, and secondly, the case of free molecular flow, where $\lambda > R$.

The first case is quite commonly known and the result is

$$F/L = 8 \pi \mu_l U \qquad (2.A.1)$$

Where μ_1 is the viscosity of the gas at high pressures. This viscosity can generally be written as

$$\mu_1 = \rho \lambda v_t/2 \qquad (2.A.2)$$

Where ρ is the density of the gas and v_t the thermal velocity. The numerical constant is just an order of magnitude. The derivation of this formula can be found in any text book on gas kinetics. Since $\rho\lambda$ is independent of pressure, it follows the viscosity μ_1 is independent of pressure.

Let us now consider the case of free molecular flow. Again the gas density is ρ, the flow velocity U and the mass of one molecule is M. The number of molecules entering the tube per unit time now equals

$$(\rho/M)\ U\ \pi\ R^2 \qquad (2.A.3)$$

When we follow the path of a single molecule entering the tube it will hit the wall after a distance in the order of R. At such a collision, it looses its momentum in the direction of flow and will be scattered in a random direction. Assuming there is a thermal equilibrium between the wall and the gas the momentum exchange due to the thermal velocity averaged over many molecules will be zero. The effective momentum exchange will therefore be MU. Now it will keep on colliding with the wall and move in all kinds of directions, until it collides with another molecule and takes up the transport velocity U again. Between this collision and the first one with the wall, the net transport and momentum change will again be zero.

Now it moves again over a distance R, collides with the wall and again looses its momentum in the transport direction. This goes on until it leaves the tube. The total number of effective collisions will then be L/R, while the net momentum exchange per effective collision is MU. The total force per unit length will now be

$$F/L = \pi\ \rho\ U^2\ R \qquad (2.A.4)$$

We can now introduce an apparent viscosity (μ_2) in analogy with equation (2.A.1)

$$\mu_2 = \rho\ R\ U/8 \qquad (2.A.5)$$

The ratio of the two viscosities is

$$\frac{\mu_1}{\mu_2} = 4 \frac{\lambda}{R} \frac{v_t}{U} \qquad (2.A.6)$$

Hence, it follows that the apparent viscosity decreases at low pressures because λ is larger than R and v_t, order of 500 m/s, is much larger than U, order of 0.01 m/s.

2.B THE LEAST-SQUARES SEARCH PROCEDURE

In this appendix we shall briefly discuss the least-squares procedure we used and its theoretical background. We will not give a complete analysis since this would be too lengthy.

Our assumption is that we have performed N independent measurements which gave values y_i. We also assume that these values have a Gaussian distribution with a standard deviation σ_i. Of course we do not know the real value of each variable we measured, but we can put the likelihood of it to be equal to x as

$$A(x|y_i,\sigma_i) \sim \exp\left(-\frac{1}{2}\left(\frac{x - y_i}{\sigma_i}\right)^2\right) \qquad (2.B.1)$$

We now also have a model $f_i(\underline{p})$ for each variable dependent on M independent parameters p_j, denoted as $\underline{p}$. We can write

$$A(f_i(\underline{p})|y_i,\sigma_i) \sim \exp\left(-\frac{1}{2}\left(\frac{f_i(\underline{p}) - y_i}{\sigma_i}\right)^2\right) \qquad (2.B.2)$$

or

$$A(\underline{f}(\underline{p})|y_i,\sigma_i) \sim \exp\left(-\frac{1}{2}\sum_i\left(\frac{f_i(\underline{p}) - y_i}{\sigma_i}\right)^2\right) \qquad (2.B.3)$$

where $\underline{f}(\underline{p})$ is the vector of the N models $f_i(\underline{p})$. We now want to find the most likely parameters. From equation (2.B.3) it can be seen this is the case if

$$Q = \frac{1}{2}\sum_i\left(\frac{f_i(\underline{p}) - y_i}{\sigma_i}\right)^2 \qquad (2.B.4)$$

is minimal. Suppose this is true for $\underline{p} = \underline{q}$. We now linearize $\underline{f}(\underline{p})$ with respect to $\underline{p}$ at $\underline{q}$. So

$$f_i(\underline{p}) = f_i(\underline{q}) + \sum_j \frac{\delta f_i}{\delta p_j}\bigg|_{\underline{p}=\underline{q}} (p_j - q_j) \qquad (2.B.5)$$

Putting this into equation (2.B.4) it follows Q is in its extremum if

$$\sum_i \frac{f_i(\underline{q}) - y_i}{\sigma_i} \frac{\delta f_i}{\delta p_j}\bigg|_{\underline{p}=\underline{q}} = 0 \quad (j = 1,M) \qquad (2.B.6)$$

So the solution of the least-squares problem is the solution of equation (2.B.6). Generally, equation (2.B.6) cannot be solved directly, but an iteration is necessary. Suppose our momentarily best set of parameters is $\underline{r}$. We can then write

$$f_i(\underline{q}) = f_i(\underline{r}) + \sum_k \frac{\delta f_i}{\delta p_k}\bigg|_{\underline{p}=\underline{r}} (q_k - r_k) \qquad (2.B.7)$$

and also

$$\frac{\delta f_i}{\delta p_j}\bigg|_{\underline{p}=\underline{q}} = \frac{\delta f_i}{\delta p_j}\bigg|_{\underline{p}=\underline{r}} \qquad (2.B.8)$$

Putting this into equation (2.B.6) we get

$$\sum_i \frac{f_i(\underline{r}) - y_i - \sum_k \frac{\delta f_i}{\delta p_k}\Big|_{\underline{p}=\underline{r}} (q_k - r_k)}{\sigma_i} \frac{\delta f_i}{\delta p_j}\bigg|_{\underline{p}=\underline{r}} = 0 \quad (j=1,M) \qquad (2.B.9)$$

which is a set of linear equations in $q_k - r_k$ and therefore in q_k. The parameters found are used as the best fit for a new iteration until the change in the parameters is below a certain value, e.g. their error, or until Q does not decrease any more.

When $\underline{q}$ is found we can write equation (2.B.4) using equations (2.B.5) and (2.B.6) as

$$Q = \frac{1}{2} \sum_i \left(\frac{f_i(\underline{q}) - y_i}{\sigma_i}\right)^2 + (\underline{p} - \underline{q})^T A^T A (\underline{p} - \underline{q}) \qquad (2.B.10)$$

where A is a M×N matrix given by

$$A_{ij} = \frac{1}{\sigma_i} \frac{\delta f_i}{\delta p_j}\bigg|_{\underline{p}=\underline{q}} \qquad (2.B.11)$$

Of course, the parameter set $\underline{q}$ is not exactly true, but given our experiments, it is the most likely one. Therefore we also need the errors in the parameters, i.e. their variance, defined by

$$V(p_j,p_k) = E((p_j - q_j)\ (p_k - q_k)) \tag{2.B.12}$$

E(x) is the expected value of x geven y_i and σ_i. The likelihood of $\underline{p}$ given $\underline{q}$, y_i and σ_i using equations (2.B.3) and (2.B.10) is

$$\Lambda(\underline{p}|\underline{q},y_i,\sigma_i) \sim \exp[-(\underline{p}-\underline{q})^T A^T A(\underline{p}-\underline{q})] \tag{2.B.13}$$

Using

$$V = (A^T A)^{-1} \tag{2.B.14}$$

where V is a M×M matrix, it can be derived that

$$V(p_j,p_k) = V_{jk} \tag{2.B.15}$$

It can also be derived that

$$E(Q) = N \tag{2.B.16}$$

$$E((\underline{p}-\underline{q})^T A^T A(\underline{p}-\underline{q})) = M \tag{2.B.17}$$

and therefore using equation (2.B.10)

$$E(\frac{1}{2} \sum_i (\frac{f_i(\underline{q}) - y_i}{\sigma_i})^2) = N-M \tag{2.B.18}$$

This summation can also be calculated after the parameters have been found. Equation (2.B.18) gives us then a check on our model, since it is derived using the overall assumption that if we could measure the real values of the variables, so σ_i=0, then also our model would fit to this measurement exactly, so $f_i(\underline{q}) - y_i = 0$.

Some final remarks are:

- The variables need not all be of the same dimension, since the division by the error makes each term in the summation always dimensionless.
- Of course, all the parameters have to be independent. If this is not so, parameters have to be skipped until an independent set is obtained. Otherwise, an infinite number of parameter combinations would give the same solution. In practice, also parameters which are almost dependent have to be skipped, where almost depends on

the accuracy of the computer used. The easiest way to do this skipping in a program is to put the value of a dependent parameter to zero. So in fact another equation is added to the equations in in equation (2.B.9), making the parameters independent again.

- A non-linear least-squares can have more minima. But there is always only one global minimum. If it is thought that the minimum found by the procedure is not the global one, e.g. the summation in equation (2.B.18) is much larger than N-M, other starting values of $\underline{q}$ for the iteration can be tried.

3 THE EFFECT OF INTERSTITIAL GAS ON MILLING, PART 2

Published in Powder Technology
Coauthors: K. Rietema and S. Stemerding.

3.0 ABSTRACT

In a previous paper (1) results were presented on the effect of interstitial gas on the milling characteristics of one specific fine powder in a ball mill. This second paper gives more data on two other powders, cracking catalyst and hematite, together with those on the powder used in the earlier experiments, quartz sand. The effects found are similar for each of the three powders: increasing gas pressure or viscosity of the gas or both inside the mill increases the rate of breakage and decreases the fineness of the daughter particles of a milling event. The overall milling speed or production rate as well as the ultimate fineness of the product improved when increasing pressure or viscosity of the gas.

On the basis of these results a comparison is made with wet milling. It appears that milling at a pressure of around 10 bar is a good alternative for the milling of fine powders.

3.1 INTRODUCTION

In a previous paper (1) we reported on the effect of interstitial gas on the milling characteristics of quartz sand in a laboratory size ball mill. The results of this first paper encouraged us to continue the investigation into the effect of interstitial gas on milling. In this second paper we present results of this investigation on two other powders, i.e. hematite and cracking catalyst. These two powders are quite different in characteristics, except for the size range. They also differ widely from the quartz sand.

In the previous paper an analysis is given which indicates when interaction between powder particles and the surrounding gas can be expected to have noticeable influence. A more accurate analysis is given by Rietema (2), who considers the situation which arises in powder hand-

ling as a result of the continuous reshuffling of the powder, causing gas to be entrapped into the powder. This gas tries to escape from the powder which in this way becomes fluidized. The thus generated interaction between gas and powder becomes important when the typical settling time of the powder is long as compared to the characteristic turnover time of the powder. This leads to the following condition which has to be satisfied

$$N_g = \frac{\rho_d \, g \, d_s^2}{\mu \, U_a} << 100 \qquad (3.1)$$

In other words, if this condition is satisfied gas-powder interaction can be expected to have a bearing on powder behavior. The dimensionless number, N_g, will henceforth be called the gas-powder-interaction number. Putting in some typical values leads to

$$d_p << 100 \ \mu m \qquad (3.2)$$

So interaction will only be important for rather fine powders, where the upper value of 100 μm is of course only a rough estimate, especially since not only the particle size but also the particle size distribution should be taken into account.

The gas-powder interaction leads to a higher porosity: the gas, that is entrapped during the agitation, fluidizes the powder while flowing out and, in this way, the settling of the powder after the agitation is slowed down. The smaller the gas-powder-interaction number, the higher the average porosity will be. The increase in porosity in turn will enhance the flowability. Of course, there is a maximum to this, since at very high porosities part of the gas will escape as bubbles. (Note that the higher the gas influence the lower the gas-powder-interaction number).

Here it should be put forward that in particle mechanics the effective gas viscosity is generally not an independent gas parameter, but depends also on the particle size involved: when the free path of the gas molecules becomes comparable to the pore size the effective gas viscosity drastically decreases and thus the gas-powder interaction diminishes.

Another property of such fine powders is their cohesiveness. Cohesion is of great influence on the nature of fluidization and since this phenomenon is so closely related to the interaction between gas and powder in a mill, cohesion will most likely also influence the gas-powder interaction. Interparticle forces may stabilize the powder structure so that the powder will be fluidized homogeneously and the formation of gas bubbles is prevented. Hence, the time required for escape of the gas is extended to that in the case of a less cohesive powder. Thus the general flowability of a powder after agitation may be improved by increasing its cohesiveness.

Of course, this improvement will not continue forever when the interparticle forces keep increasing, since at very large cohesiveness it will become impossible to expand the powder homogeneously. In that case vertical channels arise in the powder mass through which the gas can easily escape (channeling). However, at not too large cohesiveness, when the powder is continuously reshuffled by stirring or other means, the particle-contacts are frequently broken as well as the gas channels. So the gas cannot escape as easily with the result that yet the powder will expand.

As reported by Piepers (3), at elevated pressures, above 1 bar absolute, the surrounding gas may increase the cohesiveness due to adsorption of gas at the surface of the particles. Thus it must be expected that when gas pressure is increased from absolute zero to pressures above 1 bar the flowability of fine powders is increased: firstly under 1 bar due to the increase of the effective gas viscosity, then, above 1 bar, due to the adsorption of gas at the particle surfaces.

This difference in flowability was visually confirmed indeed during milling experiments at various pressure levels. When looking through a glass flange at one end of the mill, it appeared that at low pressures the powder forms a rather compact layer on the wall of the mill which moves up together with the balls and finally falls down in discrete packages of powder to become part again of the layer on the wall. A very thin layer is even carried around completely, although it is incidentally broken up by falling balls. At elevated pressures the lower part of the mill is filled with a very airy powder mass, which

more or less looks like a liquid. A thin layer moves up with the balls and falls down again on the mass thus aerating the mass.

3.2 CHARACTERIZATION OF POWDERS USED IN THE MILLING EXPERIMENTS

In order to further investigate the effects found in the earlier experiments, new experiments were carried out with two powders of which the milling characteristics differ from those of the quartz sand used previously. Data on these two powders as well as the quartz can be found in table 3.1. Photos 3.1 to 3.3 show the different powders.

The cracking catalyst is a powder, the particles of which consist of aggregates formed by spray drying of a suspension of very small particles, size less than 1 μm. These aggregates, which have a high internal porosity, are rather easy to break. Of course, it is much more difficult to mill the elementary, very small particles. However, the resulting particles of any such process are far below the detection limit of the Coulter Counter, which was used for the particle-size measurement. The initial catalyst powder is slightly cohesive, while during the milling process this cohesiveness of course increases. The original powder shows a typical A-powder-behavior in Geldart's classification on the fluidization behavior of powders (4). Also after a long milling time the resulting powder remains in this category although less prominent.

The hematite on the other hand is a very cohesive powder with group-C-behavior in Geldart's classification. The powder consists of rather large particles to which an abundance of fines is adhered. The detaching of these fines is very difficult to achieve and could only be accomplished by means of ultrasonic equipment. This treatment, therefore, was applied to each sample which was taken to perform a measurement of the particle size distribution. Of course, the effective particle size inside the mill is somewhat larger due to the adherence of the fines. However, the ultrasonic treatment yielded better reproducible results.

The quartz sand of the earlier experiments was initially a free flowing powder showing B-powder-behavior in Geldart's classification. During milling the number of fines increases drastically and after some time the powder shows group-C-behavior.

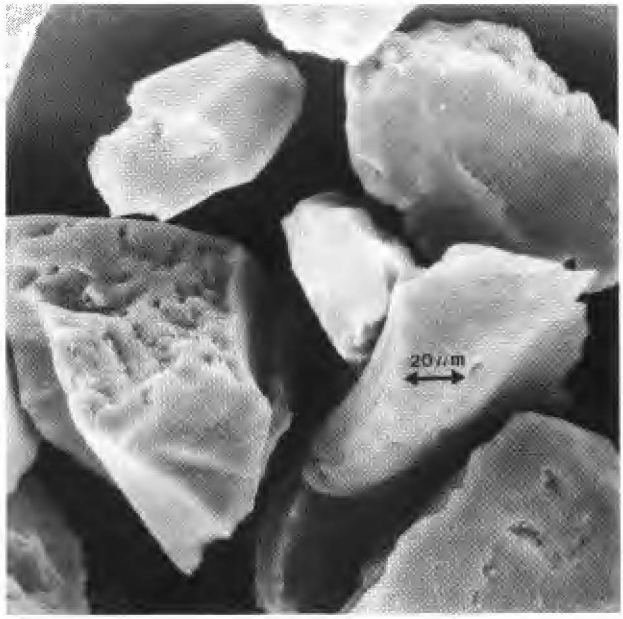

Photo 3.1. The initial quartz sand.

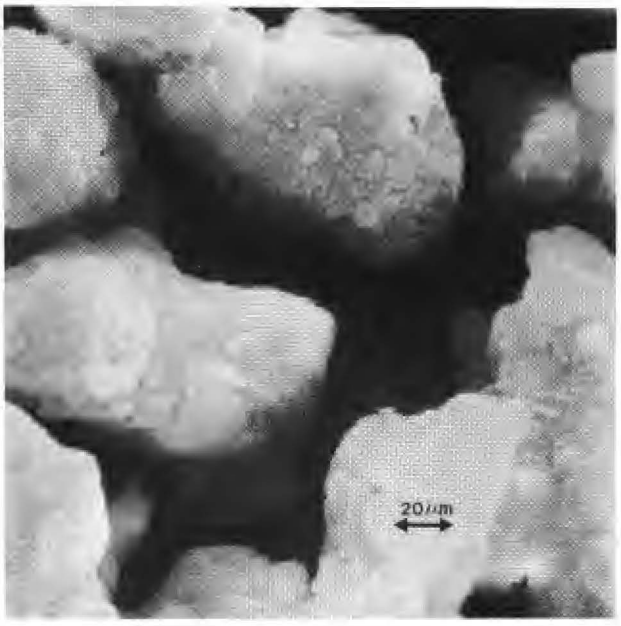

Photo 3.2. The initial cracking catalyst.

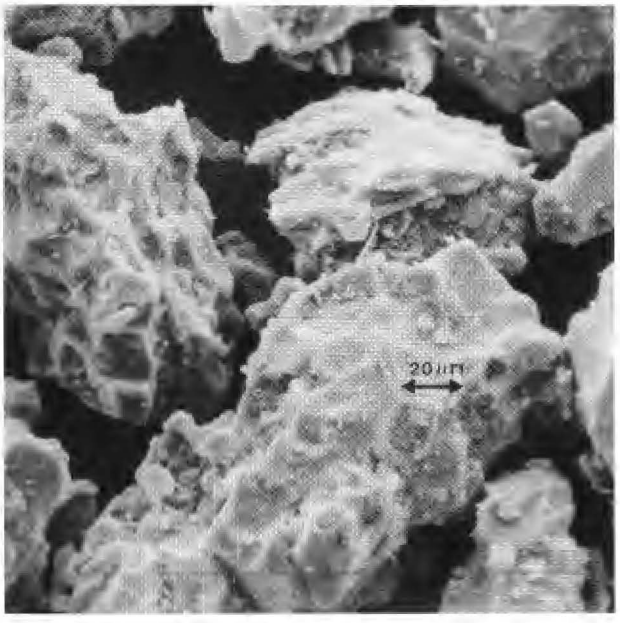

Photo 3.3. The initial hematite.

quartz sand:

ρ_d= 2600 kg/m^3, N_g= 8, main constituent SiO_2

interval	range (μm)	weight %
1	89–140	13
2	56–89	59
3	35–56	19
4	22–35	5
5	14–22	2
6	9–14	1
7	< 9	1

cracking catalyst:

ρ_d= 750 kg/m^3, N_g= 8, main constituent SiO_2-Al_2O_3

interval	range (μm)	weight %
1	66–104	34
2	42–66	48
3	26–42	17
4	17–26	1
5	11–17	0
6	7–11	0
7	< 7	0

hematite:

ρ_d= 4900 kg/m^3, N_g= 11, main constituent Fe_2O_3

interval	range (μm)	weight %
1	56–89	15
2	35–56	50
3	22–35	25
4	14–22	6
5	9–14	2
6	< 9	2

Table 3.1. Data on the powders (the dimensionless number N_g is calculated for air at 1 bar and U_a= 0.1 m/s)

3.3 EXPERIMENTAL RESULTS

As has been discussed extensively in the earlier paper (1) the milling process can be described by two different sets of parameters. First of all the rates of breakage, denoted by S_i. These parameters are defined as the total decrease per unit time of the weight fraction of a specific size interval i per unit weight present in the particular size interval due to the milling of the particles present in that interval only, or

$$S_i = -\frac{1}{w_i}\left(\frac{dw_i}{dt}\right)_{\text{milling interval i}} \tag{3.3}$$

in which w_i is the weight fraction, while interval 1 contains the largest particles.

The second set of parameters concerns the milling fineness. These parameters, generally called the breakage parameters, b_{ij}, are defined as the increment of the weight fraction of interval i that results from the milling of interval j

$$b_{ij} = -\frac{\delta w_i}{\delta w_j} = \frac{1}{S_j w_j}\left(\frac{dw_i}{dt}\right)_{\text{milling interval j}} \tag{3.4}$$

Assuming no agglomeration the milling process can be described completely with these parameters, see e.g. (5). The assumption of no agglomeration is, as will be shown later, not always justified. It leads, however, only to small errors in the parameter values, because, if agglomeration occurs, it becomes important only, when sufficient fines are present, i.e. after a long milling time. Hence, it manifests itself merely at the end of the milling process.

The experimental procedure consisted of taking small samples at regular time intervals from the mill. These samples were analyzed by a Coulter Counter. In each individual experiment about 20 to 30 samples were taken. Using the measured size distributions the two sets of parameters were established by a least-squares fit. Any more details can be found in the first paper (1), where all steps of this procedure are extensively discussed. In this first paper it is also shown that the observed milling process can indeed be described using the two

sets of parameters defined above.

Figure 3.1 shows the values of the rate of breakage for the intervals 1, 2 and 3 of the powders concerned (actual sizes are given in table 3.1) for different pressures of air. The catalyst was milled using ceramic balls; hematite and quartz using steel balls. All other experimental conditions were equal and are shown in table 3.2.

As shown in figure 3.1 all powders follow generally the same trend: the rates of breakage increase with increasing pressure. It can also be seen that for the higher rank intervals, smaller particle sizes, the effect becomes stronger. This is probably due to the fact that the milling of a higher ranking interval is of importance not before relatively long milling times, i.e. when the change of the weight fraction of the particular interval is mostly caused by milling of that interval and hardly any more by any influx of products of lower intervals. This means that the rate of breakage of the higher rank intervals is determined at a moment that the contents of the mill are finer and thus the gas influence is larger.

Figure 3.2 shows the results for the breakage parameters of the two most important size intervals. Again we see a similar behavior for each of the three powders: a general decrease in fineness with increasing pressure, because b_{21} increases, while b_{31} decreases. So more products of the milling of particles originally in interval 1 belong to interval 2, instead of to interval 3, when the pressure is increased.

mill length	195 mm
diameter	150 mm
speed of rotation	80 rpm
balls diameter	16 mm
load	240 pieces
	15 % of mill volume
powder bulk volume	15 % of mill volume

Tabel 3.2. Data on the experimental conditions.

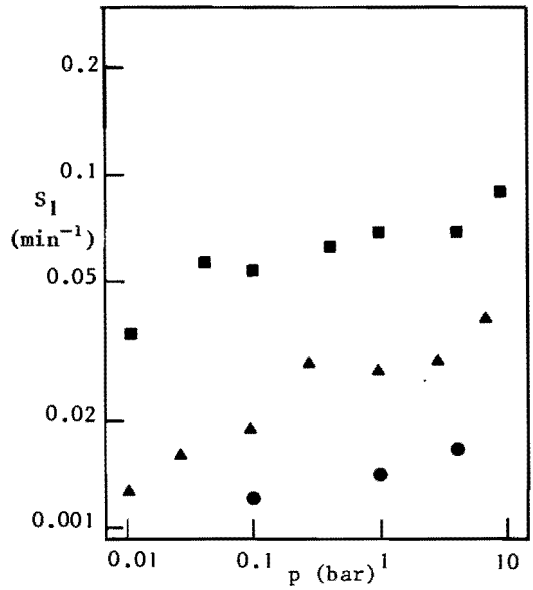

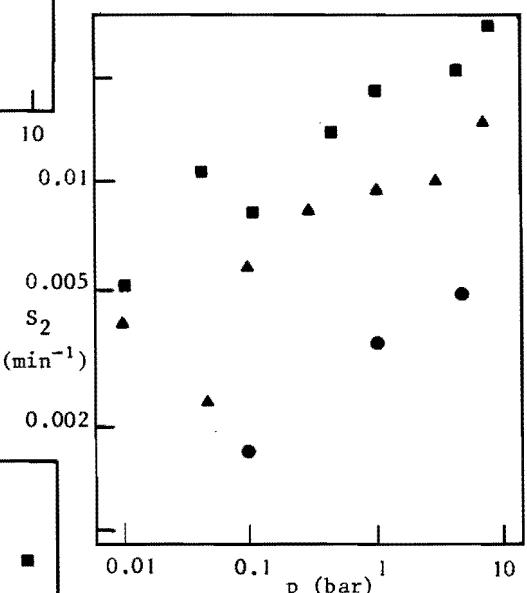

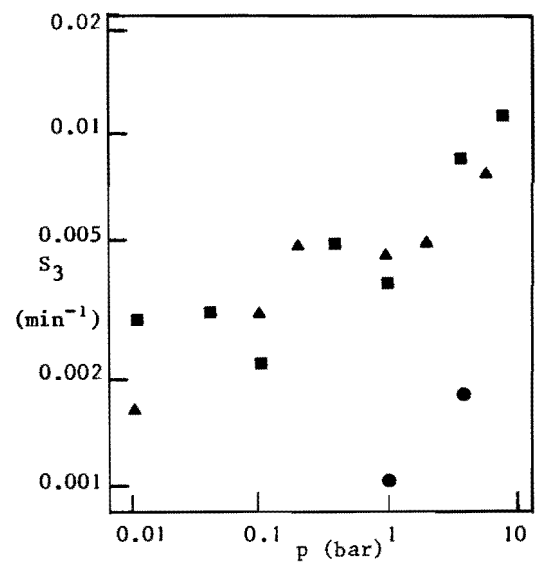

Figure 3.1. Values of the specific rates of breakage as a function of pressure of the interstitial gas for three different powders:
▲, *quartz sand,*
■, *cracking catalyst,*
●, *hematite.*

With catalyst and hematite also some experiments were carried out with neon, as the interstitial gas. Neon has a higher viscosity than air. The same effect as in the previous experiments was found: at increasing gas viscosity the rate of breakage increases, but the fineness of the process decreases. So the effect of higher pressure and that of higher viscosity are similar.

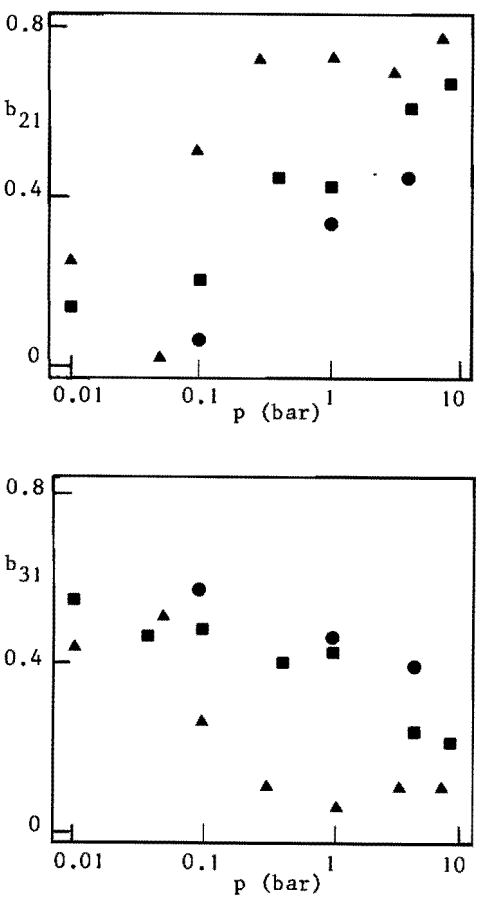

Figure 3.2. Values of the breakage parameters as a function of the pressure of the interstitial gas for three different powders:
▲, *quartz sand,*
■, *cracking catalyst,*
●, *hematite.*

3.4 DISCUSSION

3.4.1 comparison with wet milling

First of all it is interesting to make a comparison with the results of experiments found in the literature on wet milling. Unfortunately, no results could be found on the wet milling of such fine powders as we used. However, it appeared to be quite informative, as shown in figure 3.3, to compare with the results of wet milling of much coarser particles. The results of the rate of breakage versus the particle size, as represented by the lines in the left side of figure 3.3, were taken from Austin (6). He also used quartz sand, but with an initial size range from about 100 to 1000 μm. In order to be able to compare the results we brought the particle size on a dimensionless basis by relating it to the mean particle size of the interval containing the largest particles. That mean size was the same in corresponding experiments, viz. dry/wet (Austin) or non-pressurized/pressurized (ours). In a similar way the rates of breakage were made dimensionless. For dry/wet milling the rates were related to the value belonging to the first interval of wet milling. For the other combination the value of the first interval belonging to pressurized milling was used.

At the right side the cumulative breakage parameter, B, for the products of the first interval is shown. This parameter is for a given particle size defined as the fraction of the milling product of interval 1 being smaller in diameter than this given size. The data on this parameter were taken from Berube (7), who also used quartz of about the same size range as Austin. The particle size is made dimensionless in the same way as in the left figure.

Figure 3.3 now shows a great deal of similarity between the cases dry/wet and non-pressurized/pressurized respectively: the rate of breakage increases, but the fineness decreases when milling wet instead of dry, or pressurized instead of non-pressurized. The first conclusion is apparent from the figure on the left side. The second one follows from the figure on the right side: for wet milling the B-curve falls under that of dry milling. So, less of the product is smaller than a given

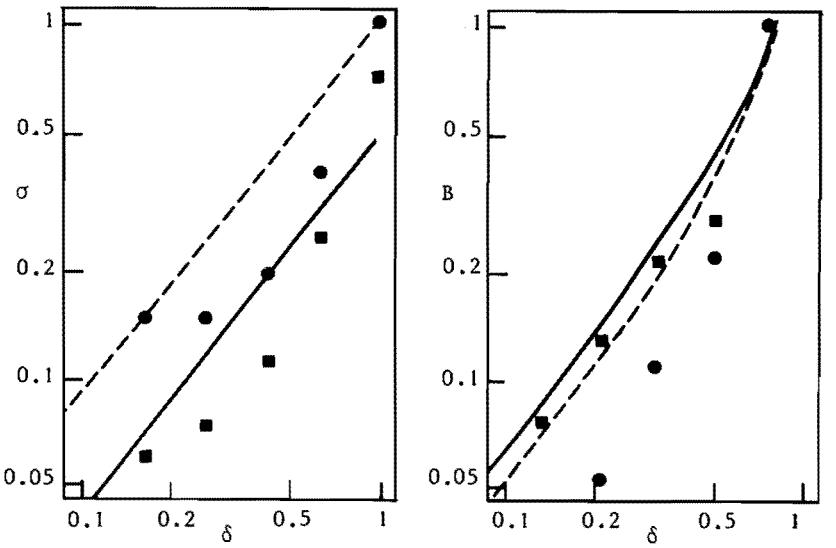

Figure 3.3. A comparison of the change in milling characteristics when converting from dry milling to wet milling versus the change when converting from non-pressurized milling to pressurized milling.
Dry milling: solid lines, wet milling: broken lines.
Non-pressurized milling: ■, pressurized milling: ●.

size limit, when milling wet. The same holds for non-pressurized/pressurized milling.

Another interesting observation in this respect made by Berube is that the rate of breakage of the lowest rank interval, i.e. with the largest particles, increases with time during wet milling. Initially it is about equal to the value during dry milling. As already mentioned in our previous paper we made the same observation when milling at elevated pressure using rather coarse initial powder: initially the milling speed is equal to the value at very low pressures (0.01 bar). When the fines content increases, the rate of breakage increases to the value obtained at elevated pressure as depicted in figure 3.1. It must be put forward here that this similarity does not necessarily mean that the two phenomena can be ascribed to the same cause. In fact, our results can be explained by a decreasing powder viscosity, due to the increase in gas-powder interaction, when the particle size

decreases and thus the gas-powder-interaction number also decreases (see formula 3.1). In the case of Berube, however, the viscosity of the slurry increases instead of decreases with the increase of the fines content. Moreover, Berube states that this increase will be only minor, since the increase of fines is rather small and he is unable to explain his results when considering the influence of the viscosity of the slurry.

An argument for wet milling against dry milling, next to the increase in the rate of breakage, is the smaller rate of agglomeration. Here again we see a similarity with pressurized milling. Figure 3.4 gives data on the effect of gas pressure on the final value of the weight fraction of the first interval, containing the largest particles. This final value was established, when after a sufficiently long milling it remained constant. Thus a steady state is reached, which results from an equilibrium between agglomeration and breakage of agglomerates. As a side remark it should be pointed out that the rate of breakage of agglomerates is probably not equal to the rate of breakage of the original particles of this interval, since the structure of agglomerates is quite different, as was detected by observation through a microscope.

Figure 3.4 now shows that the final value of the weight fraction of the first interval decreases with increasing pressure. At pressures above 3 bar or when milling in neon, higher viscosity, it even becomes zero. Whether this effect is due to a higher rate of breakage or to a lower rate of agglomeration or to both has not been investigated. However, it appears that milling at elevated pressures results in a finer product than milling at 1 bar.

3.4.2 simulation of continuous, pressurized milling

The mathematical description we used for our batch grinding experiments can easily be extended to a description for continuous milling with or without classification. Treatises on this can be found in the literature [5,8]. In essence the extension consists of introducing terms for feed and product flows in the rate equations, while assuming a stationary size distribution inside the mill. Figure 3.5 gives the

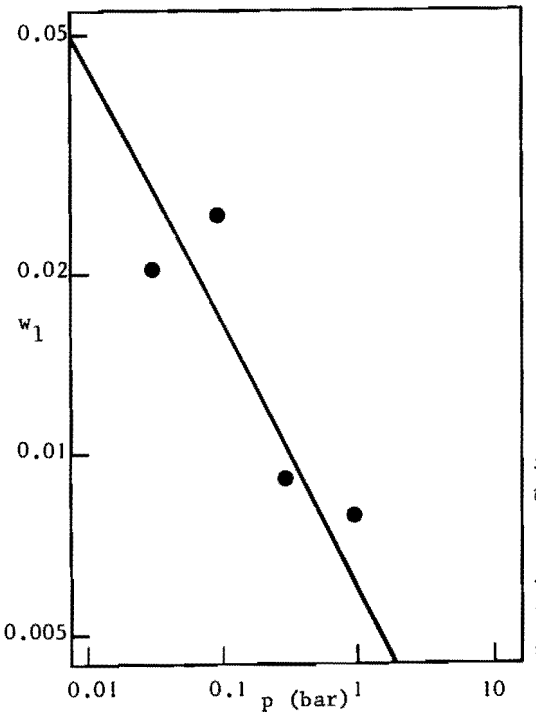

Figure 3.4. The final value of the weight fraction of the interval, containing the largest particles as a function of pressure when milling catalyst. At pressures above 3 bar, using air, the fraction becomes zero.

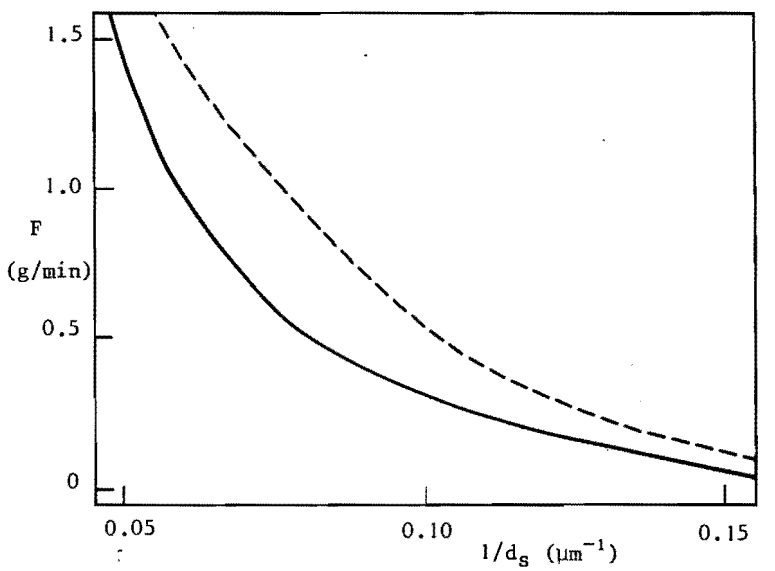

Figure 3.5. The feed rate versus the specific surface, when milling quartz sand continuously at 1 bar, solid line, and at 7 bar, broken line. The holdup in the mill was 300 g, while the specific surface of the feed was 0.017 μm^{-1}.

result of a computer simulation of continuous milling using rates of breakage and breakage parameters of quartz sand as found in our experiments for the cases of low and high pressure inside the mill. Here the feed rate versus the specific area of the product, i.e. the inverse Sauter mean diameter, d_s, is shown. In this simulation no classification was used, i.e. no recirculation of particles above a certain size limit. The mill was assumed to be fully mixed. The results show that, when a certain specific area is wanted, the feed rate can be increased by almost a factor of two by operating at a pressure of 7 bar.

Simulations on a milling circuit with classification show similar increases in production rate, i.e. the amount of powder below a given size limit produced per unit time.

3.4.3 comparison of power consumption

We compared also the power consumption for the three types of ball milling, i.e. simple non-pressurized dry milling, wet milling and pressurized dry milling. We assumed batchwise operation. Figure 3.6 shows the total power consumption as a function of product of the milling time and the relative production rate for these three cases. Data used to prepare this figure can be found in table 3.3. Since for a specific result the product of the production rate and the milling time is, of course, the determining factor, the parameter on the horizontal axis in figure 3.6 is directly a measure of the obtained results.

It shows that simple dry milling from the viewpoint of production costs is always less attractive than pressurized dry milling. When a very fine powder is wanted and thus a long milling time is necessary, wet milling finally becomes more advantageous. Of course, capital costs need also to be taken into account. These will be the lowest for dry milling and, probably, the highest for pressurized milling.

As mentioned it was assumed that finally all three processes can give the desired results. This will not always be true, since e.g. wet and pressurized milling decrease the rate of agglomeration and thus in-

crease the ultimate product fineness. During the drying process, necessary if the product needs to be dry, however, agglomeration can occur again. This disadvantage is not present when milling pressurized. This consideration in itself can be a reason for pressurized milling.

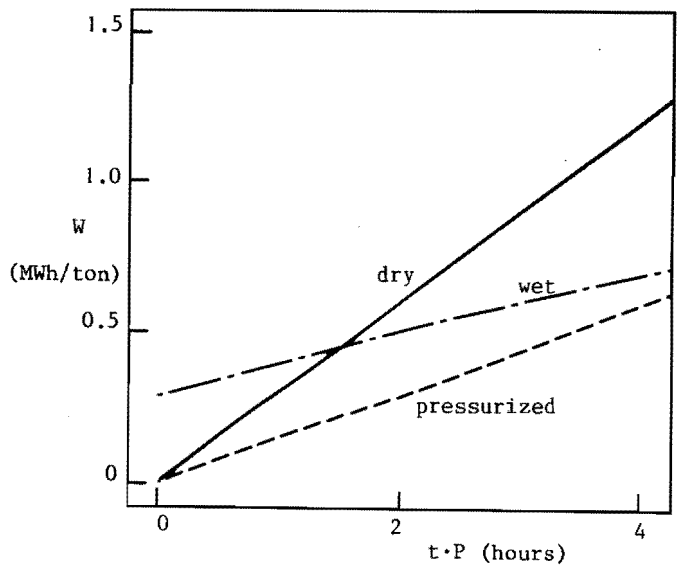

Figure 3.6. The total power used for three different types of milling versus product of the milling time and the relative production rate.

	dry	wet	pressure
power required to drive the mill (kW/ton)	300	300	300
relative production rate, p	1	3	2
drying (30 weight % water) (kWh/ton)	-	300	-
pressurization (20 bar) (kWh/ton)	-	-	12

Table 3.3. Power data for three types of milling. A mill volume of 7 m^3 per ton powder was assumed.

3.5 CONCLUSIONS

The batch experiments in the laboratory size ball mill show the following results for the gas influence on the milling of fine powders:

increasing the pressure and/or the viscosity of the interstitial gas

- increases the rate of breakage.
- decreases the fineness of the daughter fragments.
- decreases the number of agglomerates.

It appears that all these effects are quite similar to the effects obtained by wet milling of coarse powders: the total milling speed increases, while the ultimate product can be finer.

Although the gain in milling speed is somewhat smaller when milling pressurized instead of milling wet, pressurization can still be of advantage with respect to production costs, since no drying of the product is necessary. Moreover, any agglomeration during the drying process is avoided.

3.6 LIST OF SYMBOLS

b_{ij}		breakage parameter, part of milling product of interval j falling into interval i
B		cumulative breakage parameter
d_p	L	particle diameter
d_s	L	Sauter mean diameter
F	MT^{-1}	feedrate in continuous milling
g	LT^{-2}	gravitational acceleration
i		interval number
j		interval number
N_g		gas-powder-interaction number according to equation (3.1)
p	$ML^{-1}T^{-2}$	gas pressure
P		production rate of a mill relative to the production rate of that mill when milling dry
S_i	T^{-1}	rate of breakage of size interval i
t	T	time

U_a	LT^{-1}	typical speed of apparatus in which a powder is handled
w_i		weight fraction of size interval i
W	L^2T^{-2}	power required to produce an amount of milled and dried powder
δ		dimensionless particle diameter parameter
μ	$ML^{-1}T^{-1}$	gas viscosity
ρ_d	ML^{-3}	particle density
σ		dimensionless rate of breakage parameter

3.7 LITERATURE

1 W. Cottaar and K. Rietema Powder Technology 38(1984)183

2 K. Rietema Powder Technology 37(1984)5

3 H. Piepers, E.J.E. Cottaar, A.H.M. Verkooijen and K. Rietema Powder Technology 37(1984)55

4 D. Geldart Powder Technology 7(1973)285

5 L.G. Austin Powder Technology 5(1971)1

6 L.G. Austin, P.Bagga and M. Celik Powder Technology 28(1981)235

7 M.A. Berube, Y. Berube and R. le Houillier Powder Technology 23(1979)169

8 L.G. Austin, V.K. Jindal and C. Gotsis Powder Technology 22(1979)199

4 THE EFFECT OF INTERSTITIAL GAS ON MILLING: A CORRELATION BETWEEN BALL AND POWDER BEHAVIOR AND THE MILLING CHARACTERISTICS.

Submitted for publication to Powder Technology
Coauthor: K. Rietema.

4.0 ABSTRACT

In two earlier papers (1,2) the effect of interstitial gas on milling was reported. It showed that these effects were well correlated with changes in powder porosity and by consequence the changes in powder mobility due to variation of gas viscosity and pressure.

In this paper the cause of this correlation is further investigated. Starting from a close visual inspection of the processes in a ball mill a model is developed in which the milling characteristics are correlated to the ball flow and the powder behavior during ball collisions. From experiments it follows that both are influenced by powder mobility.

4.1 INTRODUCTION

In two earlier papers (1,2) we reported on our experimental results about the effect of the interstitial gas, the gas filling of the mill, on the characteristics of dry milling of fine powders, particle diameter less than 100 μm, in a ball mill. It was found that for three quite different powders (quartz sand, fresh cracking catalyst and hematite) the effect was very similar: increasing the gas viscosity, by applying different gases, and (or) the gas pressure resulted in an increase of the rate of breakage, i.e. the amount of material milled per unit of time, and in a decrease of the milling fineness, i.e. the increase in total surface when a particle is crushed.

As an example figures 4.1a and 4.1b give the rates of breakage for two powders as a function of gas pressure and gas viscosity respectively. Figures 4.2a and 4.2b show the corresponding milling fineness, which is defined as

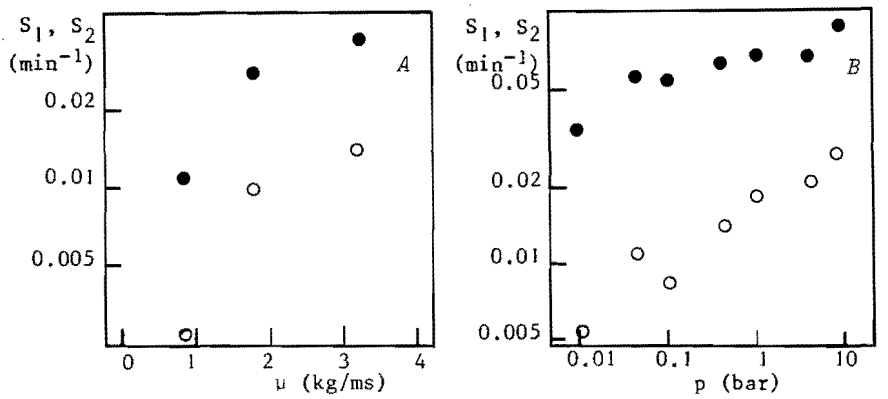

Figure 4.1 *The rates of breakage as a function of viscosity and gas pressure:*

A: quartz sand: interval 1 (●) 77 - 121 μm

2 (○) 48 - 77 μm

B: cracking catalyst: interval 1 (●) 66 - 104 μm

2 (○) 42 - 66 μm

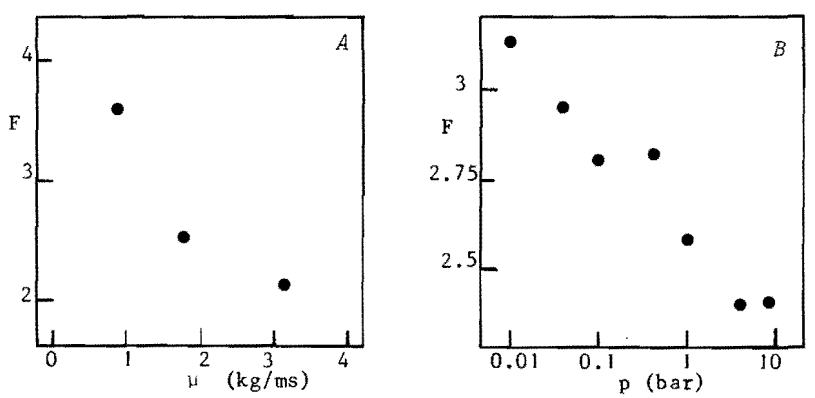

Figure 4.2. The milling fineness as a function of gas viscosity and gas pressure for a quartz sand and a cracking catalyst respectively

$$F = \sum_{i=2}^{6} b_{i1} \frac{d_1}{d_i} \qquad (4.1)$$

where b_{i1} are the breakage parameters of the first interval and d_i denotes the average size of the ith interval. Note that the minimum value of F (b_{21}=1) is given by d_1/d_2 which was 1.58 for our experiments.

It was also observed that the milling characteristics correlate well with the average porosity of the powder. The higher the gas viscosity or the higher the gas pressure the more porous the powder. The porosity in its turn influences the mobility of the powder. (The similarity between the effects of gas viscosity and pressure are explained in the first paper (1)).

The authors believe that the results of the milling experiments should be explained by the changes in powder mobility and consequently in ball behavior and ball-powder interaction. In this paper we will therefore further investigate these phenomena.

4.2 VISUAL OBSERVATION OF THE MILLING PROCESS

Before presenting our model we will describe the qualitative, visual observations made by us, since we developed our model from these observations.

As already pointed out in the first paper (1) the powder porosity, and, therefore, the powder mobility, can change quite drastically with varying gas pressure and (or) viscosity. Two extreme cases can be observed:

- At low pressure, below 0.03 bar with air, porosity and mobility of the powder are very low.
- At relative high pressure, above 0.3 bar with air, porosity and mobility are high.

In this paper we shall only consider these two extreme cases and not deal with intermediate states. Nor shall we deal with the effect of gas viscosity which is quite similar to that of pressure. Next to these two extremes of gas pressure we shall consider a variation in

Powder flow:

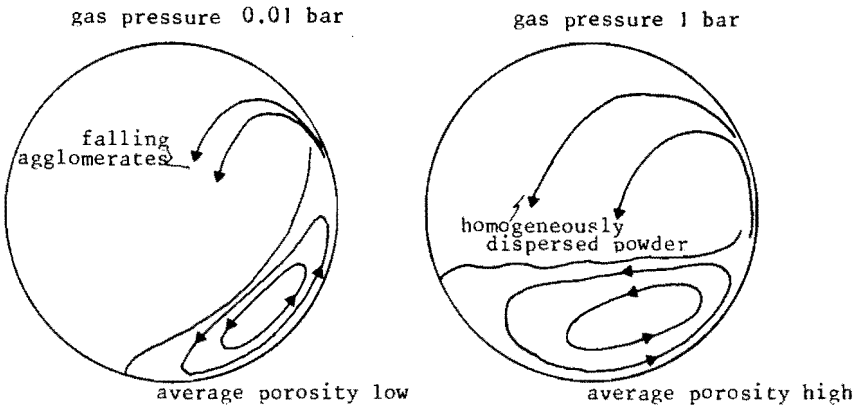

Ball movement:

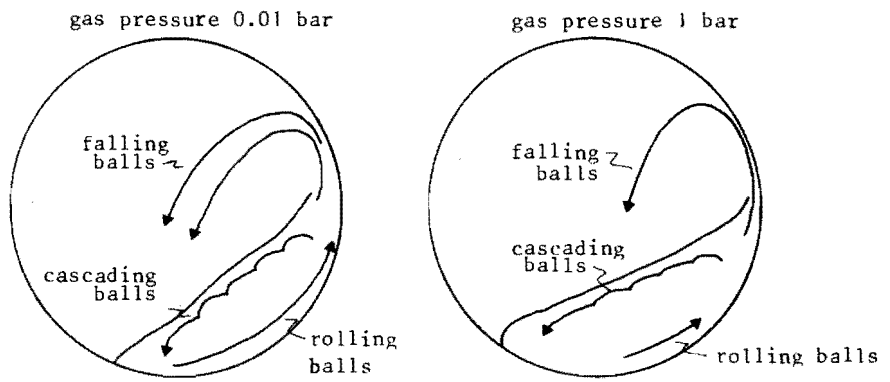

Figure 4.3. The powder flow and ball movement at two gas pressures.

ball load. The visual observations were made in the same apparatus as used for the earlier milling experiments, one metal flange being replaced by a glass one. The powder and ball flow patterns are sketched in figure 4.3. All relevant equipment parameters are given in table 4.1.

Regarding the powder flow the following observations were made:

- Low gas pressure results in a low powder porosity. Most of the powder fills the space between the balls in the lower right section of the mill and is carried upward with the balls (mill turning anti-clockwise). From a certain point the major part of the powder flows

mill	
material	steel
internal radius (R_m)	75 mm
internal length	195 mm
speed of rotation	80 rpm
balls	
material	ceramic
mass pro ball	6 gram
radius (R)	8 mm
powder	
material	fresh cracking catalyst
particle density	750 kg/m^3
mill loading	280 gram (0.5 liter)

interval	size range	init.weight
1	56 - 89 μm	22 %
2	36 - 56	53
3	22 - 36	17
4	11 - 22	5
5	9 - 14	2
6	< 9	1

Table 4.1. Conditions during the milling experiments.

down. The other part is carried upwards at the wall to the point where equilibrium is reached between the centrifugal and gravitational forces and falls down in the form of agglomerates to become a part of a thin layer on the wall.

- High gas pressure results in a high powder porosity. The powder is equally distributed between the lower left and right sections of the mill. Part of it is even fluidized: when the mill is suddenly stopped, the powder slowly collapses while deaerating. At each turn of the mill only a small portion of the powder is carried upwards after which it falls down as a neatly dispersed powder.
- The effect of the ball load on powder porosity is small.
- At low ball loads, 120 and less, and high gas pressure, the powder does not really flow around any more. Instead the powder shows a stick-slip flow along the wall of the mill. Due to the fact that

the aeration of the powder is drastically decreased the average powder porosity also decreases. It remains, however, well above the porosities observed at low pressure levels.

When considering the ball movement three different types can be distinguished. At the bottom of the mill rolling balls are observed. These balls are closely packed and move upwards. Generally there is a slip of these balls at the wall.

Over these rolling balls cascading balls can be seen. They are more loosely packed and move downwards while rolling and jumping over one another and over the rolling balls. Their falling height between two collisions is of the order of the ball radius.

Finally balls can be distinguished which fall down over a distance of typically the radius of the mill. Of course, these falling balls as well as the cascading balls have been part of the rolling balls whilst being carried upwards.

When varying gas pressure and ball load the following effects were noticed:

- At low gas pressure the number of falling balls per unit of time is is higher than at high gas pressure.
- At very low ball loads for none of the gas pressures used any falling balls were observed.
- At low gas pressure the plane in which the cascading balls come down, is steeper than at high pressure. Its slope also increases with increasing ball load.
- At high gas pressure and ball loads of 120 and less, the balls do not flow around. Instead they show a stick-slip behavior along the wall of the mill quite analogously to the behavior of the powder at these conditions.

4.3 A CORRELATION BETWEEN MILLING CHARACTERISTICS AND BALL AND POWDER BEHAVIOR

From the above observations we concluded that the effect of interstitial gas on milling may be caused by the following phenomena:

(1) The change in powder porosity and the resulting difference in powder mobility, which probably will highly influence the way of compaction of the powder during ball collisions.

(2) The change in ball movement, probably induced by the change in powder mobility, which results in different collision rates of balls falling and cascading.

(3) The change in powder distribution in the mill and the resulting difference in the thickness of the powder layers in the areas where balls collide.

In order to arrive at a more quantitative relation we introduce a set of parameters as given in table 4.2. The first and second parameter, n_f and n_c, represent the numbers of collisions per unit of time due to falling or cascading balls respectively. These parameters depend on gas pressure as well as on ball load. The contribution, if any, of rolling balls to the milling process is put equal to zero.

The third and fourth parameter, σ_{fi} and σ_{ci}, are defined as the decrease in the weight fraction of the ith interval due to one milling event of one falling or cascading ball collision respectively relative to the weight fraction of that interval. Since the state of the powder is not highly influenced by ball load, these parameters depend only on gas pressure. Of course, these parameters also vary with particle size and therefore with interval number.

The final two parameters, ϕ_f and ϕ_c, are defined as the milling fineness due to one milling event of a falling or cascading ball collision respectively. Since the overall milling fineness as defined in equation (4.1) is related to the first interval, ϕ_f and ϕ_c will also be related to the first interval. These parameters only depend on gas pressure.

Using these definitions and the definition of the rate of breakage

parameter	description	influenced by ball load	influenced by gas pressure
n_f	collision rate of balls falling	+	+
n_c	collision rate of balls cascading	+	+
σ_{fi}	weight fraction of powder from the ith interval milled in one collision of a falling ball, relative to the weight fraction	-	+
σ_{ci}	weight fraction of powder from the ith interval milled in one collision of a cascading ball, relative to the weight fraction	-	+
ϕ_f	fineness due to a collision of a falling ball	-	+
ϕ_c	fineness due to a collision of a cascading ball	-	+

Table 4.2. Parameters of the proposed correlation.

(see e.g. [1,3]) we can write

$$S_i = n_f\sigma_{fi} + n_c\sigma_{ci} \qquad (4.2)$$

When n_f, n_c and S_i are obtained by experiments at a certain gas pressure but at different ball loads, then for that gas pressure σ_{fi} and σ_{ci} can be determined from equation (4.2).

Since $n_f\sigma_{fl}$ gives the amount of powder milled by falling balls, while it obtains a fineness ϕ_f, and $n_c\sigma_{cl}$ the amount of powder milled by cascading balls, while it obtains a fineness ϕ_c, the overall milling fineness will be given by

$$F = \frac{n_f\sigma_{fl}\phi_f + n_c\sigma_{cl}\phi_c}{n_f\sigma_{fl} + n_c\sigma_{cl}} \qquad (4.3)$$

When F is now also measured at the same gas pressure and at the same ball loads as n_f, n_c and S_l, then ϕ_f and ϕ_c can be determined from equation (4.3) for that pressure.

4.4 EXPERIMENTS WITH VARYING BALL LOAD

4.4.1 milling characteristics

The experiments were carried out in the same mill as used in the previous experiments. (Data are given in table 4.1). As a powder fresh cracking catalyst was used. The sizes of the intervals used in the analysis and the initial weight distribution are also given in table 4.1. The ball load, N, in the mill was varied from 60 to 360 balls. The results of the rates of breakage for the two intervals containing the largest particles and the fineness are shown in figures 4.4 and 4.5.

The relative error in the rates of breakage are about 10% for both intervals. The absolute error in the milling fineness is about 0.1. These errors were established by repeating the experiments several times.

The method of particle size measurement and the subsequent analysis are extensively discussed in the first paper (1).

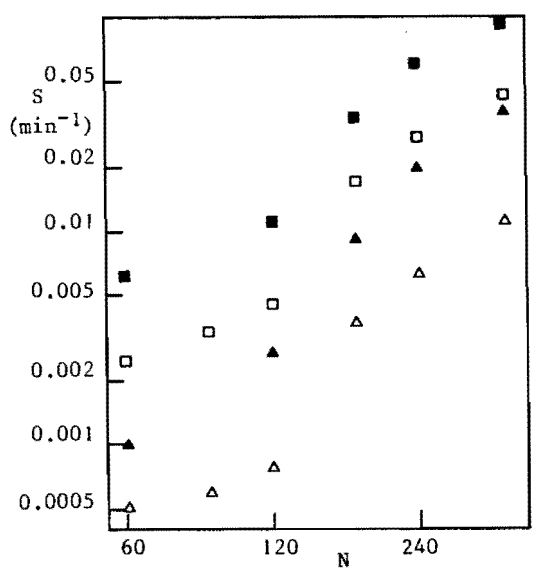

Figure 4.4. The rate of breakage as a function of ball load for two gas pressures: ■, S_1 at 1 bar; ▲, S_2 at 1 bar; □, S_1 at 0.01 bar and △ S_2 at 0.01 bar.

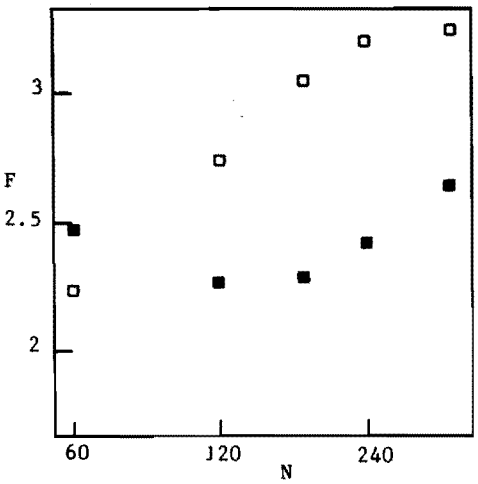

Figure 4.5. The fineness as a function of ball load at 1 bar (■) and at 0.01 bar (□) gas pressure.

4.4.2 the collision rates of balls falling

As already pointed out in the first paper (1) there is also a marked difference in the noise of the mill for the two pressure levels. At low pressure it was much louder. It appeared that there is a correlation between the noise of the mill and the collision rate of balls falling. Therefore, a method was developed to establish the collision rate of balls falling from an analysis of the noise of the mill.

When the sound of the mill was recorded by a microphone and displayed on an oscilloscope, the noise of the mill appeared to consist generally of two components. One was a low intensity signal. The other one consisted of short bursts of a much higher intensity. It showed that when no balls were falling, these bursts were absent. We therefore assigned these bursts to collisions of falling balls and assumed that each individual burst corresponded to a collision of a falling ball and by measuring the frequency of these bursts the collision rate of balls falling was established. The method is further elaborated in appendix 4.A.

The result is shown in figure 4.6. The relative, systematic error in the values obtained is estimated at 10%.

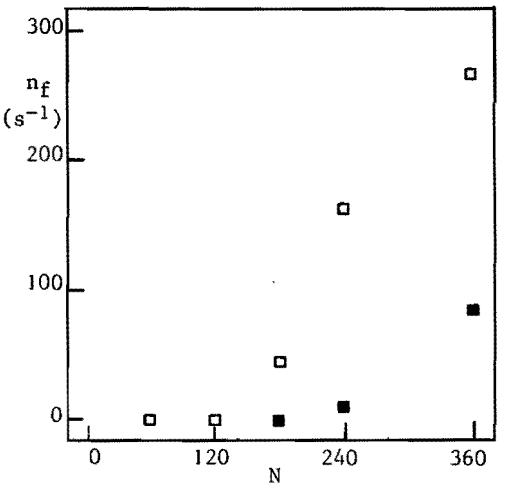

Figure 4.6. The collision rate of balls falling at 0.01 bar (□) and 1 bar (■) as a function of ball load.

4.4.3 the collision rate of balls cascading

To determine the collision rate of balls cascading the power consumption of the mill was measured. This power consumption, M, consists of three contributions:

(1) The power required to drive the empty mill (M_e)

(2) The power required to carry up the powder in the mill (M_p)

(3) The power required to carry up the balls. Since all of these balls eventually either fall or cascade down, this contribution to the power consumption consists of two parts. The first part is required to carry up the falling balls (M_f), the second to carry up the cascading balls (M_c)

So

$$M = M_e + M_p + M_f + M_c \qquad (4.4)$$

Since we were not able to obtain absolute values of the power consumption, all power values will be given relative to the power required to drive the empty mill, M_e.

The results of the total power consumption are given in figure 4.7. It shows that most power is required to drive the empty mill (the value of $(M-M_e)/M_e$ is at most 0.22). The relative error in the value of $(M-M_e)/M_e$ is about 10%.

The value of M_p was established in the following way. Firstly the power consumption of the mill was measured with only powder present. This yielded values of M_p/M_e of 0.019 at a high pressure level (0.035 at a low pressure level). Secondly we measured the power consumption when the mill was filled with balls only (240) and compared it to the power consumption at a high pressure level and at the same ball load but now in the presence of powder. Assuming that at a high pressure level (high powder mobility) the ball movement is not influenced by the powder, this yielded for a high pressure level a value of 0.045 for M_p/M_e.

At a high pressure level the power required to drive the powder was now obtained through inter- and extrapolation. So at a high pressure level

$$M_p/M_e = 0.019 + 0.026 \frac{N}{240} \qquad (4.5)$$

For a low pressure level the power needed to carry up the powder cannot be obtained as directly as at a high level, since the powder, as observed visually, highly influences the ball flow. Nonetheless it is assumed that the influence of ball load on the power consumption due to the powder is independent of pressure. So at a low pressure level

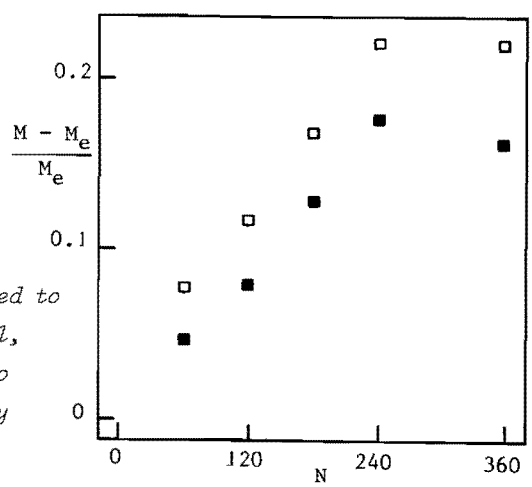

Figure 4.7. The power required to drive the filling of the mill, powder and balls, relative to the powder to drive the empty mill at 0.01 bar (□) and 1 bar (■).

$$M_p/M_e = 0.035 + 0.026 \frac{N}{240} \qquad (4.6)$$

To calculate the contribution to the power consumption due to ball movement it is assumed that the power input for one ball when being carried upwards is proportional to the height over which it is carried upwards, i.e. to the height over which it will eventually fall down. For a falling ball this height is assumed to be equal to the mill radius, R_m. For a cascading ball it is assumed that between two collisions it falls over a distance of typically the ball radius R. So

$$M_f/M_e = C'R_m n_f \qquad (4.7)$$

$$M_c/M_e = C'R\, n_c \qquad (4.8)$$

Using equations (4.4),(4.7) and (4.8) we get

$$\frac{M - M_e - M_p}{M_e} = C \left(\frac{R_m}{R} n_f + n_c \right) \qquad (4.9)$$

with $C = C' \cdot R$.

To get an estimate of C it was reasoned that at a ball load of 360 balls and at a low pressure level the collision rate of balls cascading must be very low, at most a few hundred per second. The main reason is that at this ball load the total power consumption is equal to that at 240 balls, while the collision rate of balls falling is much higher. Since R_m/R is about equal to ten, the collision rate of balls cascading must have been drastically decreased. Using a value of n_c of 300 s^{-1} at these conditions results in a value for C of $4.87 \cdot 10^{-5}$s. The final results for the collision rates of balls falling and cascading are given in table 4.3.

The relative systematic error in the values of the collision rate of balls cascading is estimated at 20% for most conditions. The only real exception is at a ball load of 360 balls at a low pressure level, where the error may be as large as 100%. The sources of these errors are the error in the power consumption measurements, the error in the collision rate of balls falling and finally the error in the estimation of the constant C.

0.01 bar absolute (low powder mobility)

N	$(M-M_e)/M_e$	M_p/M_e	n_f	n_c
0		0.035		
60	0.08	0.042	0	780
120	0.12	0.048	0	1480
180	0.17	0.055	50	1860
240	0.22	0.061	165	1620
360	0.22	0.074	270	300

1 bar absolute (high powder mobility)

N	$(M-M_e)/M_e$	M_p/M_e	n_f	n_c
0		0.019		
60	0.05	0.026	0	490
120	0.08	0.032	0	980
180	0.13	0.039	0	1870
240	0.18	0.045	10	2670
360	0.16	0.058	90	1200

Table 4.3. Results on the collision rates of balls falling and cascading for two pressure levels as a function of ball load. ($C = 4.87 \cdot 10^{-5}$ s, $R_m/R = 10$).

4.5 RESULTS

Using the experimental data the parameters describing individual milling events were calculated using equations (4.2) and (4.3) by a least-squares fitting procedure. The results are given in table 4.4. Since at a high pressure level ball and powder flow at ball loads of 120 and less are quite different from the flow at higher ball loads only the experimental data for ball loads of 180 and higher are used. At a low pressure level the whole range of ball loads was used.

The errors given in table 4.4 are statistical errors due to spread in the experimental data. As mentioned already the collision rates of balls falling and cascading have a systematic error too. This will create corresponding systematic errors in σ_{fi} and σ_{ci}. The systematic error in σ_{fi} will therefore be of the order of 10% and in σ_{ci} of the

	1 bar absolute (high powder mobility)			0.01 bar absolute (low powder mobility)		
interval	1	2	3	1	2	3
$\sigma_{fi} \cdot 10^6$	13 ± 2	5.4 ± 0.8	1.9 ± 0.4	2.5 ± 0.2	0.7 ± 0.1	0.22 ± 0.05
$\sigma_{ci} \cdot 10^8$	33 ± 3	8.9 ± 0.9	3.0 ± 0.4	5.4 ± 0.1	1.0 ± 0.1	0.34 ± 0.08
σ_{fi}/σ_{ci}	39	61	63	46	65	65
σ_{fl}/σ_{fi}	1	2.4	6.8	1	3.8	11
σ_{cl}/σ_{ci}	1	3.7	11	1	5.4	16
ϕ_f	2.7 ± 0.1			3.4 ± 0.2		
ϕ_c	2.4 ± 0.1			2.5 ± 0.1		

Table 4.4. Results on the milling parameters of individual milling events for two pressure levels. At 1 bar the experiments at ball loads of 180, 240 and 360 were used. At 0.01 bar the ball loads used were 60, 120, 180, 240 and 360.

order of 20%. The systematic errors in the fineness parameters are much lower and well below the statistical error.

From these results it can be observed that:

(1) At either pressure level the amount of material milled by a falling ball is much larger than the amount of material milled by a cascading ball.

(2) The amount of milled material at the higher pressure level is always larger than at the lower level. This holds for both falling and cascading balls. Moreover, the difference is larger for smaller particles (higher intervals).

(3) At decreasing particle size the amount of milled material decreases sharper for cascading balls than for falling balls.

(4) At either pressure level the milling fineness due to a falling ball is higher than the milling fineness due to a cascading ball.

(5) The milling fineness due to a falling ball is higher at the lower pressure level than at the higher level.

(6) The milling fineness due to a cascading ball is about equal for either pressure level.

4.6 DISCUSSION

Firstly it should be remarked that the amount of experimental data is not sufficient to prove that the equations (4.2) and (4.3) give a complete description of the milling process. Our experiments only give the values of the parameters of the model, assuming the equations give indeed a complete description. Of course, our model was not just made up, but was developed from visual observations.

At the higher pressure level the results of the experiments at the loads of 60 and 120 could not be brought in line with those obtained at higher ball loads. The rates of breakage were much too small. This is in accordance with the visual observation that at these ball loads and pressure neither the balls nor the powder do really flow.

In the literature it is quite common to describe the rate of breakage by a unique relation to the particle diameter (e.g. 4,5):

$$S \sim d^{\alpha} \qquad (4.10)$$

in which α is independent of other conditions. Our results show that this relation in general does not apply. E.g. at a higher pressure level for falling balls the exponent α would be about 2, for cascading balls it would be about 2.8. Although at constant conditions (e.g. mill radius and speed) relation (4.10) may still be useful, care should be taken when the conditions are changed, as in scaling up, since the ratio of falling and cascading balls, and therefore α, may change.

Since as derived by Rietema (6) the influence of interstitial gas depends on the circumferential speed of the apparatus under consideration, also the state of the powder depends on this speed and therefore the scale of the apparatus. This in its turn influences the ratio of falling and cascading balls as well as the result of an individual event. This may again change the exponent α.

Similar considerations hold, of course, for the milling fineness.

Finally it is worth mentioning that our experiments show that crushing experiments on individual particles [7,8,9], cannot reveal all the information on the milling characteristics. E.g. at either pressure level falling balls enter the powder with the same kinetic energy, the resulting milling fineness is however different. These effects, which are due to differences in powder mobility, were occasionally noted before in the literature [10,11].

4.7 CONCLUSIONS

From the experiments on the ball movement it can be concluded that this movement depends on ball load as well as on the powder mobility.

The amount of material milled in one milling event and the resulting fineness of such an event depends on kinetic ball energy as well as on the powder mobility.

In order to arrive at a complete understanding of the milling process in addition to actual milling experiments separate experiments should be carried out on ball movement, on powder flow and on ball-powder interaction during collisions.

4.8 LIST OF SYMBOLS

b_{i1}		breakage parameter of first interval
C'	$L^{-1}T$	constant in mill power relation
C	T	constant in mill power relation
d	L	particle diameter
F		overall milling fineness
i		interval number
M	ML^2T^{-3}	total power consumption of the mill
M_c	ML^2T^{-3}	power consumption due to cascading balls
M_e	ML^2T^{-3}	power consumption of the empty mill
M_f	ML^2T^{-3}	power consumption due to falling balls
M_p	ML^2T^{-3}	power consumption due to the powder
N		ball load in the mill
n_c	T^{-1}	collision rate of balls cascading
n_f	T^{-1}	collision rate of balls falling

p	$ML^{-1}T^{-2}$	gas pressure
R	L	radius of a ball
R_m	L	internal radius of the mill
S	T^{-1}	rate of breakage
α		constant in equation (4.10)
μ	$ML^{-1}T^{-1}$	gas viscosity
σ_c		relative amount of powder milled by one cascading ball
σ_f		relative amount of powder milled by one falling ball
ϕ_c		milling fineness due to a cascading ball
ϕ_f		milling fineness due to a falling ball

4.9 LITERATURE

1 W. Cottaar and K. Rietema Powder Technology 38(1984)183

2 W. Cottaar, K. Rietema and S. Stemerding
to be published in Powder Techn.

3 L.G. Austin Powder Technology 5(1971)1

4 L.G. Austin, K. Shoji and P.T. Luckie
Powder Technology 14(1976)71

5 L.G. Austin, P. Bagga and M. Celik
Powder Technology 28(1981)235

6 K. Rietema Powder Technology 37(1984)5

7 B. Buss and H. Schubert Powder Technology 4(1970)117

8 S. Baumgardt, B. Buss, P. May and H. Schubert
Powder Technology 8(1973)107

9 S.R. Krogh Powder Technology 27(1980)171

10 J.M. Crowley Powder Technology 15(1976)133

11 L.G. Austin and P. Bagga Powder Technology 28(1981)83

APPENDIX

4.A NOISE ANALYSIS OF THE MILL

In this appendix a noise analysis will be discussed, which is used to obtain the number of falling balls per unit of time. The first aim of this analysis was to obtain an amplitudo distribution of this noise $Q(A)$, where $Q(A)\Delta A$ denotes the chance that the noise consists of a sinusoidal wave with its amplitudo in the range $A-\frac{1}{2}\Delta A$ to $A+\frac{1}{2}\Delta A$.

To reach this aim the noise of the mill, or more precisely the pressure fluctuation, was recorded by a microphone, amplified and then sampled by a microcomputer. The sampling frequency was 10 KHz. Thus a distribution R(y) was obtained, where $R(y)\Delta y$ denotes the chance that at any given time the absolute value of the deviation of the noise level from zero is in the range $y-\frac{1}{2}\Delta y$ to $y+\frac{1}{2}\Delta y$.

Of course, Q and R are not the same functions. For example when the noise would consist of only one sinusoidal wave with a fixed amplitudo A, then

$$Q(A) = \delta(A) \tag{4.A.1}$$

where δ denotes the deltafunction. And

$$R(y) = R_0(y) = \begin{cases} \frac{2/\pi}{\sqrt{A^2-y^2}} & y \leq A \\ 0 & y > A \end{cases} \tag{4.A.2}$$

Generally R(y) can be written as

$$R(y) = \int_y^\infty \frac{2/\pi}{\sqrt{A^2-y^2}}\, Q(A)\, dA \tag{4.A.3}$$

So R(y), the measured distribution, is the result of the convolution of $R_0(y)$ and Q(A), the wanted amplitudo distribution. Similarly Q(A) can now be obtained by a deconvolution, when R(y) is measured.

The next goal was to derive from the obtained amplitudo distribution Q(A), the number of falling balls per unit of time. Here the following assumptions are made, which are supported by observation of the noise signal on an oscilloscope:

- One falling ball gives an amplitudo larger than a level A_b during a time Δt_b.
- There is no other noise with an amplitudo larger than A_b present.

If the number of balls falling per unit time is equal to n_f, then the fraction of time, f, during which the amplitudo of the noise signal is larger than A_b is given by

$$f = n_f \Delta t_b \exp(-n_f \Delta t_b) \tag{4.A.4}$$

The exponential term on the rightside of the equation accounts for the chance of two or more balls colliding almost simultaneously.

In accordance to the definition of the amplitudo distribution f can also be written as

$$f = \int_{A_b}^{\infty} Q(A)\, dA \qquad (4.A.5)$$

Using values of A_b and Δt_b obtained from visual inspection of the noise signal using (4.A.5) and (4.A.4) the number of falling balls, n_f, can be obtained.

5 THE EFFECT OF INTERSTITIAL GAS ON MIXING OF FINE POWDERS

Submitted for publication to Powder Technology
Coauthors: A. Heijnen and K. Rietema

5.0 ABSTRACT

In our research program on the effect of interstitial gas on the handling of fine powders the influence on mixing was investigated.

Two types of mixing were investigated: the mixing of two powders of which all relevant properties were equal and two powders with widely different properties. The experiments were performed in a rotating drum. Powder composition was established with a probe, which measured the optical reflectivity of the powder. This method proved to be fast and easy while being accurate enough.

From the experiments it can be concluded that for powders with (nearly) equal properties the speed of mixing can be increased by increasing the gas viscosity and/or gas pressure. For powders, which show a segregative behavior, the final quality of the mix can, however, be improved by lowering the gas viscosity and/or gas pressure.

5.1 INTRODUCTION

In a research program on the influence of interstitial gas on the handling of fine powders we already reported extensively on the effects of interstitial gas on milling [1,2,3]. These effects appeared to be caused by changes in powder porosity and hence in the powder mobility due to differences in gas viscosity and gas pressure. Summarizing these changes were:

- At increasing gas viscosity the powder porosity and mobility increase.
- When decreasing the gas pressure from ambient pressure to values of typically 0.01 bar, the powder porosity and mobility decrease. This change is actually analogue to the first one, since at such low pressures the effective gas viscosity for powders decreases.

- When increasing the gas pressure from ambient pressure to values of typically 10 bar the powder porosity and mobility increase. This change can most probably be ascribed to the increase in particle interaction due to gas adsorption, but is not yet fully understood. It is quite analogue to similar phenomena observed by us in fluidization (4).

Rietema (5) derived a criterion, when gas influence might be expected,

$$N_g = \frac{\rho_d \, d_p^2 \, g}{\mu \, U_a} << 100 \qquad (5.1)$$

The smaller the value of the gas-powder-interaction number, N_g, the larger the gas-powder interaction. Since this gas influence already has a remarkable effect on milling, it might be expected there is also a dependency of the mixing behavior of fine powders on the interstitial gas. Therefore, we also undertook an effort in this field of powder handling.

5.2 DESCRIPTION OF THE MIXING PROCESS

In this section we will discuss methods to describe the mixing process. Since all experiments were performed in a horizontal drum, we will confine ourselves to methods to be used in this geometry. Moreover, about equal amounts of powder with roughly the same particle size were mixed. Mixing is therefore purely stochastic and the concept of ordered mixtures due to adherence of small particles on large particles will not be applicable.

There are generally two ways to describe a mixing pocess. In one the actual process is described by transport equations. In the other description the (final) result of the process is given. This is mostly done by the variance in composition between samples of a given size, drawn from the mixture. We will discuss both methods below. Extensive discussions can be found in the literature (6,7).

5.2.1 description by transport equations

Considering only binary mixtures, where no convective processes are present in the direction under consideration, the dependence of the composition c with time t and position x is given by

$$\frac{dc}{dt} = \frac{d}{dx} D \frac{dc}{dx} \qquad (5.2)$$

Where D is called the diffusion coefficient.

By definition the composition is zero if only one powder is present and one if only the other is present. If in a given sample the bulk volumina of both powders are equal it will be 0.5.

We will use this equation to describe the axial mixing in a horizontally rotating drum. Initially one half of the drum is filled with one powder, the other half with another. Setting x=0 at the middle of the drum and the length to L, this leads to the initial condition

$$c(t=0) = \begin{cases} 1 & 0 < x \leq \frac{1}{2}L \\ 0.5 & x = 0 \\ 0 & -\frac{1}{2}L \leq x < 0 \end{cases} \qquad (5.3)$$

The boundary conditions are

$$\frac{dc}{dx} = 0 \qquad x = \pm\frac{1}{2}L \qquad (5.4)$$

since no transport is possible through the flanges at the end of the drum.

5.2.2 description of final result

When the powder properties become more and more different the description of a mixing process using equation (5.2) becomes less and less meaningfull. This is due to the fact that segregation processes can generally not be adequately described by this equation. Since for such processes up till now no adequate alternative descriptions are available, we will take resource to describing the mixing process by way of describing the final result.

This final result will be quantified by means of introducing a va-

riance σ of the composition in the direction under consideration. This variance is defined as

$$\sigma^2 = \int (c - \bar{c})^2 dx \Big/ \int dx \qquad (5.5)$$

Where $\bar{c}$ denotes the average value of the composition.

Generally, the composition is only known at certain positions. The integral then reduces to a summation

$$\sigma^2 = \frac{1}{m-1} \sum_{i=1}^{m} (c_i - \bar{c})^2 \qquad (5.6)$$

And

$$\bar{c} = \frac{1}{m} \sum_{i=m}^{m} c_i \qquad (5.7)$$

It is both allowed to measure the compositions at regular intervals along the direction under consideration and to measure it at random positions.

5.3 EXPERIMENTAL SET-UP

5.3.1 the sampling method

To measure the local composition of a powder mixture we used a method based on a difference in the optical reflectivity of the powders to be mixed. A schematical drawing is given in figure 5.1. The main advantage of this method is the measuring speed: the probe is inserted into the powder, and instantaneously the composition can be read from a calibration graph.

Of course, the method has its disadvantages:

- The powders to be mixed must be optically different. In a research project this can be obtained by coating one of the powders.
- The sample size is unknown. At best only a fair estimate can be calculated. Therefore, the method cannot be used to investigate mixing on microscale. Only an overall mixing process can be studied.
- The optical reflectivity appeared to depend on the porosity. If, however, care was taken during calibration this effect could be

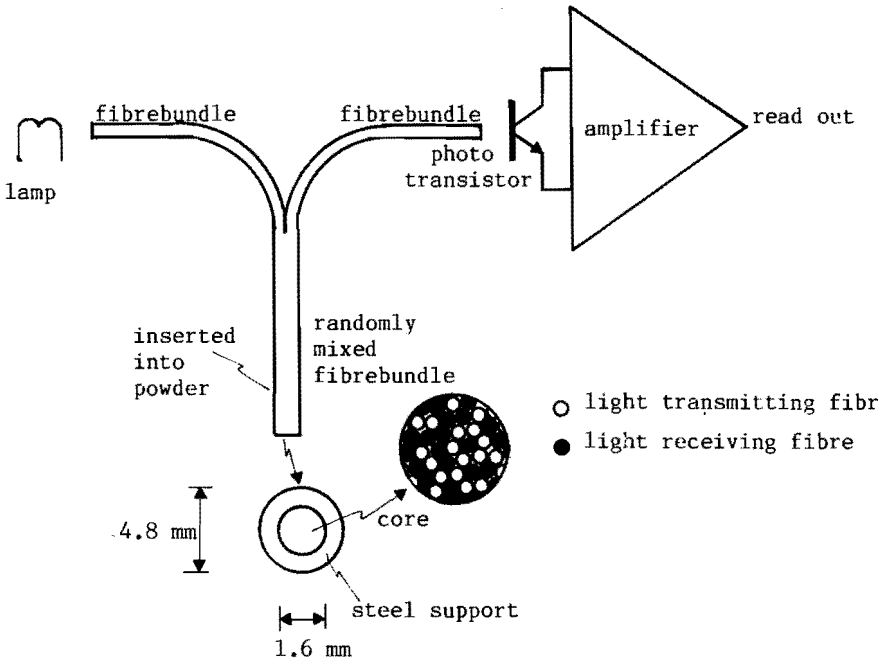

Figure 5.1. A schematical drawing of the optical probe.

largely eliminated when measuring in a stationary powder. The effect, however, makes the probe useless when a flowing powder is monitored, since in such a case the porosity may show large deviarions at the tip of the probe. Not the least, of course, due to disturbances caused by the probe itself-

In the experiments the probe behaved quite well and since it has also been used to study the segregation of powders in a fluidized bed with equal satisfactory results. The absolute error, when the composition of a powder mixture ranging from 0 to 1 was established, was about 0.02 over the whole range.

5.3.2 experimental procedures

5.3.2.1 experiments on the diffusion coefficient

Figure 5.2 shows the schematics of the experimetal set-up. Initially each half of the drum is filled with one powder. The bulk volumina of both powders are equal. During an individual experiment the drum is

rotated for several intervals. After each interval the powder composition at the position of the nine sampling holes is established. At each sampling hole an average composition is obtained by measuring at a number (5-10) of random radial positions. Of course, the drum is filled with the desired gas at the desired pressure before rotating. The gas handling system used is quite analogue to the one used in the milling experiments (1).

Then the data on the powder composition are fitted to the solution of equation (5.2) using a least-squares fitting procedure described before (1).

5.3.2.2 experiments on variances

To establish the degree of mixing two types of variance were used. One was a measure of any segregation process in the radial direction, σ_r, the other of any in the axial direction, σ_a. They were obtained in the following way:

(1) Through each sampling hole (i) a number of n measurements is done at several radial positions. Each measurement is denoted by c_{ij} ($i = 1,9$, $j = 1,n$).

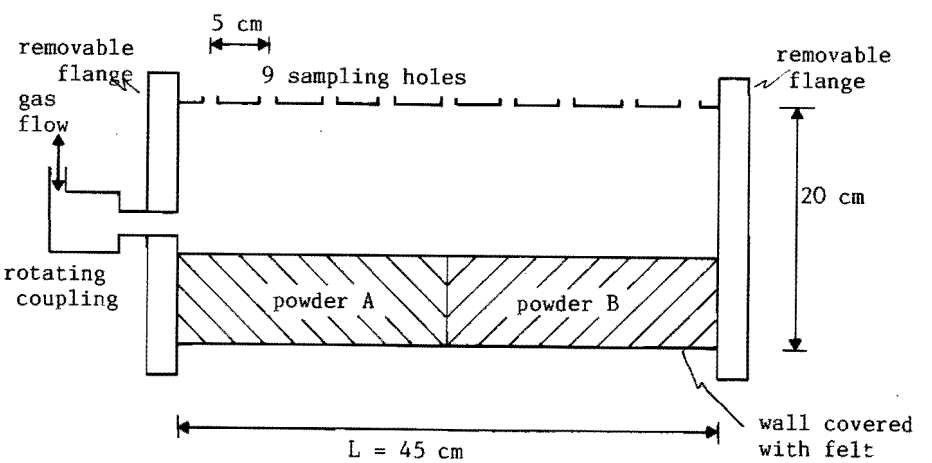

Figure 5.2. Geometry of the mixing drum.

(2) Of each sampling hole the mean value, c_i, and the variance, σ_i, of the powder composition are now given by

$$c_i = \frac{1}{n} \sum_{j=1}^{n} c_{ij} \tag{5.8}$$

$$\sigma_i = \{\frac{1}{n-1} \sum_{j=1}^{n} (c_{ij} - c_i)^2\}^{0.5} \tag{5.9}$$

(3) Since σ_i is a measure of the variance in the radial direction at one axial position, the average of σ_i over the whole drum will be a measure of the demixing in the radial direction. Thus we define

$$\sigma_r := \frac{1}{9} \sum_{i=1}^{9} \sigma_i \tag{5.10}$$

(4) Similarly any differences in c_i between different sampling holes are a measure of demixing in the axial direction. We therefore define

$$\sigma_a := \{\frac{1}{8} \sum_{i=1}^{9} (c_i - \bar{c})^2\}^{0.5} \tag{5.11}$$

Using

$$\bar{c} = \frac{1}{9} \sum_{i=1}^{9} c_i \tag{5.12}$$

In the experiments both σ_r and σ_a were measured as a function of time. The actual measuring procedure was quite the same as in the experiments on the diffusion coefficient. Only the obtained results were analyzed in a different way.

5.3.3 powders and combinations used

Table 5.1 shows the data on the powders used in the experiments. Table 5.2 shows the combinations of powders used.

In the first series actually the self diffusion of fresh cracking catalyst was studied. To enable us to follow the mixing process part of the powder was colored by Indian Ink. Care was taken that the differences in other properties, such as particle size distribution and

	FCC1	FCC2	Magnetite
d_p (µm)	0 - 100	0 - 200	0 - 250
d_s (µm)	53	60	84
ρ_d (kg/m³)	680	800	5090
ρ_b (kg/m³)	400	520	3400
ε_0	0.41	0.35	0.33
N_g [1]	10	16	196
type of fluidization [2]	A	A	B
color	white	white	black

Table 5.1. Data on powders used in mixing experiments.
FCC = Fresh Cracking Catalyst
1) The gas-powder-interaction number is calculated for air at 1 bar and an apparatus speed of 0.1 m/s.
2) According to Geldart's classification (8).

type of experiment	powder combination
diffusion coefficient	FCC1 - FCC1
variances	FCC2 - Magnetite

Table 5.2. Types of experiments and powder combinations used.

fluidization behavior, between the uncolored and colored particles were small. To reach this aim the powder which should remain white was treated in the same way as the powder to be colored, except that no Ink was added (e.g. it was also wetted in alcohol, dried and sieved again). The fresh cracking catalyst is a well flowing powder and can be homogeneously fluidized.

In the second series the mixing result, represented by the variances, of a combination of fresh cracking catalyst and magnetite is studied. This powder combination shows a high degree of demixing due to the large difference in powder properties (particle size and weight). E.g. it was very difficult to obtain full mixes of different compositions needed for the calibration of the sampling apparatus. The fresh cracking catalyst again was a well flowing powder, which could be homoge-

neously fluidized. The magnetite was a free flowing powder, which only showed heterogeneous fluidization.

5.4 RESULTS

5.4.1 diffusion coefficient for FCC1-FCC1

Figure 5.3 shows the result of a single mixing experiment. It shows that a description using equations (5.2) through (5.4) is indeed valid for the self-mixing of this powder.

Figure 5.4 shows the result of the diffusion coefficient, when different gased are used. This result is in accordance with our expecta-

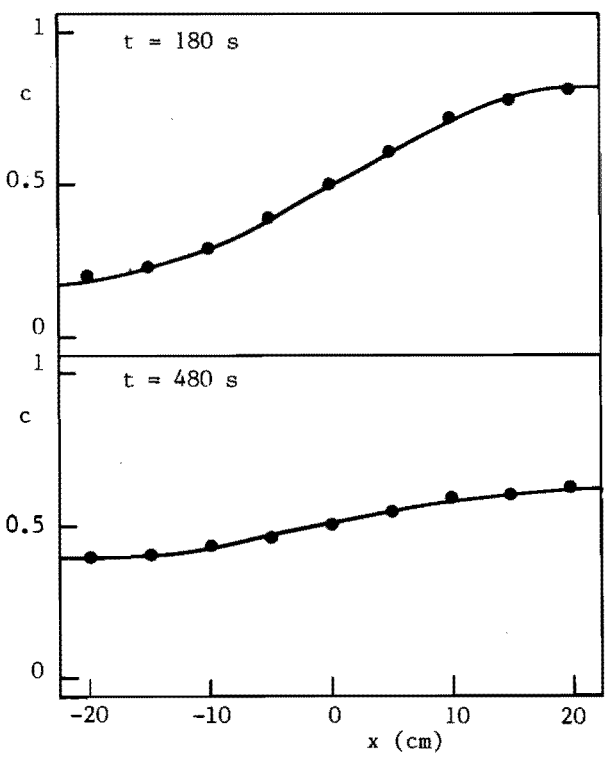

Figure 5.3. The measured (dots) and computed (drawn lines) composition as a function of the axial position in the drum at two moments for the powder combination FCC1-FCC1 when mixing in argon at 8.4 bar and a speed of rotation of 60 rpm. (D = 0.74 cm²/s)

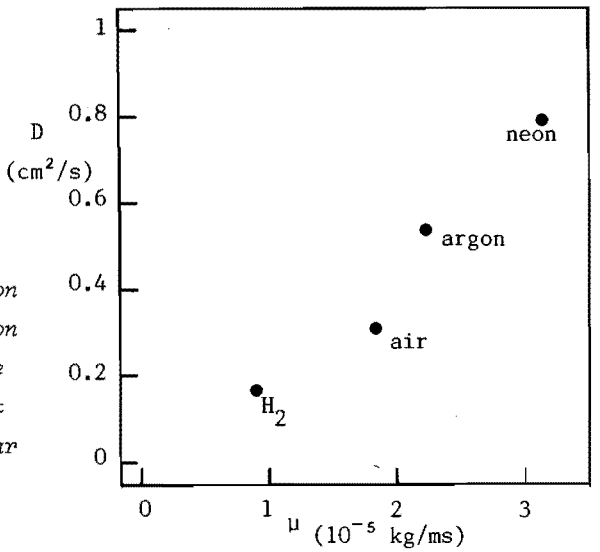

Figure 5.4. The diffusion coefficient as a function of gas viscosity for the combination FCC1-FCC1 at a gas pressure of 1.8 bar and a speed of 60 rpm.

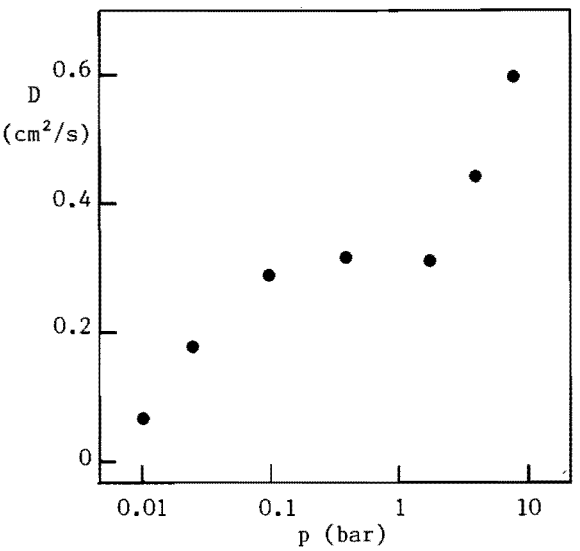

Figure 5.5. The diffusion coefficient as a function of gas pressure for the combination FCC1-FCC1 at a speed of 60 rpm. The gas used was air.

tion: at higher gas viscosities the porosity of the powder and therefore the mobility of the powder increase. An increase in mobility will in its turn create an increase in the diffusion coefficient.

Figure 5.5 shows the diffusion coefficient as a function of pressure. Again the behavior of the diffusion coefficient can be explained by the changes in powder mobility.

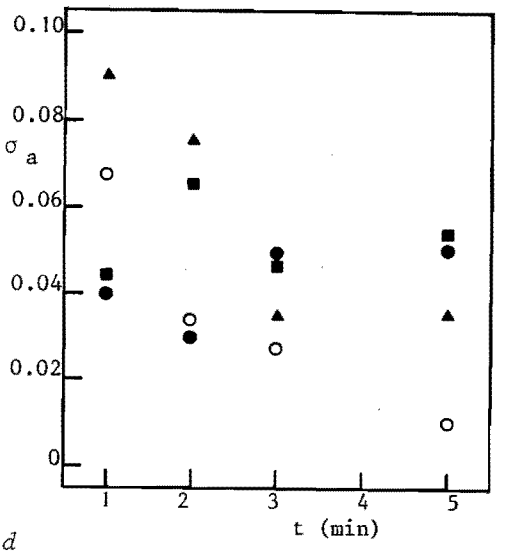

Figure 5.6. The variance in the axial direction for the combination FCC2-Magnetite as a function of time for four cases:
● *argon at 1 bar,* ▲ *air at 1 bar,* ○ *air at 0.01 bar and* ■ *hydrogen at 1 bar. The speed was 60 rpm.*

5.4.2 variances for the combination FCC2-magnetite

Figure 5.6 shows the result for the variance in the axial direction. At short mixing times no systematic gas influence can be detected. After approximately 5 minutes the values remained constant. Here it clearly shows that a very low gas viscosity (air, 0.01 bar) gives a much better mix, lower variance, than higher gas viscosities. At higher gas viscosities there appears to be no influence of gas viscosity on the variance.

Figure 5.7 shows the result for the variance in the radial direction. Here never any gas influence can be detected.

Similar observations were made by us for a somewhat different but also segregative system. Here the speed of the apparatus was varied. Again it showed that a higher gas-powder-interaction number, i.e. lower speed, lowered the axial variance. Also the radial variance was lower at a lower speed.

These observations can be understood in the following way: an increase in the gas-powder-interaction number decreases the mobility of the

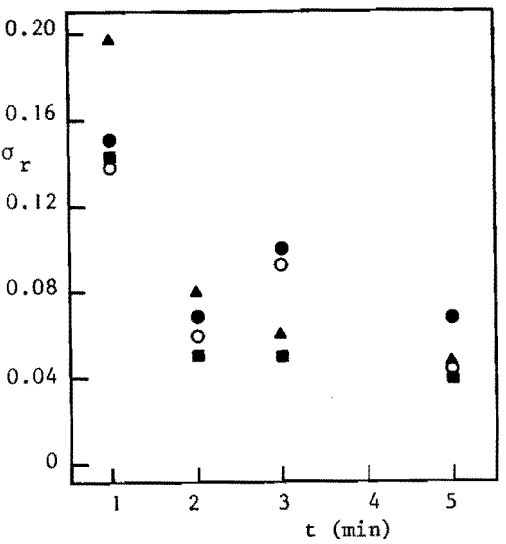

Figure 5.7. The variance in the radial direction for the combination FCC2-Magnetite as a function of time for four cases: ● *argon at 1 bar,* ▲ *air at 1 bar,* ○ *air at 0.01 bar and* ■ *hydrogen at 1 bar. The speed was 60 rpm.*

powder particles. Thus particles will have less chance to segregate. These results show a great similarity with those of Nienow and Rowe (9) for the segregation of powders in fluidized beds.

5.5 CONCLUSIONS

For fine powders with about equal properties the average speed of mixing may be increased by decreasing the gas-powder-interaction number. This implies that it is generally favourable to mix such powders in an apparatus which induces high powder velocities.

For powders, which show a tendency to segregate, i.e. unmixing, it is favourable to keep the gas-powder-interaction number high. Such powders should be mixed in an apparatus which only creates low powder velocities. The segregation can also be diminished by mixing under vacuum conditions.

5.6 LIST OF SYMBOLS

c		powder composition
d_p	L	particle size

d_s	L	Sauter mean diameter
D	L^2T^{-1}	diffusion coefficient
g	LT^{-2}	gravitational acceleration
L	L	length of the drum
N_g		gas-powder-interaction number defined by equation(5.1)
i		index indicating sampling hole
j		index indicating measurements at one sampling hole
n		number of measurements at one sampling hole
p	$ML^{-1}T^{-2}$	gas pressure
t	T	time
U_a	LT^{-1}	typical speed of powder handling apparatus
x	L	position in apparatus
ε_0		packed porosity
μ	$ML^{-1}T^{-1}$	gas viscosity
ρ_b	ML^{-3}	bulk density at packed porosity
ρ_d	ML^{-3}	particle density
σ		variance in composition
σ_a		variance in axial direction
σ_r		variance in radial direction

5.7 LITERATURE

1 W. Cottaar and K. Rietema Powder Technology 38(1984)183

2 W. Cottaar, K. Rietema and S. Stemerding to be published in Powder Techn.

3 W. Cottaar and K. Rietema submitted to Powder Technology

4 H. Piepers, W. Cottaar, A. Verkooijen and K. Rietema Powder Technology 37(1984)55

5 K. Rietema Powder Technology 37(1984)5

6 K. Sommer J. Powder & Bulk Solids Technology 3(1974)4

7 K. Sommer Fortschritte der Verfahrenstechnik 19(1981)189

8 D. Geldart Powder Technology 7(1973)285

9 P. Rowe and A. Nienow Powder Technology 15(1976)141

6 A THEORETICAL STUDY ON THE INFLUENCE OF GAS ADSORPTION ON INTERPARTICLE FORCES IN POWDERS

6.0 ABSTRACT

Using data from the literature and some additional experiments it is investigated if the interparticle forces in general and more specifically the cohesion between particles is influenced by the physi-sorption of gases.

In this otherwise theoretical study the force to be applied to a particle to obtain a specific distance from a plane is derived from the total energy of the system of particle and plane. This energy consists of three terms: molecular interaction energy between the particle and the plane, elastic energy due to deformation of the particle and adsorption energy of the gas.

It is concluded that gas adsorption may indeed quite heavily influence the interparticle forces and cohesion (increase up to a factor three). The degree of influence is determined by the type of gas and the gas pressure.

6.1 INTRODUCTION

In the past two decades considerable attention has been paid to the interaction forces between particles [1,2,3]. A quite detailed overview was already reported by Krupp [4]. This continuing interest is not remarkable, since with the ever increasing industrial use of very fine powders, this particle interaction plays an ever more important role in industrial processes.

Also attention has been paid to the relation between interparticle forces and powder properties like the tensile strength [5,6] and the fluidization behavior [7].

Lately it has been shown that there is evidence that interparticle forces are not only dependent on particle properties, but are also influenced by the surrounding gas due to adsorption [8,9]. In this paper

we will investigate if such is indeed possible. We will only deal with the influence of physi-sorption, i.e. reversible adsorption.

In the investigation we will deal with the case of a spherical particle with radius R in contact with an infinitely large and flat plane. Both particle and plane consist of the same substance. The results of such a geometry, e.g. the cohesion, are equal to the results of two particles with radii R_1 and R_2 with $R=R_1R_2/(R_1+R_2)$. The actual values of the radii to be used for any numerical calculations should not be the actual radii of the particles but the radii of the surface asperities.

6.2 DERIVATION OF THE INTERACTION FORCE FROM THE ENERGY

A system of a spherical particle and a flat plane is considered. The distance between the centre of the particle and the surface of the plane is denoted by L. This distance L can be controlled by applying an external force, F, to the particle. The maximum value of this force will be called the cohesion, C.

Suppose the energy, U, of the system is known as a function of L, then the force F is given by

$$F = \frac{dU}{dL} \tag{6.1}$$

It will now be shown how to calculate this energy as a function of L for two different cases: that of a unflattened particle and that of a flattened particle. A flattened particle is a particle that is so close to the plane that due to repulsive forces its initial shape has changed.

The assumed geometry of the flattened particle is shown in figure 6.1. Here it follows

$$L = R + z - h \tag{6.2}$$

with z the distance between the surfaces and h the flattening of the particle. It may be clear that the system still has one degree of freedom, since equation (6.2) contains two variables (z and h). Since a system always tends to the lowest possible energy it follows that at

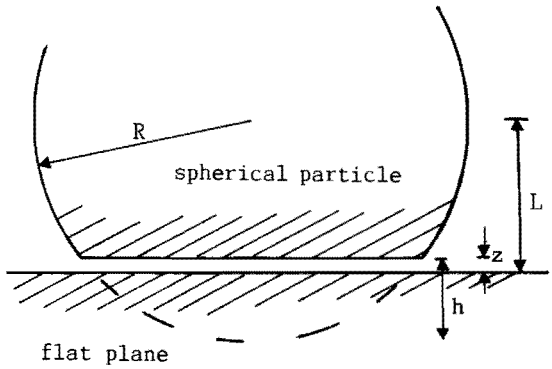

Figure 6.1. The geometry of a flattened particle adhering to a plane.

equilibrium

$$\left.\frac{dU}{dz}\right|_L = \left.\frac{dU}{dh}\right|_L = 0 \qquad (6.3)$$

or

$$\left.\frac{dU}{dz}\right|_L = \frac{\delta U}{\delta z} + \frac{\delta U}{\delta h}\left.\frac{dh}{dz}\right|_L = \frac{\delta U}{\delta z} + \frac{\delta U}{\delta h} = 0 \qquad (6.4)$$

Knowing the energy as a function of h and z relations (6.2) and (6.4) give for each value of L values of h and z and thus a value of the energy of the system.

For an unflattened particle the situation is simpler. Here the flattening, h, always equals zero and therefore no degree of freedom is left. It therefore directly follows

$$F = \frac{dU}{dz} \qquad (6.5)$$

It is noteworthy that in this analysis the distance, z, between the surfaces need not be constant. This was, however, assumed by other authors [1,3]. Johnson et al. [2] assumed a constant surface energy of both the particle and the plane, which is equivalent to assuming a constant distance z.

6.3 THE ENERGY OF THE SYSTEM

The total energy, U, consists of the following contributions:

- The molecular energy due to the interaction between the molecules of the particle and the plane, U_m.

- The elastic energy due to the deformation of the particle, U_H.
- The molecular adsorption energy due to the interaction between the adsorbed gas molecules and the molecules of the particle and the plane, U_g.

The first two contributions have also been used by other authors. It is assumed that all contributions are independent. E.g. the molecular energy due to interaction between particle and plane is not influenced by adsorbed gas molecules.

6.3.1 the molecular energy, U_m

The molecular energy due to the interaction between molecules of the particle and molecules of the plane is calculated using a Lennard-Jones potential for the interaction between two molecules. This potential is given by

$$V_{ss}(r) = C_{ss}\left(\frac{1}{2}\frac{r_{ss}^6}{r^{12}} - \frac{1}{r^6}\right) \qquad (6.6)$$

Where r is distance between the molecules and C_{ss} and r_{ss} are parameters dependent on the molecules involved.

The total molecular energy of the system can be calculated by summing all interactions. So

$$U_m(h,z) = \int_{particle} \int_{plane} n_s n_s V_{ss}(r)\, d^3x\, d^3y \qquad (6.7)$$

Where n_s is the density of molecules in the solid and the plane.

For a flattened particle (see figure 6.1) this results in

$$U_m(h,z) = \frac{A_{ss}R}{6z}\left\{-(1 + \frac{h}{z}) + \frac{1}{60}\frac{r_{ss}^6}{z^6}(\frac{1}{7} + \frac{h}{z})\right\} \qquad (6.8)$$

where A_{ss} is the Hamaker constant for solid-solid interaction, given by

$$A_{ss} = \pi^2 n_s^2 C_{ss} \qquad (6.9)$$

It is generally possible to obtain values of A_{ss} in more direct ways without using an intermolecular potential (10).

For an unflattened particle (h=0) the result is

$$U_m(h=0,z) = \frac{A_{ss} R}{6z}\left\{-1 + \frac{r_{ss}^6}{420\, z^6}\right\} \qquad (6.10)$$

6.3.2 the elastic energy, U_H

The energy due to the elastic deformation of a sphere follows from Hertz's theory [11]. For a flattened particle it follows approximately

$$U_H(h,z) = \frac{8}{15}\frac{\sqrt{2R}}{K} h^{5/2} \qquad (6.11)$$

where K is defined as

$$K = \frac{1 - \nu^2}{Y} \qquad (6.12)$$

with ν the Poisson ratio and Y the Young's modulus of the material under consideration.

Actually the elastic energy results also from molecular energy, but this time between molecules of the particle. In principle it can be calculated from the energy change due to the small displacements of the molecules in the particle when the particle is deformed.

For an unflattened particle the elastic energy is of course zero.

It should be pointed out that the shape of the particle as sketched in figure 6.1 is, of course, not the real shape. Deviations are, however, small and since our goal is to study the influence of gas adsorption we will not discuss this here. More on this subject can be found in the literature [e.g. 1,2].

6.3.3 the energy due to adsorbed gas, U_g

To calculate this energy two things must be known. First of all the binding energy, $U_c(y)$, of a single molecule, which is bound between two planes with a distance y, has to be determined. Secondly the density of molecules adsorbed per unit surface, $N_c(y)$, must also be known. The total energy due to adsorbed gas then equals

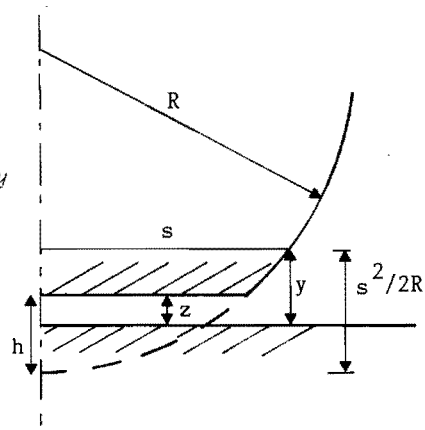

Figure 6.2. Sketch of the geometry for the calculation of the energy due to gas adsorption.

$$U_g(h,z) = \int_0^\infty N_c(y)\, U_c(y)\, 2\pi s\, ds \tag{6.13}$$

Where the distance y is given by (see also figure 6.2)

$$y = \begin{cases} z & (s < \sqrt{2Rh}) \\ z + \frac{s^2}{2R} - h & (s \geq \sqrt{2Rh}) \end{cases} \tag{6.14}$$

Thus equation (6.14) can be rewritten as

$$U_g(h,z) = N_c(z)\, U_c(z)\, 2\pi R h + 2\pi R \int_z^\infty N_c(y)\, U_c(y)\, dy \tag{6.15}$$

The calculation of the energy U_c is carried out in appendix 6.A. There for the interaction between the molecules of the solid and the gas also a Lennard-Jones potential is assumed (see equation (6.6)). The result is

$$U_c(y) = -\frac{4U_a}{\sqrt{2}} \left\{ -\frac{3r_{gs}^3}{y^3} + \frac{8r_{gs}^9}{y^9} \right\} \tag{6.16}$$

Where U_a is the binding energy of a gas molecule to a single plane of the solid. This energy will be determined from data in the literature.

The calculation of the density of adsorbed gas molecules is shown in appendix 6.B. The result is

$$N_c(y) = \frac{1}{r_{gg}^2} \frac{\delta \exp((-U_c(y) + U_a)/kT)}{1 + \delta \exp((-U_c(y) + U_a)/kT)} \tag{6.17}$$

The parameter δ is defined in appendix 6.B as

$$\delta = \frac{N_a}{N_{0a} - N_a} \tag{6.18}$$

where N_a is the number of adsorbed molecules at a free surface and N_{0a} the number of adsorption sites. Both are determined experimentally.

6.3.4 the total energy

The total energy of the system can now be written as

$$U(h,z) = U_m(h,z) + U_H(h,z) + U_g(h,z) \tag{6.19}$$

Introducing the following dimensionless parameters

$$\varepsilon = \frac{6\,U\,r_{ss}}{A_{ss}R} \qquad \eta = h/r_{ss}$$

$$\psi = \frac{48\sqrt{2}}{15}\,\frac{r_{ss}^{7/2}}{A_{ss}K\sqrt{R}} \qquad \zeta = z/r_{ss} \qquad \zeta' = z/r_{gs}$$

$$\lambda = L/r_{ss} \tag{6.20}$$

$$\alpha = -\frac{48\pi}{\sqrt{2}}\,\frac{U_a}{A_{ss}} \qquad \rho = R/r_{ss}$$

$$\tau = -\frac{U_a}{kT} \qquad \xi = y/r_{gs}$$

this relation can be written in a dimensionless form

$$\varepsilon(\eta,\zeta) = -\left(\frac{1}{\zeta} + \frac{\eta}{\zeta}\right) + \frac{1}{60}\left(\frac{1}{7\zeta^7} + \frac{\eta}{\zeta^8}\right) + \psi\eta^{5/2}$$

$$+ \alpha\left\{\Theta_c(\zeta')\,\varepsilon_c(\zeta')\,\eta + \frac{r_{gs}}{r_{ss}}\int_{\zeta'}^{\infty}\Theta_c(\xi)\,\varepsilon_c(\xi)\,d\xi\right\}\frac{r_{ss}^2}{r_{gg}^2} \tag{6.21}$$

where

$$\varepsilon_c(\xi) = -\frac{3}{\xi^3} + \frac{8}{\xi^9} \tag{6.22}$$

and

$$\Theta_c(\xi) = \frac{\delta\,\exp((-4/\sqrt{2}\,\varepsilon_c(\xi) - 1)\tau)}{1 + \delta\,\exp((-4/\sqrt{2}\,\varepsilon_c(\xi) - 1)\tau)} \tag{6.23}$$

In the remainder of this paper it is assumed that the values of r_{ss}, r_{gs} and r_{gg} are equal. Generally this will not be exactly true, but the influence of any differences will be small. This assumption implies that the dimensionless parameters ζ and ζ' are also equal. Using equation (6.21) equation (6.4) can now be written as

$$\frac{\delta\varepsilon}{\delta\zeta} + \frac{\delta\varepsilon}{\delta\eta} = \frac{2\eta}{\zeta^3} - \frac{2\eta}{15\zeta^9} - \frac{5\psi}{2}\eta^{3/2} + \alpha\,\eta\,\frac{\delta(\Theta_c(\zeta)\cdot\varepsilon_c(\zeta))}{\delta\zeta} = 0 \qquad (6.24)$$

and equation (6.2) as

$$\lambda - \rho = \zeta - \eta \qquad (6.25)$$

6.4 RANGES OF DIMENSIONLESS PARAMETERS

6.4.1 the parameter ψ

From data given by Visser [10] it follows that for almost all materials the Hamaker constant, A_{ss}, is in the range of $5\cdot10^{-20}$J through $50\cdot10^{-20}$J. It is also clear from these data that the actual values of A_{ss} obtained through different methods for one specific substance show large discrepancies. Differences may be up to a factor five.

The value of the parameter, K, which expresses the mechanical behavior of the particle, is for most materials (e.g. ionic crystals and metals) in the range of $5\cdot10^{-11}m^2/N$ through $2\cdot10^{-11}m^2/N$ [3]. For synthetic materials it is generally about a factor ten higher. For r_{ss}, the distance at which two molecules are at rest, the value will generally be of the order of $3.5\cdot10^{-10}$m.

For the radius, R, of the particle or more precisely the asperity, we will use a value of 0.1 μm [4]. Since the parameter ψ only depends on the square root of this radius any changes in the value of R will not change the range of ψ very drastically.

Finally it therefore follows

$1 < \psi < 40$ ionic crystals, metals

$1 < \psi < 4$ synthetic materials, flour, potato starch (6.26)

6.4.2 the parameter α

Using equation (6.9) for the Hamaker constant for solid-solid interaction and equation (6.A.3) for the binding energy of a single gas molecule to the solid surface parameter α can be written as

$$\alpha = \frac{64\, C_{gs}}{3\, r_{gs}^3 n_s C_{ss}} \qquad (6.27)$$

Using relation (4) of Visser [10] for the Hamaker constant between different substances

$$A_{gs} = \sqrt{A_{gg} \cdot A_{ss}} \qquad (6.28)$$

and again using equation (6.9) it follows

$$\alpha = \frac{64\pi}{3 r_{gs}^3} (C_{gg}/A_{ss})^{\frac{1}{2}} \qquad (6.29)$$

Table 6.1 shows some results for different gas/powder combinations.

	cracking catalyst (Al_2O_3, [10] $A_{ss} = 16 \cdot 10^{-20}$ J)	quartz sand (SiO_2, [10] $A_{ss} = 20 \cdot 10^{-20}$ J)
argon ($C_{gg} = 6 \cdot 10^{-78}$ Jm^6, [12,13,14])	10	9
nitrogen ($C_{gg} = 3 \cdot 10^{-78}$ Jm^6, [15])	7	6
hydrogen ($C_{gg} = 1 \cdot 10^{-78}$ Jm^6, [16])	4	3
neon ($C_{gg} = 6 \cdot 10^{-79}$ Jm^6, [13,17])	3	3

Table 6.1. Examples of the value of α for some gas/powder combinations ($r_{gs} = 3.5 \cdot 10^{-10}$ m)

6.4.3 the parameter τ

Similarly the parameter τ can be written, using equations (6.A.3), (6.9) and (6.28), as

$$\tau = \frac{4\sqrt{2}}{9} \frac{\sqrt{A_{ss} C_{gg}}}{r_{gs}^3 kT} \qquad (6.30)$$

Table 6.2 gives some examples.

The values of τ thus obtained are in good agreement with those calculated by Steele [18], who uses a much more refined method. E.g. for the adsorption on graphitized carbon ($A_{ss}=30 \cdot 10^{-20}$ J [10]) he states values of 4 and 1.8 for argon and neon respectively. Equation (6.27) would yield values of 4.9 and 1.5 respectively.

	cracking catalyst (Al_2O_3, [10] $A_{ss}= 16 \cdot 10^{-20}$ J)	quartz sand (SiO_2, [10] $A_{ss}= 20 \cdot 10^{-20}$ J)
argon ($C_{gg}= 6 \cdot 10^{-78}$ Jm^6, [12,13,14])	4	4
nitrogen ($C_{gg}= 3 \cdot 10^{-78}$ Jm^6, [15])	3	3
hydrogen ($C_{gg}= 1 \cdot 10^{-78}$ Jm^6, [16])	1.5	1.6
neon ($C_{gg}= 6 \cdot 10^{-79}$ Jm^6, [13,17])	1.1	1.3

Table 6.2. Examples of the value of τ for some gas/powder combinations at room temperature ($T = 293$ K, $r_{gs}= 3.5 \cdot 10^{-10}$ m)

6.4.4 the parameter δ

This parameter is defined by equation (6.18) as

$$\delta = \frac{N_a}{N_{0a} - N_a}$$

Where N_a is the number of adsorbed gas molecules and N_{0a} is the total number of available adsorption sites, both per unit of surface.

The value of N_a is measured by the apparatus described in appendix 6.C in the range of pressures of 1-20 bar at room temperature. The value of N_{0a} is established by a one point BET method (19).

Figure 6.3 shows δ as a function of pressure for three gas/powder combinations. As explained in appendix 6.B, δ is proportional to the pressure. This indeed appears to be true. Table 6.3 shows the result for some gas/powder combinations investigated.

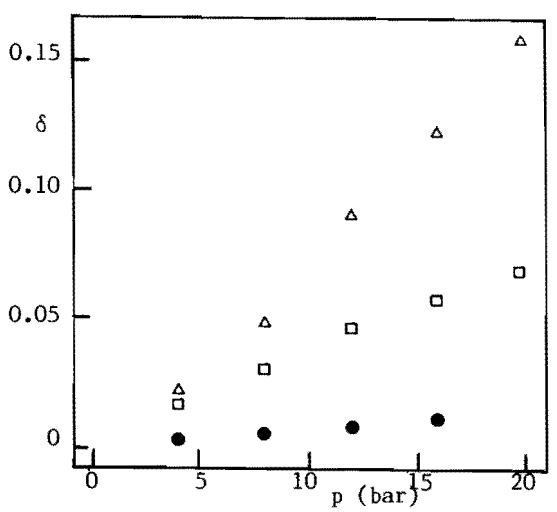

Figure 6.3. The parameter δ (a measure for the amount of adsorped gas at a free surface) as a function of gas pressure for three cases:

- ● *hydrogen on cracking catalyst,*
- □ *argon on cracking catalyst,*
- △ *nitrogen on quartz sand.*

	cracking catalyst	quartz sand
argon	0.0036	0.0060
nitrogen	0.0040	0.0063
hydrogen	0.0007	0.0021
neon	0.0001	0.0015

Table 6.3. Examples of the experimentally established values of δ/p (1/bar) for some gas/powder combinations at room temperature.

6.5 CALCULATION AND DISCUSSION

Figure 6.4 shows the result for the dimensionless force as a function of distance between the particle and the plane. This dimensionless force is given by

$$\phi = \frac{6 F r_{ss}^2}{A_{ss} R} = \frac{d\varepsilon}{d\lambda} \qquad (6.31)$$

or

$$F = \frac{\phi A_{ss} R}{6 r_{ss}^2} \qquad (6.32)$$

The curve for a pressure of 0 bar is, of course, equal to the curve without any gas influence. A negative value of ϕ represents a repulsive force between the particle and the plane: to reach the corresponding values of λ-ρ the particle must be pressed onto the plane with a force F. Positive values represent an attractive force between the particle and the plane.

At higher values of the gas pressure there is at a certain value of λ-ρ a sudden decrease in the force. This step-wise transition is due to the fact that at higher values of λ-ρ it is energetically more favorable to form a single mono-layer of gas molecules between the particle and the plane (see figure 6.5).

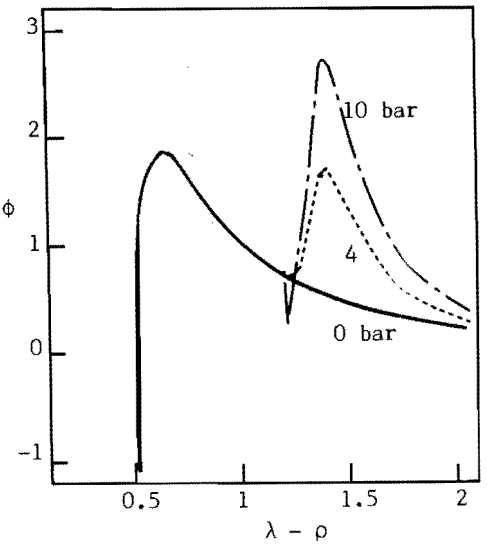

Figure 6.4. The dimensionless interaction force as a function of the particle-plane distance for the case of nitrogen adsorbed on cracking catalyst for three pressures ($\alpha = 7$, $\tau = 3$, $\delta/p = 0.004/bar$, $\psi = 20$).

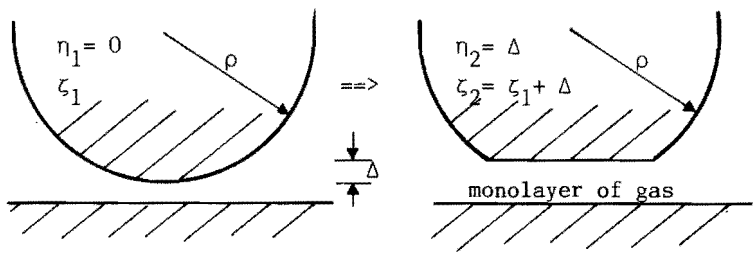

Figure 6.5. The transition from the state of an unflattened particle to the state of a flattened particle with an adsorbed monolayer between the particle and the plane. The total energy of the system is equal in both states.

It clearly shows in figure 6.4, that at high gas pressures the cohesion increases due to the gas adsorption.

Figure 6.6 shows the result of a similar calculation as the one of figure 6.4 but now with a smaller hardness parameter ψ (e.g. a smaller hardness or a larger radius). Comparison with figure 6.4 shows that at low values of λ-ρ the force dependence on λ-ρ is heavily influenced by the hardness parameter ψ. The maximum value of the force, the cohesion, is however not influenced by the hardness parameter. This is due to the fact that the maximum is always reached at a value of η (or h)

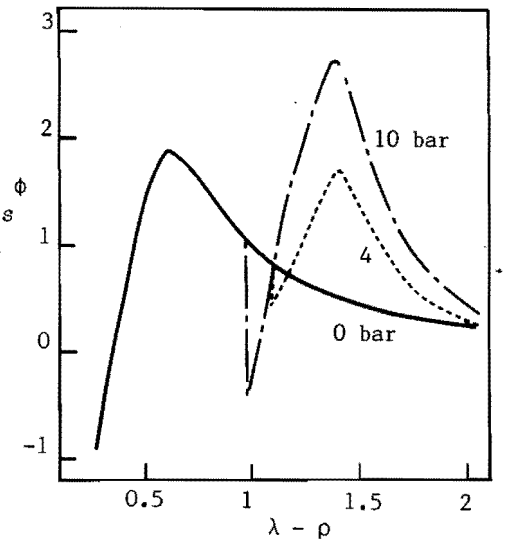

Figure 6.6. The dimensionless interaction force as a function of particle-plane distance for the same system as figure 6.4, but with a decreased hardness (α = 7, τ = 3, δ/p = 0.004/bar, ψ = 2).

close to zero. As may be clear from equation (6.21) the contribution of the hardness to the force is equal to $\psi\eta^{3/2}$. So indeed for η close to zero the contribution of the hardness is also close to zero.

The fact that the maximum is reached at values of η close to zero can be understood in the following way. If flattening of a particle occurs repulsive molecular forces become important. Since the repulsive molecular energy changes very much with small changes of the distance ζ, any changes in the distance λ will mostly induce changes of the flattening η (compare equation (6.25)). Thus it follows as a first approximation

$$\phi = \frac{d\varepsilon}{d\lambda} = \frac{d\varepsilon}{d\eta} \tag{6.33}$$

The maximum is reached if

$$\frac{d\phi}{d\lambda} = \frac{d\phi}{d\eta} = \frac{d^2\varepsilon}{d\eta^2} \sim \psi\ \eta^{\frac{1}{2}} = 0 \tag{6.34}$$

So indeed the maximum is reached at $\eta \approx 0$. Of course, an exact, but very complex, calculation can be carried out to calculate the exact value of η at which the maximum is reached.

It can also be seen in figure 6.6 that the transition to a monolayer of adsorbed gas occurs at lower values of $\lambda - \rho$. This can be understood

in the following way: the adsorption energy of this monolayer is about proportional to the flattening (first term in equation (6.15)), the elastic energy is proportional to the flattening to the power 2.5 (equation (6.11)). Since the transition occurs when both energy contributions are about equal, for a lower hardness a higher flattening occurs. Since ζ is about constant for the monolayer, equation (6.25) shows that a higher flattening, η, indeed implies a lower $\lambda-\rho$. Of course, there is also some change in the molecular energy which we neglected in this reasoning.

Figure 6.7 shows the result of a similar calculation as that of figure 6.4, but now with argon as the adsorbing gas. Note the different scale of the y-axis. Comparison with figure 6.4 shows that the cohesion is more influenced by gas adsorption for argon than for nitrogen. This is due to the fact that the total adsorption energy of adsorbed gas is higher for argon than for nitrogen. Also the transition to a monolayer occurs at lower values of $\lambda - \rho$ due to this higher adsorption energy.

Figure 6.8 finally shows the result of the cohesion force as a function of gas pressure for cracking catalyst for four different gases. This dimensionless cohesion is defined by

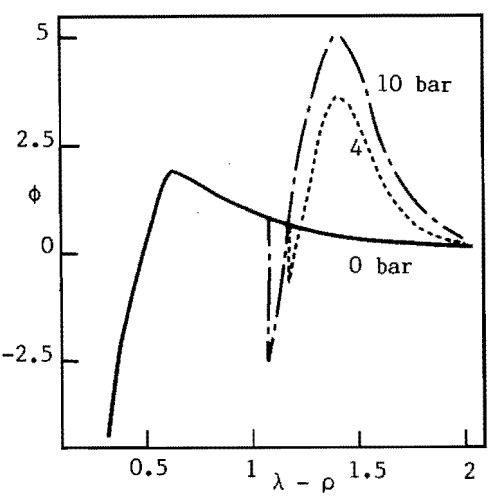

Figure 6.7. The dimensionless interaction force as a function of the particle-plane distance for the case of argon adsorbed on cracking catalyst for three pressures (α = 10, τ = 4, δ/p = 0.036/bar, ψ = 20)

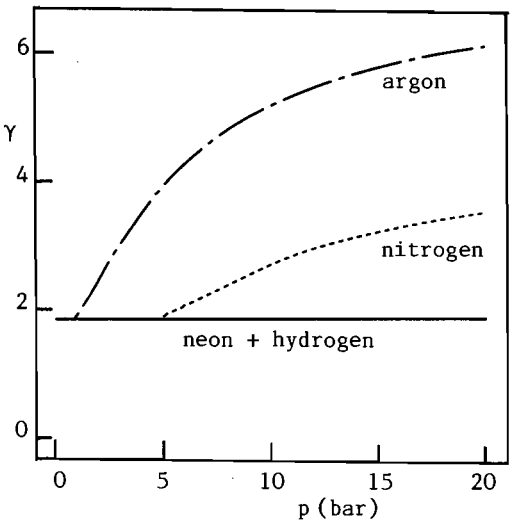

Figure 6.8. The dimensionless cohesion as a function of gas pressure for cracking catalyst. For data on gas adsorption parameters see tables 6.1-6.3.

$$\gamma = \frac{6\, r_{ss}^2\, C}{A_{ss} R} = \phi_{max} \qquad (6.35)$$

As already stated the cohesion is practically independent of the hardness of the material of the particle and the plane. This was also observed by other authors [2]. Moreover, it shows that the relative increase in the cohesion due to gas adsorption is also independent of the radius of the particle, c.q. the asperity radius. This is clarified by the fact that none of the dimensionless parameters dealing with the gas adsorption (α, τ and δ) contain the radius, R.

For the quartz sand quite similar results were obtained.

6.6 CONCLUSIONS

The relation between interparticle distance and force may be influenced by gas adsorption. The presence and degree of the influence depend on the type of gas and the gas pressure.

The cohesion of the particles may also be influenced by gas adsorption. The relative increase may be up to a factor three. The presence and degree of the influence depend on the type of gas and on the gas pressure. The relative degree of this influence does neither depend on the radius of the particles involved nor on the hardness of the particles.

6.7 LIST OF SYMBOLS

A_{ij}	ML^2T^{-2}	Hamaker constant for the interaction between substances i and j
C	MLT^{-2}	cohesion (maximum of force)
C_{ij}	ML^8T^{-2}	constant in Lennard-Jones potential for substances i and j
F	MLT^{-2}	external force applied to the particle
h	L	flattening
K	$M^{-1}LT^2$	constant defined by equation (6.12)
L	L	distance between the centre of the particle and the surface of the plane
n_i	L^{-3}	density of molecules in substance i
N	L^{-2}	density of adsorbed gas molecules
N_0	L^{-2}	maximum density of adsorbed gas molecules
p	$ML^{-1}T^{-2}$	gas pressure
r	L	intermolecular distance
r_{ij}	L	constant in Lennard-Jones potential for substances i and j
R	L	radius of the particle
s	L	distance to centre line of the particle/plane system
T	Θ	absolute temperature
U	ML^2T^{-2}	energy
V_{ij}	ML^2T^{-2}	intermolecular potential for substances i and j
y	L	distance between the surface of the particle and the plane
Y	$ML^{-1}T^{-2}$	Young's modulus
z	L	smallest distance between the surfaces of the particle and the plane

6.7.1 dimensionless parameters

α	ratio of constants for molecular solid/solid interaction and gas adsorption
γ	cohesion
δ	measure of adsorbed gas density defined by equation (6.18)

ε	energy
η	flattening of the particle
Θ	density of adsorbed gas molecules
ζ	smallest distance between the surfaces of the particle and the plane
λ	distance between the centre of the particle and the surface of the plane
ν	Poisson ratio
ξ	distance between the surfaces of the particle and the plane
ρ	radius of the particle
τ	ratio of adsorption energy and thermal energy
ϕ	external force applied to the particle
ψ	ratio of constants for molecular solid/solid interaction and elastic energy

6.7.2 indices

a	gas adsorption at a free surface
c	gas adsorption between two surfaces
g	gas
H	elastic (Hertz)
m	molecular
s	solid

6.7.3 physical constants

k $1.38 \cdot 10^{-23}$ J/K

6.8 LITERATURE

1	B.V. Derjaguin, V.M. Muller and Y.D. Toporov	J.Coll.Interf.Sci. 53(1975)314
2	K.L. Johnson, K. Kendall and A.D. Roberts	Proc.R.Soc.Lond.A 324(1971)301
3	B. Dahneke	J.Coll.Interf.Sci. 40(1972)1
4	H. Krupp	Adv.Coll.Interf.Sci. 1(1967)111
5	D.C.-H. Cheng	Chem.Eng.Sci. 23(1968)1405

6 J. Tsubaki and G. Jimbo Powder Technology 38(1984)219

7 O. Molerus Powder Technology 33(1982)81

8 K. Rietema Powder Technology 37(1984)5

9 H. Piepers, E. Cottaar, A. Verkooijen and K. Rietema Powder Technology 37(1984)55

10 J. Visser Adv.Coll.Interf.Sci. 3(1972)331

11 H. Hertz Miscellaneous papers, 1896, London: Macmillan

12 H. Beijerinck, P. van der Kam, E. Cottaar and N. Verster J.Chem.Phys. 75(1981)1570

13 K. Tang, J. Norbeck and P. Certain J.Chem.Phys. 64(1976)3063

14 R. Aziz and H. Chen J.Chem.Phys. 67(1977)5719

15 T. MacRury, W. Steele and B. Berne J.Chem.Phys. 64(1976)1288

16 J. Farrar and Y. Lee J.Chem.Phys. 57(1972)5492

17 J. Farrar, Y. Lee, V. Golmann and M. Klein Chem. Phys. Lett. 19(1973)359

18 W.A. Steele The interaction of gases with solid surfaces, Pergamon Press 1974

19 R. Johne and D. Severin Chem.-Ing. Techn. 37(1965)57

APPENDICES

6.A INTERACTION ENERGY BETWEEN A GAS AND A SOLID

For the interaction energy between an individual gas molecule and an individual molecule of the solid we assume a Lennard-Jones potential

$$V_{gs}(r) = C_{gs}\left(-\frac{1}{r^6} + \frac{r_{gs}^6}{2r^{12}} \right) \qquad (6.A.1)$$

The energy of a single gas molecule which is at a distance d of a solid plane is then given by

$$U_a(d) = 2\pi n_s \int_0^{\pi/2} \left\{ \int_{d/\cos\theta}^{\infty} V_{gs}(r)\, r^2 dr \right\} \sin\theta\, d\theta$$

$$= 2\pi n_s C_{gs}\left(-\frac{1}{6d^3} + \frac{r_{gs}^6}{144d^9} \right) \qquad (6.A.2)$$

This energy is at its minimum for $d=r_{gs}/\sqrt{2}$. The binding energy of a single gas molecule is therefore given by

$$U_a = - \frac{4\sqrt{2}\,\pi\, n_s C_{gs}}{9\, r_{gs}^3} \qquad (6.A.3)$$

If the case of a single gas molecule between two solid planes at a distance y is considered, the energy is

$$U_c(y,d) = U_a(d) + U_a(y-d) \qquad (6.A.4)$$

Where d is the distance to one of the planes.

For low values of y ($y < 2r_{gs}$) this function has a minimum at $d=\frac{1}{2}y$. For higher values two minima will occur. As long as y is not too large, the value of the energy in these minima does not differ very much from the value at $d=\frac{1}{2}y$. Therefore, we will write the binding energy between two planes as

$$U_c(y) = U_a(\tfrac{1}{2}y) + U_a(\tfrac{1}{2}y) = - \frac{4U_a}{\sqrt{2}} \left(- \frac{3r_{gs}^3}{y^3} + \frac{8r_{gs}^9}{y^9} \right) \qquad (6.A.5)$$

6.B DENSITY OF ADSORBED MOLECULES

The system of the free gas and the adsorbed gas at a free surface is considered. It is assumed there is equilibrium. Then the chemical potential, μ_g, for the free gas must be equal to the chemical potential, μ_a, of the adsorbed gas

$$\mu_g = \mu_a = U_a + kT \log \frac{N_a}{N_{0a} - N_a} \qquad (6.B.1)$$

Where N_a is the number of adsorbed gas molecules and N_{0a} the number of adsorption sites at the free surface.

The same holds, of course, for the adsorption between two planes at distance y. Thus

$$\mu_g = \mu_c = U_c(y) + kT \log \frac{N_c(y)}{N_{0c} - N_c(y)} \qquad (6.B.2)$$

If all conditions, e.g. temperature and pressure, are the same it therefore follows

$$\frac{N_c(y)}{N_{0c} - N_c(y)} = \frac{N_a}{N_{0a} - N_a} \exp((-U_c(y) + U_a)/kT) \qquad (6.B.3)$$

Since the surface covered by one gas molecule is of the order of r_{gg}^2 it follows

$$N_c(y) = \frac{1}{r_{gg}^2} \frac{\delta \exp((-U_c(y) + U_a)/kT)}{1 + \delta \exp((-U_c(y) + U_a)/kT)} \qquad (6.B.4)$$

Using the definition

$$\delta = \frac{N_a}{N_{0a} - N_a} \qquad (6.B.5)$$

Since the chemical potential of a free, ideal gas is proportional to the logarithm of the gas pressure it follows from equation (6.B.1) that δ is also proportional to the pressure.

6.C THE SORPTION MEASUREMENTS

6.C.1 introduction

To measure the physi-sorption of gases and powders at elevated pressures an experimental set-up was constructed as shown in figure 6.C.1. In its essence the used technique is a volumetric one: the lack of gas due to adsorption (or the surplus due to desorption) is measured by a differential pressure transducer. All volumina are chosen in such a way that if no sorption would take place the differential pressure would be zero.

In this section we will treat the gas as an ideal gas. Using more accurate descriptions of a real gas, e.g. using virial coefficients, hardly increases the accuracy of the results.

6.C.2 the adsorption measurements

The procedure followed in this measurement is given in table 6.C.1. From a simple mol balance it can be derived that the total amount of adsorbed gas in moles at a pressure p_1, $n_a(p_1)$, is equal to

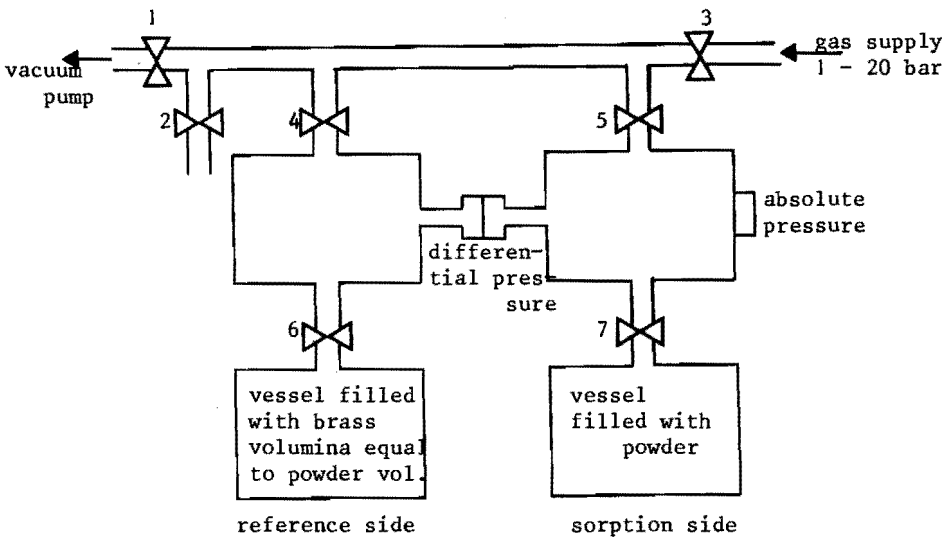

Figure 6.C.1. Schematics of the set-up for the sorption measurements.

$$n_a(p_1) = \frac{-\Delta p\,(V_s - V_p) - p_1(V_c - V_p)}{RT} \qquad (6.C.1)$$

Where Δp is the pressure difference between the sorption and the reference side, V_s is the total volume below valve 5 (valve 7 opened), V_p is the skeleton volume of the powder, p_1 is the absolute pressure at the sorption side, V_c is the required skeleton volume of the powder (i.e. the volume necessary to get no pressure difference, if no sorption is present), R is the gas constant and T is the absolute temperature.

Since the absolute pressure, p_1, is orders of magnitude larger than the differential pressure, Δp, it may be clear from equation (6.C.1) that the accuracy to be reached is determined by the accuracy in $V_c - V_p$. The required skeleton volume, V_c, is obtained through a calibration procedure. The error is generally of the order of 0.01%. The error in V_p, established by measurements with a pyknometer, was generally about 0.1%. The lowest sorption, n_{am}, which can therefore be measured is equal to

adsorption measurement

step	valves (x = closed)							pressure (upper right)	action
	1	2	3	4	5	6	7		
1		x	x					0 bar	evacuation
2	x	x				x	x	p_0	filling of upper vessels
3	x	x	x	x	x			p_1	measurement
4	x		x					1 bar	deflating

desorption measurement

step	valves (x = closed)							pressure (upper right)	action
	1	2	3	4	5	6	7		
1	x	x						p_0	filling of all vessels
2	x		x			x	x	1 bar	deflating
3		x	x			x	x	0 bar	evacuation of upper vessels
4	x	x	x	x	x			p_1	measurement
5	x		x					1 bar	deflating

Table 6.C.1. The followed procedures for the sorption measurements. When proceeding to a next step first all valves to be closed are closed, then valves to be opened are opened. Valves 4 and 5 and 6 and 7 are always opened or closed simultaneously.

$$n_{am}(p_1) = 10^{-3} \frac{p_1 V_p}{RT} \qquad (6.C.2)$$

Or at 10 bar

$$n_{am}(10)/V_p = 0.04 \text{ mol/m}^3 \qquad (6.C.3)$$

Or using a skeleton weight of 3000 kg/m^3

$$N_{am}(10)/m_p = 1.4 \cdot 10^{-5} \text{ mol/kg} \qquad (6.C.4)$$

Where m_p denotes the powder mass. Taking e.g. a molar weight of the gas of 30 gr this leads to a weighing accuracy of $4 \cdot 10^{-7}$, when a gravimetric method would be used. Such is however unreachable, without taking resource to very exotic weighing techniques. This shows the advantage of a volumetric method for gasadsorption.

The duration of a single measurement is about three hours. One hour is needed for a proper evacuation of all vessels. The second hour is needed to fill the two upper vessels with gas. This takes such a long time since all small pressure fluctuations must be damped out. The final hour is needed for the pressure difference to settle, after the valves between the lower and upper vessels are opened.

6.C.3 the desorption measurement

The procedure followed in this measurement is also given in table 6.C.1. Now it can be derived that

$$n_a(p_0) = \frac{\Delta p\ (V_s - V_p) + p_1(V_c - V_p)}{RT} + n_a(p_1) \qquad (6.C.5)$$

Where p_0 is the pressure at which the lower vessels were originally filled (step 1). The sorption at the final pressure p_1 has to be known. Generally it is measured by the adsorption technique.

The lowest measurable value of the sorption which can be measured is now determined by the absolute errors in p_1V_p/RT and in $n_a(p_1)$. Since both errors are equal (see the previous section), it follows

$$n_a(p_0) = 2 \cdot 10^{-3}\ \frac{p_1 \cdot V_p}{RT} \qquad (6.C.6)$$

Since p_0 is about twice as large as p_1, it follows again

$$n_a(10)/V_p = 0.04\ \text{mol/m}^3 \qquad (6.C.7)$$

So the accuracy of both the adsorption and the desorption technique are equal.

6.C.4 the calibration technique

In the equations (6.C.1) and (6.C.5) in which the sorption is calculated, two parameters, V_s and V_c, are still unknown. These where established by the following calibration procedure:

- Instead of the powder a known volume of steel balls, V_b, is placed in the lower sorption vessel.
- A measurement is done similar to the adsorption or desorption mea-

surement.

- Since the sorption is practically zero from equation (6.C.1) (or (6.C.5)) it can be derived:

$$\Delta p\ (V_s - V_b) + p_1(V_c - V_b) = 0 \qquad (6.C.8)$$

- Using different ball volumina, V_b, and initial pressures, p_0, resulting in many values of Δp and p_1, V_s and V_c can be determined by a least-squares fitting procedure.

7 GENERAL OVERVIEW

7.1 INTRODUCTION

It is evident from the previous chapters that the interstitial gas does influence the behavior of the powder through interaction with the powder particles. All influences noted in the milling and mixing experiments created by applying gases with different viscosities and/or pressures can be explained by the differences in porosity of the powder and the accompanying differences in mobility and cohesion of the powder. That this influence on the porosity does have such a remarkable effect on the powder behavior is due to the fact that the mobility and the cohesion show a very strong dependency on the porosity.

Two distinct types of gas influence could be distinguished. They are shortly discussed below.

7.2 THE HYDRODYNAMIC GAS-POWDER INTERACTION

This interaction is due to the fact that a powder, which is aerated during reshuffling in the apparatus under consideration, takes a certain time to fully deaerate. If this time of deaeration is long compared to the cycle time of the reshuffling (at least) part of the powder is continuously in an aerated state. Rietema (1) derived a criterion when gas influence can be expected:

$$N_g = \frac{\rho_d \, g \, d_p^2}{\mu \, U_a} << 100 \qquad (7.1)$$

The dimensionless number N_g is called the gas-powder-interaction number. It should be noted that the smaller this number, the higher the gas influence.

Figure 7.1 shows the result of a series of experiments in a rotating drum in which both the apparatus speed U_a and the gas viscosity μ are varied. All particle properties were kept constant. In this particular case the limiting value of the number N_g, at which gas influence resulting in a partly expanded powder became noticeable, was around 7. It also clearly shows that the lower the number, i.e. the higher the gas

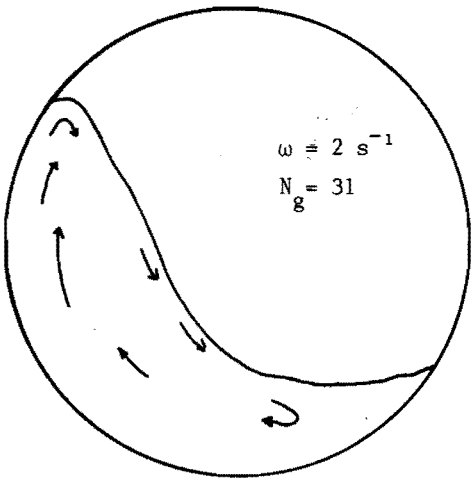

hydrogen $\mu = 0.88 \cdot 10^{-5}$ kg/ms

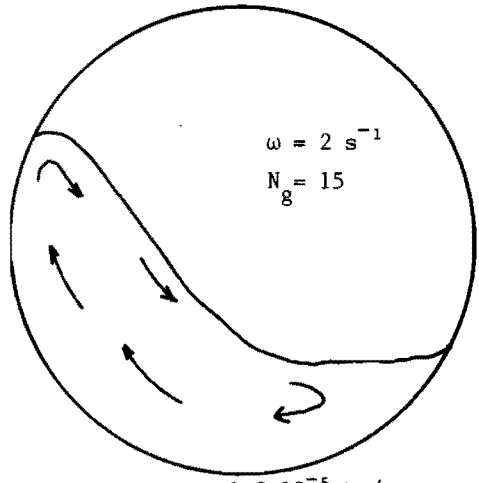

air $\mu = 1.8 \cdot 10^{-5}$ kg/ms

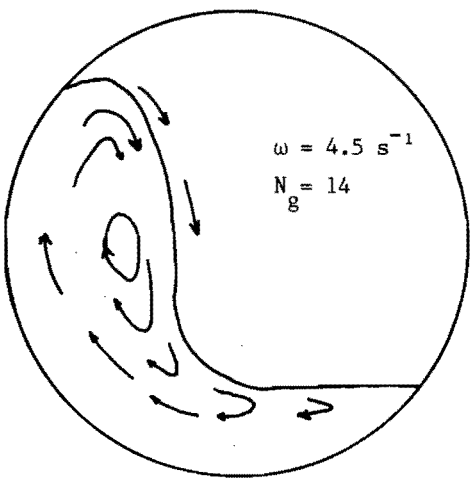

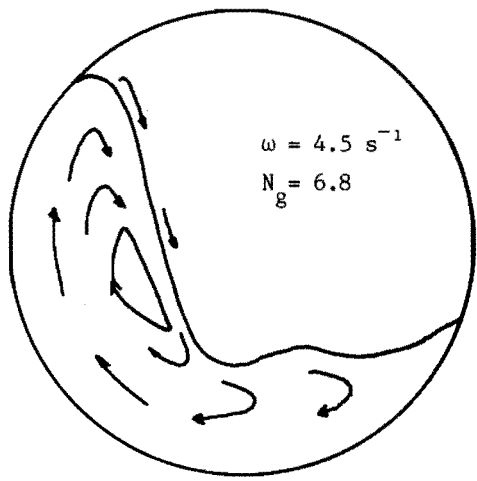

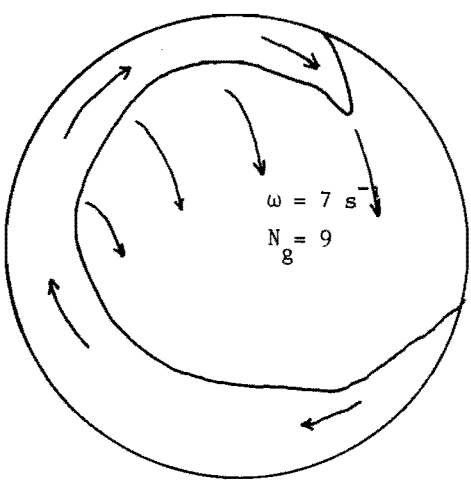

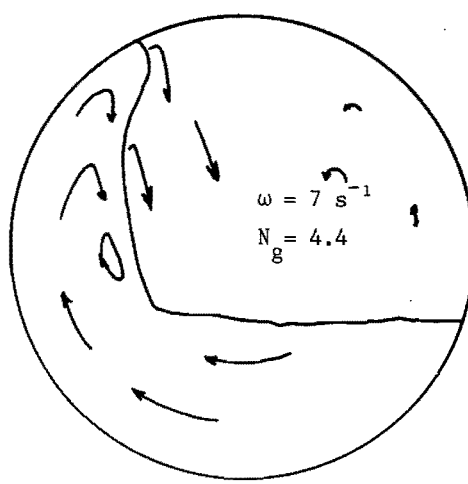

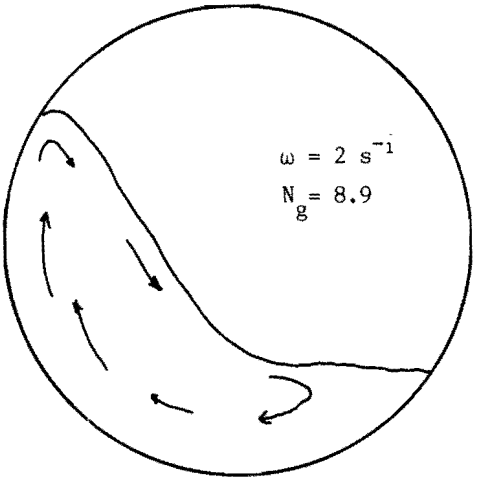

neon $\mu = 3.1 \cdot 10^{-5}$ kg/ms

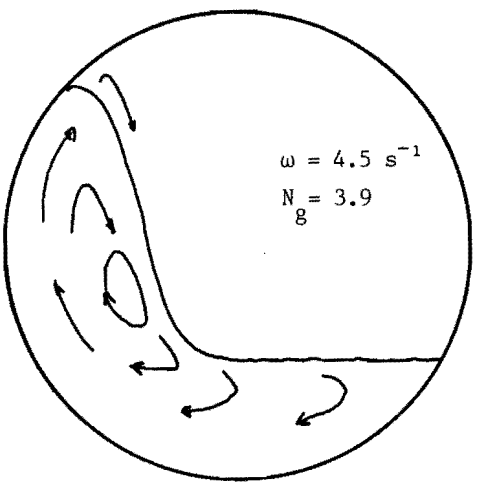

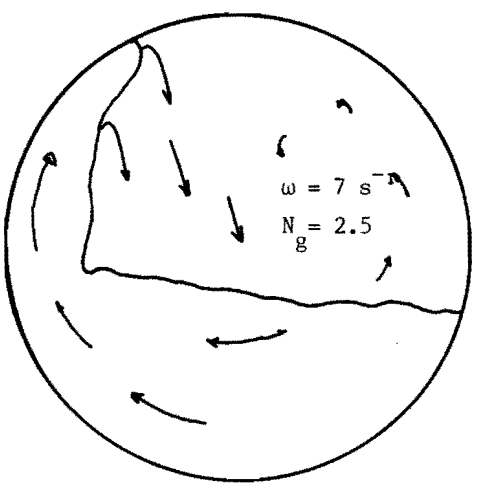

Figure 7.1. The visually observed powder surface and powder flow of a fresh cracking catalyst (d_p = 63-80 μm, ρ_p = 800 kg/m³) for three different gases at three speeds of rotation. Radius of the drum is 0.075 m. Depth of the drum is 0.02 m.

influence, the more powder is in the expanded state.

Two remarks must be made on this influence. The first is that for fine powders the gas viscosity is generally not an independent gas parameter. At low absolute pressures the free path of the gas molecules becomes of the order of the particle diameter, which results in a drastical decrease of the effective gas viscosity. For particles with a diameter of 10 μm this effect sets in around 0.1 bar.

The second remark is that the number N_g, generally, depends on the scale of the apparatus, since the speed of the apparatus depends on this scale in most cases. E.g. for ball mills, which are run at a constant fraction of the critical speed, the number N_g is inversely proportional to the square root of the radius of the mill. So when the scale is increased, the number N_g decreases and thus the gas influence increases. As may be clear from the previous chapters this may have important consequences for the processes involved.

7.3 THE INFLUENCE OF GAS ADSORPTION ON PARTICLE COHESION

This influence is studied theoretically in chapter 6. The result of this influence is that the maximum porosity of the aerated powder is increased. This can be explained by the theory developed by Mutsers [2,3,4], which states that the larger the interparticle forces the larger the stabilizing forces in an aerated powder will be. Hence, the formation of gas bubbles, which cause a very fast deaeration of the powder, is still prevented at higher porosities.

That gas adsorption does indeed influence the interparticle cohesion and thus the powder cohesion is shown in figure 7.2. Here the calculated cohesion is compared to the measured cohesion. A strong correlation is evident.

When in the future more pressurized installations will be used in powder handling these effects may also become important. Since gas adsorption is also very dependent on the absolute temperature, also the temperature will effect this influence.

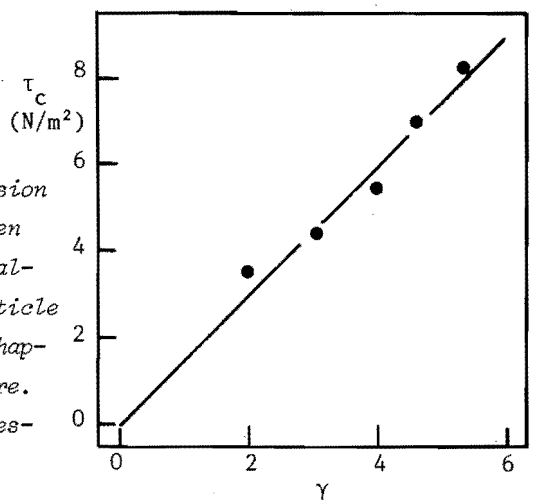

Figure 7.2. The powder cohesion of cracking catalyst as given by Rietema (1) versus the calculated (dimensionless) particle cohesion as calculated in chapter 6 for an argon atmosphere. The parameter is the gas pressure.

7.4 USAGE OF GAS INFLUENCE IN POWDER HANDLING PRACTICE

Apart from the deeper insight in some powder handling processes, which was obtained is this research project, the influence of the interstitial gas may also be directly used to improve these processes.

As already noted in chapter 4 pressurized milling for example may be a good alternative to the wet milling of a powder with respect to production costs. When the powder is needed in the dry state after the milling, pressurized milling is even more advantageous since no drying is necessary (with its accompanying agglomeration of particles), while the obtained result is close to that of wet milling. Pressurized milling will also yield a better result than ordinary dry milling.

In mixing the most useful result of using gas influence is the mixing of powders with a high tendency to segregate at a very low gas pressure, i.e. under vacuum conditions. Mixing will then only occur through convective processes. Due to the very low powder porosity diffusive mixing is almost absent. At the same time this very low porosity will, however, also inhibit the segregation of particles. So the mixing process will be slow but in the end effective.

Another possible usage may be the transport in vessels of segregating powder mixes under vacuum conditions. Thus preventing, or at least slowing down, any segregation.

Since gas viscosity and pressure so markedly influence the powder behavior gas influence may occasionally also be useful in creating some special circumstances which are otherwise unobtainable.

7.5 LITERATURE

1	K. Rietema	Powder Technology 37(1984)5
2	S. Mutsers	thesis, T.H. Eindhoven 1977
3	S. Mutsers and K. Rietema	Powder Technology 24(1979)57
4	S. Mutsers and K. Rietema	Powder Technology 24(1979)65

SAMENVATTING

In dit proefschrift worden de resultaten beschreven van een onderzoek naar de invloed van het interstitiële gas, het gas tussen de poederdeeltjes, op het gedrag van fijne, stromende poeders. Twee invloeden moeten worden onderscheiden:

- een hydrodynamische interaktie ten gevolge van een verschil in snelheid tussen het gas en de poederdeeltjes,
- een eventuele verhoging van de onderlinge deeltjeskrachten ten gevolge van mogelijke adsorptie van het gas aan het oppervlak van de deeltjes.

De eerste invloed heeft in het algemeen tot gevolg dat het poeder in apparaten waarin het wordt bewerkt, een hogere porositeit verkrijgt, dan die het in een dergelijk apparaat zou hebben bij afwezigheid van deze invloed. De hogere porositeit heeft een hogere poedermobiliteit tot gevolg. De belangrijkste grootheden, die deze invloed bepalen, zijn de gasviskositeit en de deeltjesdiameter.

De tweede invloed, welke vooral merkbaar is bij verhoogde drukken (10 tot 20 bar) heeft tot gevolg dat de maximale porositeit, die het poeder bereiken kan, wordt verhoogd en daarmee samenhangend de mobiliteit wordt vergroot. Ten gevolge van de grotere interaktiekrachten tussen de deeltjes (grotere kohesie) kan het beluchte poeder namelijk een lossere struktuur bereiken zonder instabiel te worden (belvorming).

Voor twee praktische vormen van poederbewerkingen, malen en mengen, is de uiteindelijke betekenis van deze twee gasinvloeden voor het proces onderzocht.

Bij malen bleken de eigenschappen van het gas zowel de maalsnelheid (de gewichtsfraktie gemalen poeder per tijdseenheid) als de maalfijnheid (de fijnheid van de gemalen poederdeeltjes) te beïnvloeden. Ook de uiteindelijke fijnheid van het maalprodukt wordt beïnvloed door het gas. Het onderzoek toont aan dat onder bepaalde omstandigheden het droog malen van een poeder in een molen onder verhoogde druk een goed alternatief kan zijn voor het nat malen, dan wel een verbetering

kan geven ten opzichte van normaal droog malen.

De beïnvloeding van het poedergedrag door het gas en de daaruit volgende beïnvloeding van het maalproces is ook gebruikt om een beter inzicht te verkrijgen in de verschijnselen welke van belang zijn voor het malen in een kogelmolen. Het bleek mogelijk twee typen van kogelgedrag te onderscheiden, die elk bijdroegen tot het maalproces, en de bijdragen van elk te kwantificeren. Ook de porositeit van het poeder bleek invloed te hebben op deze bijdragen. Kennis als deze kan van groot nut zijn bij de schaalvergroting van kogelmolens.

Ook op het menggedrag van poeders bleek de gasfase invloed te hebben. In het algemeen geldt dat voor poeders, welke geen neiging tot segregatie vertonen, de mengsnelheid verhoogd kan worden door de mobiliteit, respektievelijk de porositeit, van de poeders te vergroten. Dit kan bereikt worden door uit te gaan van een gas met een hoge viskositeit en/of te werken bij verhoogde druk. Voor poeders, welke wel neiging tot segregatie vertonen, dient de mobiliteit juist zo laag mogelijk gehouden te worden om uitzakken van deeltjes te bemoeilijken. Dit kan men bewerkstelligen door te werken met een lage gasviskositeit en/of bij verlaagde druk (vakuum).

De invloed van de adsorptie van gas op de deeltjeskrachten is ook theoretisch onderzocht. Op grond van literatuurgegevens en enige aanvullende experimenten kon worden aangetoond dat een dergelijke invloed inderdaad aanwezig is. De invloed is sterk afhankelijk van het type gas.

De eindkonklusie van het onderzoek kan luiden dat het interstitiële gas inderdaad een duidelijke invloed op het gedrag van fijne poeders heeft en dat deze invloed van belang is bij de verschillende poederbewerkingen.

SUMMARY

This thesis reports on a research project on the influence of interstitial gas, i.e. the gas in the pores between the powder particles, on the behavior of fine, flowing powders. Two influences must be distinguished:

- a hydrodynamic interaction due to a slip velocity between the gas and the particles,
- a possible increase of the interparticle forces due to adsorption of the gas at the surface of the particles.

The first influence generally causes that the porosity of the powder in the apparatus under consideration is higher than it would be without this influence. This increased porosity in its turn increases the mobility of the powder. The main parameters controlling this influence are the gas viscosity and the particle size.

The second influence, which is mostly noticeable at elevated gas pressures (10 through 20 bar), causes an increased maximum porosity of the powder. This is due to the fact that due to the increased interparticle forces the powder can reach a more open structure without becoming instable (creation of gas bubbles). The increased maximum porosity again increases the mobility.

For two applications in the field of powder handling the effects of these two influences of interstitial gas have been further investigated. These applications were the dry milling and dry mixing of fine powders.

For milling the properties of the gas influenced both the rate of breakage, i.e. the fraction of the powder milled per unit of time, and the milling fineness, i.e. the fineness of the milled particles. Also the ultimate fineness of the product was influenced by the interstitial gas. It is shown that the dry milling of a powder in a mill at an elevated gas pressure can be a good alternative to the wet milling of such a powder. Milling at an elevated pressure will also cause an improvement in comparison with ordinary dry milling.

The influence of the gas on the powder behavior and the resulting influence on the milling process has also been used to obtain a better insight in the most important processes occuring in a ball mill. Two types of ball movement, falling and cascading balls, each contributing to the milling process, could be distinguished. The contribution of each could be quantified. Also the powder porosity appeared to influence these contributions. The knowledge thus obtained can be of great value whan scaling up.

Also the mixing behavior of fine powders appeared to be influenced by the interstitial gas. Generally it can be stated that powders, which show no tendency to segregation, can be more quickly mixed by increasing the powder porosity, c.q. the mobility. This can be done by using a more viscous gas and/or an increased gas pressure in the mixer. Powders, however, which will easily segregate, can better be mixed in a state of low powder mobility. This one can reach by mixing in a low viscosity gas and/or at low gas pressure (vacuum).

The influence of the adsorption of gas on the interparticle forces has also been investigated theoretically. Using data from the literature and some additional experiments it is shown that such an influence is indeed present. The degree of the influence is very dependent on the type of gas used.

The final conclusion of this research is that the interstitial gas indeed does influence the behavior of fine powders and that this influence has its consequences for practical applications of powder handling.

LEVENSBERICHT

20 aug 1956	geboren te Heerlen
1974	eindexamen gymnasium-B aan het Bernardinus-college te Heerlen
1974 - 1980	studie aan de afdeling Technische Natuurkunde van de TH Eindhoven
1980 - 1984	als wetenschappelijk ambtenaar van de stichting FOM werkzaam aan de afdeling Scheikundige Technologie van de TH Eindhoven
1985 -	werkzaam als ontwikkelaar bij de hoofdindustriegroep Licht van de Nederlandse Philips Bedrijven B.V.

ACKNOWLEDGEMENT

The project of which this thesis is a result was a part of the program of Technical Physics and Innovation (Technische Natuurkunde en Innovatie) of the Foundation for Fundamental Research on Matter (Stichting Fundamenteel Onderzoek der Materie, FOM). It was also financially supported by the Foundation for Technical Sciences (Stichting voor de Technische Wetenschappen, STW), the future technical science branch of the Foundation for Pure Research (Stichting Zuiver Wetenschappelijk Onderzoek, ZWO).

STELLINGEN

behorend bij het proefschrift van E.J.E. Cottaar

1 Het is onjuist aan het oppervlak van vaste stoffen een oppervlakte-energie toe te kennen.

dit proefschrift, hoofdstuk 6

K.L. Johnson e.a., Proc.R.Soc.Lond.A 423(1971)301

B.V. Derjaguin e.a.,J.Coll.Interf.Sci. 53(1975)314

2 De als "flow properties" in de literatuur omschreven eigenschappen van poeders beschrijven niet, zoals de term suggereert, de stromingseigenschappen, maar slechts de overgang van een stilstaand naar een stromend poeder.

3 De door Sommer gegeven beschrijving van het mengen van poeders is niet invariant voor een verandering in de definitie van de konsentratie.

K. Sommer, Fortschr.d.Verfahrenst. 19(1981)189

4 Gezien de bij de huidige stand van de kennis van het gedrag van poeders zeer beperkte geldigheid van numerieke korrelaties en de daar tegenover staande grote variatie in de eigenschappen van poeders, is het geven van en zoeken naar dergelijke numerieke korrelaties in het algemeen een zinloze zaak. De voortgang van de kennis over poeders is voorlopig meer gebaat bij goede kwalitatieve beschrijvingen van het waargenomen gedrag.

5 Het door Vaessen ontwikkelde model voor de impulsoverdracht tussen een plasma en daarin gespoten metaaldeeltjes is onnodig ingewikkeld. Een eenvoudig laminair model geeft, gezien de onzekerheid in de verschillende parameters, een even nauwkeurig beeld.

P.H. Vaessen, proefschrift TH Eindhoven 1984

6 Bij de sporenelementenanalyse met behulp van PIXE (proton induced X-ray emission) is de keuze van de dragermaterialen en het ontwikkelen van standaardmethoden voor de monsterbereiding minstens even belangrijk als het ontwikkelen van de uiteindelijke analyseapparatuur en -programmatuur.

H.P.M. Kivits, proefschrift TH Eindhoven 1980

7 Bij het gebruik van tracerdeeltjes ten behoeve van het bestuderen van het gedrag van een stromend medium dient men zorgvuldig te onderzoeken of en in hoeverre te verwachten is dat het gedrag van de tracerdeeltjes overeenkomt met dat van het te onderzoeken medium.

8 Na de invoering van de twee-fasen struktuur in het wetenschappelijk onderwijs lijkt het zinvoller de aanduiding "universiteit" in de aanduiding "hogeschool" te veranderen in plaats van de omgekeerde wijziging zoals voorgesteld door de Nederlandse regering.

16 april 1985